TECHNISCHE UNIVERSITÄT MÜNCHEN

Department Chemie
Lehrstuhl für Biotechnologie

Co-chaperone interactions in the Hsp90 chaperone cycle

Jing Li

Vollständiger Abdruck der von der Fakultät für Chemie der Technischen Universität München zur Erlangung des akademischen Grades eines Doktors der Naturwissenschaften genehmigten Dissertation.

Vorsitzender:	Univ.-Prof.Dr. L. Hintermann
Prüfer der Dissertation :	1. Univ.-Prof.Dr.J.Buchner
	2. Univ.-Prof.Dr.S.Weinkauf
	3. Univ.-Prof.Dr.M.Sattler

Die Dissertation wurde am 20.10.2011 bei der Technischen Universität München eingereicht und durch die Fakultät für Chemie am 09.12.2011 angenommen

To My Family

1. Summary

Hsp90 is an evolutionally conserved and highly abundant molecular chaperone that is essential in eukaryotes. It interacts with more than 200 clients proteins and promotes their maturation and activation. Therefore Hsp90 is involved in almost all physiological events such as signal transduction, cell cycle progression and transcription regulation. Hsp90 does not act alone, but with various accessory proteins, called co-chaperones. They regulate different aspects of Hsp90 function such as activation or inhibition of the ATPase activity and recruitment of specific client proteins. Different Hsp90/co-chaperone complexes have been found during the maturation of client proteins, and the client proteins must pass through these complexes to achieve their active conformation.

In this thesis, the complexes formed by Hsp90 and co-chaperones were characterized and the progression of the chaperone cycle was investigated. Co-chaperones such as Hop/Sti1, Aha1, Cpr6 and p23/Sba1 were labeled at cysteine residues and subjected to analytical ultracentrifugation (aUC) with fluorescence detection to examine the oligomerization states and the complex formation with Hsp90 and other co-chaperones. With labeled Hsp90 single cysteine variants, fluorescence resonance energy transfer (FRET) assays were established to trace the association and disassociation kinetics of the co-chaperone interactions. In addition, other biochemical, biophysical and *in vivo* methods were used to analyze these interactions. In this work, the co-chaperone Hop/Sti1 was first shown to be a monomeric protein but not a dimeric protein as previously reported. A new asymmetric intermediate complex containing Hsp90, Hop/Sti1 and the peptidylprolyl isomerase (PPIases), which is important for the progression of the chaperone cycle was identified and investigated. Also, the mechanism of the exit of Hop/Sti1 from the Hsp90 chaperone cycle was elucidated.

Another co-chaperone, Aha1, the most prominent Hsp90 ATPase activator, had been shown to have strong influence on the function of Hsp90. It interacts with the N- and M-domains of Hsp90 and induces the repositioning of the domain orientation. However, the role of Aha1 in the progression of the chaperone cycle remained

unclear. In this work, Aha1 was shown to be a new conformation-dependent co-chaperone as it has much higher affinity to the closed conformation of Hsp90. It completely expelled Hop/Sti1 from Hsp90 together with Cpr6 and nucleotides in the absence of p23/Sba1. Moreover, Aha1 formed a mixed complex with Cpr6 and stimulated the ATPase activity of Hsp90 synergistically. The cooperative binding of these three proteins was found and verified.

The human Hsp90 co-chaperones, aryl-hydrocarbon receptor interacting protein (AIP) and aryl-hydrocarbon receptor interacting protein like-1 (AIPL1) are homologous proteins with 49% sequence identity. Comparative studies in this thesis indicated that both proteins do not possess PPIase activity, but that AIPL1 is an active molecular chaperone. The unique C-terminal proline-rich domain in AIPL1 is essential for its chaperone activity and acts as a negative regulator for the interaction with Hsp90.

Taken together, new experimental techniques such as aUC and FRET enabled us to further dissect the chaperone cycle of Hsp90 and increase our understanding of the Hsp90 machinery.

Zusammenfassung

Hsp90 ist ein evolutionär hoch konserviertes und weit verbreitetes molekulares Chaperon. Es interagiert mit mehr als 200 Substratproteinen und fördert deren Reifung und Aktivierung. Deshalb ist Hsp90 in fast allen physiologischen Vorgängen, wie Signaltransduktion, Zellzyklus und Transkription, involviert. Hsp90 agiert dabei nicht alleine, sondern mit Hilfe von Co-Chaperonen. Diese regulieren unterschiedliche Aspekte der Hsp90-Funktion, wie Aktivierung/Inhibierung der ATPase Aktivität und die Rekrutierung spezifischer Substratproteine. Unterschiedliche Hsp90/Co-Chaperon-Komplexe konnten während der Reifung von Substratproteinen gefunden werden. Dabei müssen die Substrate diese Komplexe durchlaufen um ihre aktive Konformation zu erhalten.

In dieser Arbeit wurden die Komplexe, die Hsp90 mit den Co-Chaperonen bildet, charakterisiert und ihr Verhalten im Chaperonzyklus untersucht. Die Co-Chaperone wie Hop/Sti1, Aha1, Cpr6 und p23/Sba1 wurden dabei an Cysteinresten mit einem Fluoreszenzfarbstoff markiert und mittels analytischer Ultrazentrifugation (aUZ) wurde der Oligomerisierungsstatus und die Komplexbildung mit Hsp90 untersucht. Zur Bestimmung der Assoziations- und Dissoziationskinetiken der Hsp90/Co-chaperon-Komplexe wurde ein Fluoreszenz Resonanz Energie Transfer (FRET) System etabliert. Zusätzlich wurden weitere biochemische, biophysikalische und *in vivo* Methoden angewendet, um diese Interaktionen zu analysieren. In dieser Arbeit konnte erstmals gezeigt werden, dass das Co-Chaperon Hop/Sti1 als Monomer, und nicht wie früher beschrieben als Dimer, vorliegt. Ein neuer und für den Verlauf des Chaperonzyklus wichtiger assymetrischer Intermediat-Komplex bestehend aus Hsp90, Hop/Sti1 und einer Peptidylprolyl-Isomerase (PPIase) wurde identifiziert und charakterisiert. Des Weiteren wurden die Voraussetzungen für die Verdrängung von Hop/Sti1 aus dem Hsp90 Komplex aufgeklärt.

Aha1, ein weiteres Co-Chaperon und der wohl bedeutendste Hsp90 ATPase Aktivator, besitzt einen starken Einfluss auf die Hsp90 Funktion. Es interagiert mit der N-terminalen und der Mitteldomäne von Hsp90 und induziert dabei eine Neuausrichtung der Domänen. Die Rolle von Aha1 für den Chaperonzyklus blieb

jedoch unklar. In dieser Arbeit konnte gezeigt werden, dass Aha1 ein neues konformationsabhängiges Co-Chaperon ist, da es eine wesentlich höhere Affinität zur geschlossenen Form von Hsp90 besitzt. Durch Aha1 kommt es in Gegenwert von Cpr6 und Nukleotid und in Abwesenheit von p23/Sba1 zur vollständigen Verdrängung von Hop/Sti1 aus dem Hsp90 Komplex. Dabei bildet Aha1 einen gemischten Komplex mit Cpr6 und Hsp90 und stimuliert zusätzlich die ATPase Aktivität von Hsp90. Die kooperative Bindung dieser drei Proteine konnte hier gezeigt und verifiziert werden.

Aryl-hydrocarbon receptor interacting protein (AIP) und Aryl-hydrocarbon receptor interacting protein like-1 (AIPL1), zwei humane Hsp90 Co-Chaperone, sind homologe Proteine und besitzen eine 49%ige Sequenzidentität. Vergleichende Studien in dieser Arbeit zeigen, dass beide Proteine keine PPIase Aktivität besitzen, jedoch AIPL1 ein aktives molekulares Chaperon ist. Die C-terminale Prolin-reiche Domäne von AIPL1 ist dabei essentiell für die Chaperon-Aktivität und agiert als negativer Regulator der Hsp90 Interaktion.

Zusammengefasst ermöglichten neue Techniken wie die Kombination von Fluoreszenzspektrorkopie und analytische Ultrazentrifugation und das FRET-System den Chaperonzyklus von Hsp90 detaillier zu analysieren und somit das Hsp90 Chaperonnetzwerk besser zu verstehen.

2. Introduction

2.1 Protein folding

Proteins are the most versatile biological molecules and essential for all organisms. Almost all the physiological activities such as muscle movement, food digestion, control of senses, defense against infection, are supported by various proteins. Except intrinsically unstructured protein, which is lack of stable tertiary structure (2), in order to perform its function, protein must be folded into a defined three-dimensional conformation, so called native state (3). The physical process by which an unstructured polypeptide folds into a functional tertiary structure is called protein folding (4,5).

In 1970s, Anfinsen developed the famous hypothesis that the native conformation is determined by the amino acid sequence based on the experiments on the spontaneous folding of Ribonulcease A (4). In the following forty years, the extensive studies allow us to gain a much deeper understanding on the theory of protein folding.

The classic model of folding pathway was proposed by Levinthal in 1968, based on his points, proteins have to fold through some directed process to reach their native conformation (6). Folding intermediates such as molten globule state and unstable transient states were reported during the research of protein folding, which support this model (7-9). However, this model is challenged by the discovery of parallel folding pathways, for example, in the folding process of lysozyme and cytochrome c (9-11).

The new model which use the language of “folding funnel” and “energy landscape” was developed based on the *in vitro* protein denaturation and refolding experiments (Fig. 1) (3,12,13). This theory provides a statistical description of the free energies of different molecular conformations. The native states locate at the bottom of the funnel which represents the global energy minimum, while the upper edge of the funnel represents the ensemble of unfolded states or denatured states with higher energy. In general, this model indicates that protein folding is a process with

decrease in energy and concomitant loss of entropy. In an ideal folding scenario, the landscape lacks deep valleys and high barriers in which the polypeptide chain smoothly reaches its native states. However, most protein fold on rough and rugged landscapes, through which the polypeptide chain has to navigate, possibly via one or more populated intermediates, to the native states (1,14).

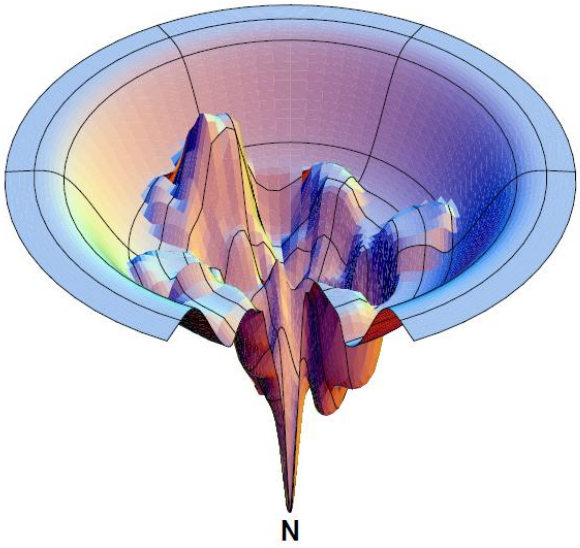

Figure 1. Model of the folding funnel

The native state N located at the bottom of the funnel in a defined state with minimal energy, whereas the unfolded state is characterized by an ensemble of high energy state at the upper edge of the funnel (1)

2.2 Protein folding in the cell

Current folding funnels, however, cannot elucidate how the polypeptide chains fold under physiological conditions since it only describes the folding behavior of an isolated single polypeptide chain at infinite dilution (15). In the living cells, the protein concentration in the cytoplasm reaches values of 200 mg/ml (16). Protein-protein interactions take place as soon as the newly synthesized polypeptide chain exits the ribosomes (17). In addition, other macromolecules such as various forms of RNA contribute to a more crowded environment (18). The crowded condition caused by high concentration of low-molecular weight cosolutes termed “molecular crowding”, which is used to describe the excluded volume effect occurred routinely in living cells (18). Interactions among different biomolecues and the crowding effects significantly alter the folding behavior of the polypeptide chain. Under such conditions, it is important to prevent the aggregation and misfolding due to unspecific interaction or

molecular crowding (19). It has been showed that aggregated and misfolded proteins are associated with neurodegenerative diseases (20,21). A generalized folding pathway is shown in Figure 2.

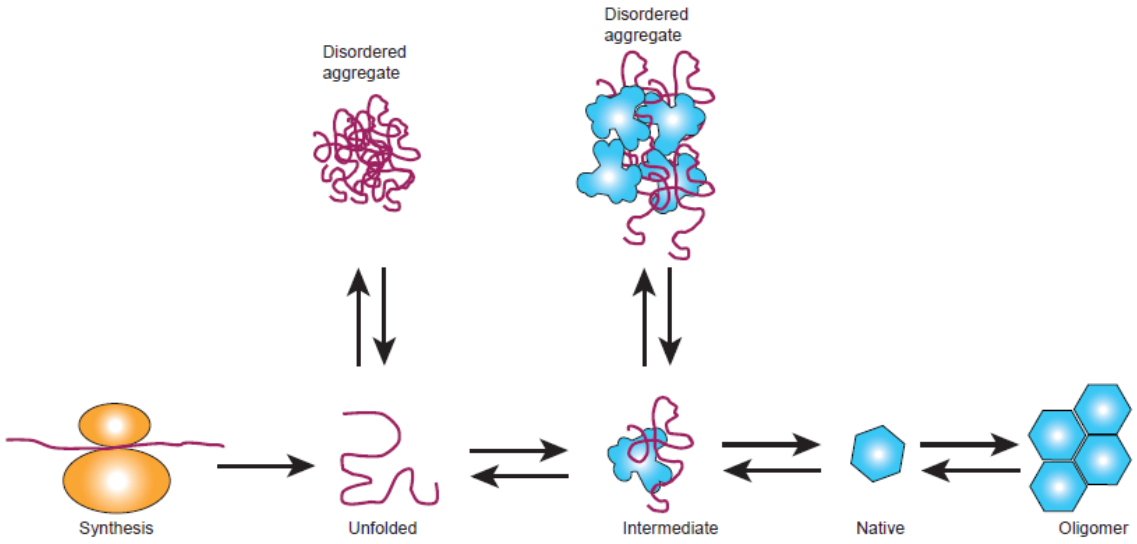

Figure 2. Protein folding pathway

Polypeptide chains (red lines) are synthesized and released from ribosome. Then they fold to their native conformations (blue hexagon) through one or more intermediate states (irregular shape in blue). Misfolded protein might form aggregates during the folding process. Figure adapted from review article 'protein folding and misfolding' (22).

2.3 Catalyzed protein folding

Refolding experiments using denatured proteins suggest that folding events of single domain globular polypeptides take place in second or even millisecond time scales (9). However, some relevant covalent reactions or conformational changes during the folding process take significantly more time, for example, the formation of correct disulfide bonds and the cis-trans isomerization of peptidyl-prolyl bonds (23,24). The cell has evolved folding mechanisms to speed up these rate-limiting processes in order to slow down the accumulation of folding intermediates, and thus prevent the aggregation during folding process (25). Protein disulfide isomerase (PDI) is the first reported folding catalyst, which accelerates the formation of correct disulfide bonds (26,27). In 1984, another enzyme, peptidylprolyl isomerase (PPIase) was

demonstrated to speed up proline cis-trans isomerization (28). So far, only these two enzymes have been found to catalyze protein folding.

PDI resides in the endoplasmic reticulum (ER), where the formation of disulfide bonds in secretory proteins occurs (29). As one of the most abundant ER proteins, PDI plays a significant role in accurate folding and quality control by accelerating the formation, isomerization and breakage of disulfide bonds (27,30). Structurally, PDI is a monomeric protein containing four catalytic and non-catalytic thioredoxin-like domains, namely, a, b, b' and a'. The catalytically active Cys-X-X-Cys motifs are located in the a and a' domains, which react with newly synthesized proteins to confer oxidoreductase activity. The non-catalytic the b and b' domains are responsible for substrate recruitment (31,32).

Unlike PDI, PPIases are ubiquitously expressed proteins and their primary function is to facilitate the *cis-trans* isomerization of peptide bonds N-terminal to proline (Pro) residues (28). PPIases are curial for *in vivo* protein folding, as nascent proteins are presumably all *trans* polypeptide chains and *cis*-X-Pro are frequently found in native proteins (33). In general, PPIases are divided into four structurally unrelated classes, the Cyclosporin A (CsA)-binding cyclophilins, the FK506-binding proteins (FKBPs), the Parvulin-like PPIase and the newly identified protein Ser/Thr phosphatase 2A (PP2A) activator PTPA (34). The knowledge on the exact cellular functions of PPIase is still limited, although cyclophilins and FKBPs have been intensively studied as the targets for the clinically used immunosuppressive drugs CsA and FK506/Rapamycin, respectively (35,36,38). PPIase activities are inhibited when these drugs are bound. However, the actions of these drugs do not involve the suppression of the enzyme activity, but instead it involves the promotion of the formation of a ternary complex with calcineurin or target of rapamycin (TOR), which results in the inhibition of calcineurin phosphatase or TOR kinase activity, respectively (34).

2.4 Molecular chaperones

Besides folding catalysts, there is another group of helper proteins which play an important role in protein folding, the molecular chaperones. The concept of molecular chaperones was introduced by Lasky in 1978. During the study of nucleosome assembly, a nuclear protein called nucleoplasmin was discovered which facilitated the assembly of nucleosome but was not part of the nucleosome. Therefore it was named “molecular chaperone” (39). 1993, R. John Ellis coined the definition: “chaperones are proteins that assist the non-covalent folding or unfolding and the assembly or disassembly of other macromolecular structures, but do not occur in these structures when the structures are performing their normal biological functions having completed the processes of folding and/or assembly (40).” In other words, a molecular chaperone interacts, stabilizes or helps non-native proteins to achieve their native conformation, but the chaperone itself is not present in the final functional structure (41). Several structurally distinct families of molecular chaperones exist in cells (Fig. 3), and many of these proteins are highly expressed under heat or other stress conditions like oxidative stress or heavy metal exposure (42,43). Hence the term “heat shock protein (Hsp)” has been widely used to name molecular chaperones (44). According to their molecular weight, chaperones are usually classified into five different families, Hsp100s, Hsp90s, Hsp70s, Hsp60s and small heat shock proteins (sHSPs). Besides *de novo* folding, chaperones are also involved in various cellular functions such as protein transport, oligomer assembly and proteolytic degradation. Interestingly, many members of the folding catalysts (PDIs and PPIases) also possess chaperone activity, and the chaperone activity is independent of their enzymatic activity (45,46).

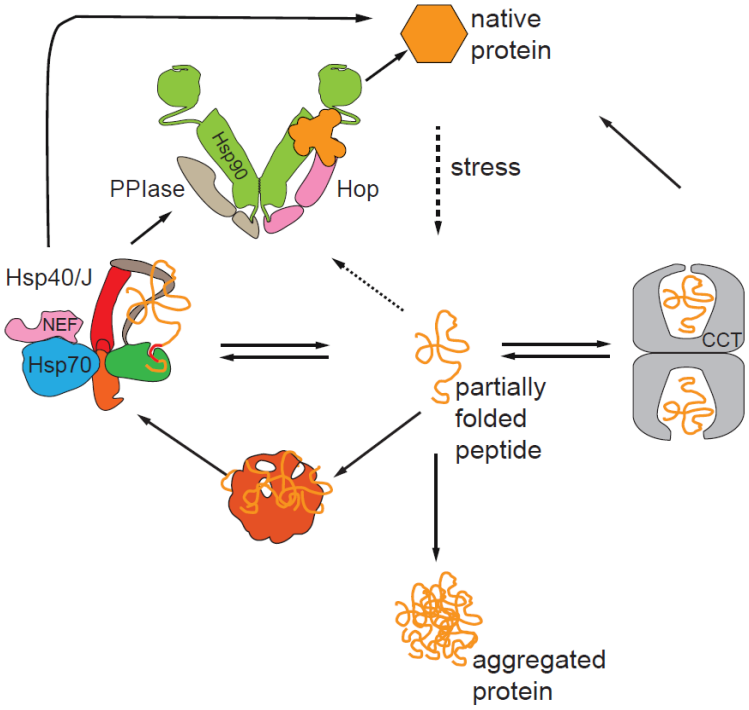

Figure 3. Molecular chaperone networks

In higher eukaryotes, the cytosolic chaperone system is composed of the Hsp70 system (blue), the Hsp90 System (green), sHsps (red) and CCT from the Hsp60 family (grey). Different chaperones from a network to facilitate the correct folding and prevent protein aggregation (47).

2.4.1 Hsp60/Chaperonin family

Chaperonins are structurally conserved large protein complexes that assist the folding of nascent protein to its functional conformation in an ATP dependent manner (48,49). They are divided into two different subgroups based on the dependency on Hsp10. Group I chaperonins (also called Hsp60s) are found in bacteria (GroEL), mitochondria (Hsp60) and chloroplasts (Cpn60). They have seven-membered rings and functionally cooperate with Hsp10 (GroES in bacteria) proteins, which form the lid of the folding cage (50-52). Group II chaperonins are present in archaea (thermosome) and the eukaryotic cytosol (TRiC, TCP-1 Ring Complex, are also called CCT for chaperonin-containing TCP1). They have eight or nine-membered rings and are functionally independent of Hsp10/GroES (53,54).

The GroEL/GroES complex in *E.coli* is the best characterized large chaperonin complex. GroEL consists of 14 identical subunits which forms two heptamer rings, with a large central cavity (55). Non-native protein with a molecular size up to 60 kDa can be bound inside this central cavity. ATP triggers the binding of GroES, which also causes a large conformational change of the chaperonin system that leads to the formation of a cage with a highly hydrophilic, negatively-charged inner wall (56). After ATP hydrolysis, encapsulated protein leaves the cage after the disassociation of GroES, which is triggered by ATP binding to the opposite ring (55,57,58).

2.4.2 Hsp100 family

The Hsp100/Clp family of chaperones is involved in various cellular activities, such as disaggregation or destruction of misfolded proteins (59,60). It belongs to the superfamily of AAA+ domain-containing ATPases. Bacteria contain several Hsp100/Clp proteins including ClpA, ClpB, ClpC, ClpP and ClpX. Similar proteins are found in plants, yeasts and mammals (61). Based on different number of nucleotides binding sites, the Hsp100/Clp family is divided into two classes. Those contain two nucleotides binding domains belongs to class 1, such as ClpA, ClpB, ClpC and yeast Hsp104. Whereas ClpX belongs to the class 2, bearing only one nucleotides binding domain (62,63). The functional forms of these AAA+ proteins are hexameric rings with a narrow pore in the middle. The energy from ATP hydrolysis enables the translocation and unfolding of the misfolded protein through the central pore (64,65). The exact molecular mechanism remains to be elucidated.

2.4.3 Hsp70 family

The Hsp70 family is one the most ubiquitous and conserved classes of chaperones, as Hsp70s exist in almost all living organisms except some archaeal species. The sequence identity between prokaryotic Hsp70, DnaK and its eukaryotic homologues is around 60% (66). In yeast, 14 different genes encode Hsp70 proteins (67). In higher eukaryotes, Hsp70s are found in the cytosol, mitochondria (mtHsp70), chloroplasts (cpHSC70) and ER (Grp78/Bip) (68-70). In mammals, there are two isoforms of cytosolic Hsp70, constitutively expressed Hsc70 and stress-inducible

Hsp70. Hsp70 is composed of three structural domains, a 44 kDa N-terminal ATPase domain followed by an 18 kDa substrate binding domain (SBD) and a 10 kDa C-terminal domain (71). Clients interact with the hydrophobic pocket in the SBD and the interaction is profoundly affected by the interaction between Hsp70 and nucleotides. In the ATP bound-state, Hsp70 has a low affinity but fast exchange rate, while the ADP bound-state shows high client affinity but slow exchange rates (66,72). Moreover, the position of the C-terminal lid is different. In the ADP-bound state, the lid moves closer to the SBD, which prevents the release of client protein (73,74). Hsp70s facilitate not only the protein folding or refolding, but also the degradation and translocation. To achieve these functions, Hsp70 works together with J-proteins (Hsp40s) and nucleotide exchange factors. These co-chaperones regulate the Hsp70 machinery by either conferring client specificity or affecting the interaction with nucleotides (71).

The Hsp70 chaperone machine does not only act alone, but also cooperates with other chaperones machines. For example, in the folding of nascent polypeptides, Hsp70 interacts with the unfolded clients and then transfers the clients to the Hsp90 chaperone machinery through the adaptor protein Hop (Hsp70-Hsp90 Organizing Protein) for the final maturation and activation (75,76). In addition, Hsp70 is also known to be involved in the refolding of the denatured protein captured by the small heat shock proteins (77-80).

2.4.4 Small heat shock proteins

In contrast to Hsp70s, the small heat shock protein (sHsp) family is the most poorly conserved class of chaperones. They share a common domain of around 100 amino acids, called α-crystallin domain, which is usually proceeded by an N-terminal region of variable length/sequence and followed by a non-conserved C-terminal tail (77,81). sHsps are found in all three kingdoms of life, except some pathogenic bacteria. Functionally, sHsps bind proteins in non-native conformations and prevent their aggregation in an ATP-independent manner (82,83). Usually sHsps collaborate with other chaperone machineries such as the Hsp70 system to refold the bound denatured substrate proteins (77). The detailed mechanism for the substrate transfer

remains to be further elucidated. Although the monomer size ranges from 12 to 43 kDa, the active form of sHsps are large oligomers, often composed of 24 subunits and activated by heat or modifications (84-87). The exact substrate binding sites remain unclear, but several studies suggest that the N-terminal region may be involved in the substrate interaction (87). Moreover, the N-terminal region is also important for the chaperone function and oligomerization of sHsps. For example, the N-terminal truncation of yeast Hsp26 and *M. tuberculosis* Hsp16.3 resulted in loss of *in vitro* chaperone activity and their disassociation to dimers or dimers/trimers, respectively (88-90).

2.4.5 Hsp90 family

Hsp90 is a highly conserved molecular chaperone that is essential in eukaryotes (91,92). Comprising 1–2 % of cytosolic protein, it is one of the most abundant proteins, even in unstressed cells (93,94). It contributes to various cellular processes including signal transduction, protein folding, intracellular transport and protein degradation.

Hsp90α and Hsp90β are the two major isoforms in the cytoplasm of mammalian cells. Hsp90α is the major form which is inducible under stress conditions, while Hsp90β is constitutively expressed (94,95). Hsp90 analogues also exist in other cellular compartments such as Grp94 in the endoplasmic reticulum, Trap-1 in the mitochondrial matrix (96-98). Interestingly, no Hsp90 gene has been found in archea and only one Hsp90 gene is present in bacteria, called HtpG (99-101). In yeast, there are also two Hsp90 isoforms in the cytosol, Hsc82 and Hsp82, of which Hsp82 is up-regulated up to 20 times under heat shock stress (91,94)

2.5 Hsp90 chaperone machinery

2.5.1 Structure and conformational dynamics of Hsp90

Hsp90 is composed of three flexibly linked domains, an N-terminal ATP binding domain (N-domain), a middle domain which regulates the ATPase activity (M-domain) and a C-terminal dimerization domain (C-domain) (Fig. 4) (102). Except the

charged linker region located between the N-terminal domain and middle domain, this domain organization is conserved from bacteria to man (75,94). As a member of the gyrase–Hsp90–histidine kinase–MutL (GHKL) family, the N-terminal domain associated closely to trap ATP (103). The ATP binding sites of Hsp90 is rather unique with Bergerat-fold characteristics. Structurally, it consists of a α- and β-sandwich motif (Fig.4c). Hsp90 ATPase inhibitors, such as geldanamycin and radicicol, are targeted to this region (104). Another interesting feature of the ATP binding region is that several conserved amino acid residues in the N-domain comprise a 'lid' (residues 100–121) that close over the nucleotide binding pocket in the ATP bound state but is open during the ADP-bound state (Fig.4c) (105). The middle domain of Hsp90 is involved in the ATP hydrolysis, as it contains crucial catalytical residues for forming the composite ATPase sites. Moreover, the middle domain contributes to the interaction sites for client proteins and some co-chaperones (106-108). Structurally, M-domain consists of a large αβα segment connecting to a small αβα segment via several short α-helices (102). The C-terminal domain consists of a curved α-helix, a three-stranded β-sheet, a three-helix coil and an extended disordered arm (102). A helix-strand segment (residues 587-610) is involved in the dimerization of Hsp90, and the conserved MEEVD motif in the disordered region serves as the docking sites for the interaction with co-chaperones which containing a tetratricopeptide repeat (TPR) clamp (Fig.6a) (109-111).

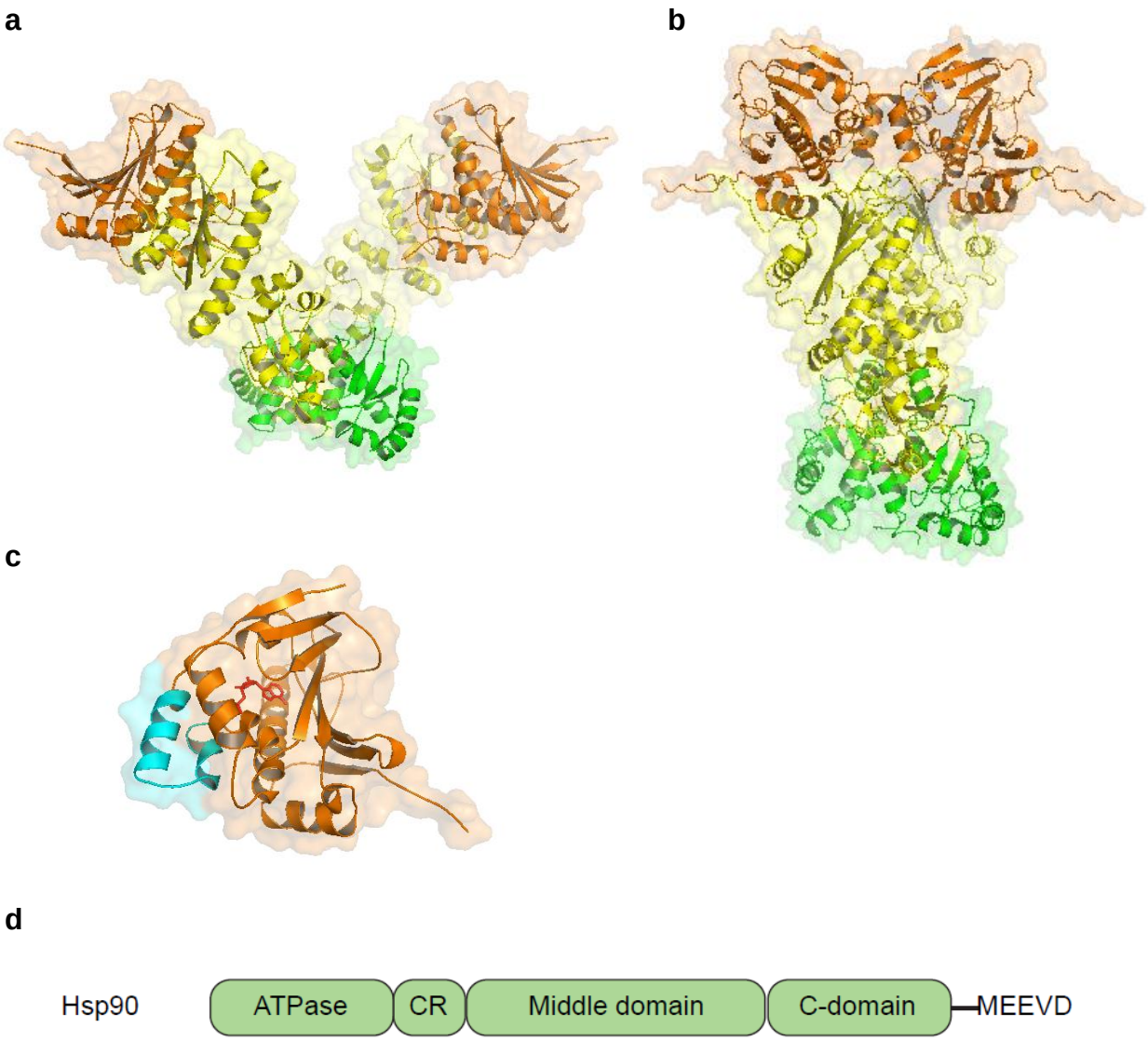

Figure 4. Crystal structures of Hsp90 in the open or closed states

The N-terminal domain is depicted in orange, the M-domain in yellow and the C-terminal domain in green. a. Structure of bacterial Hsp90 (HtpG) in the nucleotide-free state (PDB 2IOQ). b. Structure of yeast Hsp90 in the nucleotide binding state (PDB 2CG9). c. Structure of Hsp90 N-domain complex with ADP (red), the ATP lid is colored in cyan (PDB 1AH6). d. Schematic domain organization of eukaryotic Hsp90.

ATP hydrolysis is required for Hsp90 to perform its function (112,113). However, Hsp90 is a weak ATPase and turnover rates are very low, with 1 min^{-1} for yeast Hsp90 and 0.1 min^{-1} for human Hsp90 (114,115). Structural studies revealed that Hsp90 adopts a number of structurally distinct conformations, which are mainly induced by nucleotide binding and represent different function states of Hsp90

(100,116). In the apo state, Hsp90 adopts a V shape conformation, termed “open conformation”. ATP binding trigger a series of conformation changes including repositioning of the N-terminal lid region and a dramatically change in the N-M domain orientation. Finally Hsp90 reaches a more compact conformation, termed “closed conformation” in which the N-domains are dimerized (100,102). Recent biophysical studies using ensemble and single molecule FRET assays allowed to further dissect the ATP-induced conformational changes (Fig. 5) (117,118). After fast ATP binging, Hsp90 slowly reaches the first intermediate state (I1), in which the ATP lid is closed but the N-domains are still open. Then the N-terminal dimerization leads to the formation of the second intermediate state (I2), in which the M-domain repositions and interacts with N-domain. Then Hsp90 reaches a fully closed state in which ATP hydrolysis occurs. After ATP is hydrolyzed, the N- domains disassociate, release ADP, Pi and Hsp90 returns to the open conformation again (117).

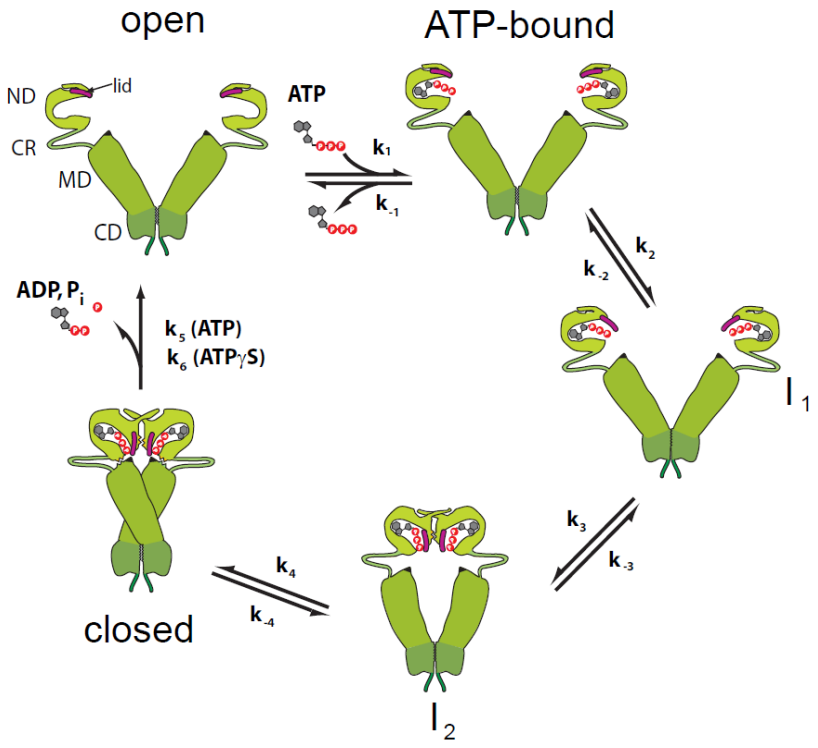

Figure 5. Conformational cycle of Hsp90

After ATP binding, conformational changes occur in the N-domain involving the movement of the ATP lid (I1). The N-domain dimerization leads to the formation of I2 and the repositioning of the N-M-domain orientation finally leading to the fully closed state of Hsp90, where ATP hydrolysis takes place (117).

Interestingly, nucleotide binding is not the only determinant for the conformational change. Recent structural studies show that the interaction with client protein also leads to a partially closed conformation of bacterial Hsp90. At the same time, the presence of the clients stimulates the ATPase activity, which has been observed for both human and bacteria Hsp90 (119,120). However, the detailed mechanism is still not well understood. Nevertheless, these results suggest that there may be a dynamic equilibrium between the different conformations of Hsp90 and this conformational plasticity is functionally important since it may allow Hsp90 to adapt to different client proteins. Moreover, the conformational cycle of Hsp90 is also regulated through the interaction with different co-chaperones.

2.5.2 Hsp90 co-chaperones

Hsp90 interacts with a large number of different co-chaperones dynamically. To date, more than 20 co-chapreones have already been identified in eukaryotic cells (75). They regulate the function of Hsp90 in different ways such as inhibition and activation of the ATPase of Hsp90 as well as recruitment of specific client proteins to the cycle (111,121). The TPR co-chaperones which recognize the C-terminal MEEVD motif in Hsp90 through a highly conserved clamp domain is a prominent example here. Structurally, TPR domain consists of degenerated 34-amino acid repeats forming two anti-parallels α helices separated by a turn. The helix-turn-helix motifs stack upon each other to form a superhelical groove, which interacts with TPR acceptor modules (Fig. 6a) (109). Those co-chaperones include Hop (yeast homologue Sti1), the protein phosphatase PP5 (yeast homologue Ppt1), and members of PPIase family, like Fkbp52, Fkbp51 and Cyp40 (yeast homologous Cpr6/Cpr7) (122-127).

Hop/Sti1 binds and stabilizes the open states of Hsp90 and thus inhibits the ATPase activity of Hsp90 (111,128,129). The presence of three TPR domains allows for its simultaneously binding to Hsp70 and Hsp90, which leads to the facilitation of client protein transfer (130). Previous biochemical studies show that the TPR1 and TPR2A domain binds to the EEVD containing C-terminal end of Hsp70 and Hsp90 (Figure 6), respectively (109,131). The exact role of TPR2B domain is as yet unknown, which

may also contribute to the interaction with Hsp90. Besides TPR domains, two linker regions were found in Sti1/Hop: One between the TPR1 and TPR2A domains, called DP1, and the other one, called DP2, which is located in the C-terminal part of Sti1/Hop (Fig. 6b). However, the exact function of these two linker domains is not clear.

Hop/Sti1 is indispensable for maintaining the hormone binding activity of the glucocorticoid receptor (GR) and progesterone receptor (PR) based on the reconstitution studies (132,133). Recent results indicate that Hop/Sti1 has an influence on many different Hsp90 clients. For example, Lin and co-workers suggests that in *Drosophila* Hop/Sti1 is important for phenotypic stability and this involves a complex of Hop/Sti1 with Hsp90 and the protein Piwi (134). S-nitrosylation or knockdown of Hop contributes to the maturation of a mutant form of the cystic fibrosis transmembrane conductance regulator (CFTR) (135), qualifying it as a new target for the treatment of cystic fibrosis.

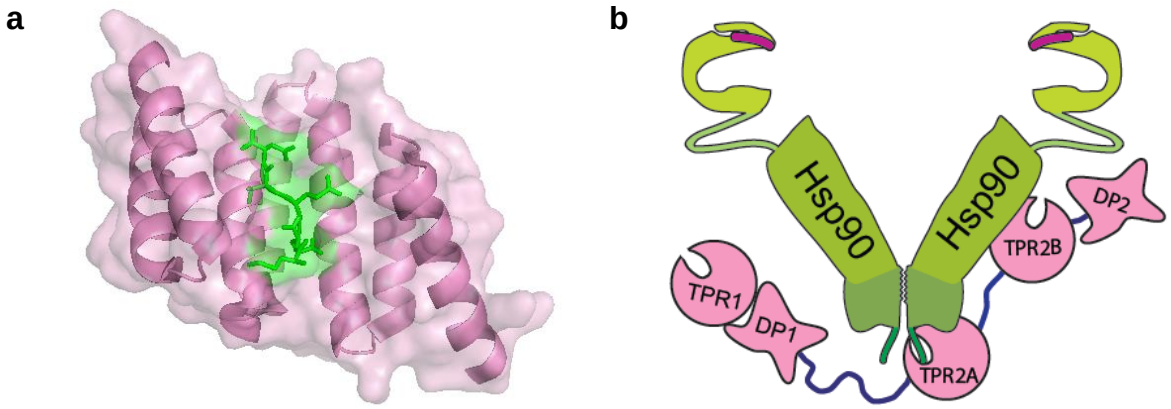

Figure 6. Interactions between Hsp90 and Hop/Sti1

a. Crystal structure of Hop TPR2A domain (pink) complex with Hsp90 MEEVD peptide (green) (PDB 3ESK)

b. Hop/Sti1 binds to the C-terminal MEEVD motif of Hsp90 through its TPR2A domain, additional binding sites in the M-domain may exist.

In contrast to Hop/Sti1, p23/Sba1 binds specifically to the closed conformation of Hsp90 (136,137). This small acidic protein contains an unstructured C-terminal tail, which is important for its intrinsic chaperone activity (138,139). p23/Sba1 was

identified as a component in steroid receptors complex together with Hsp90 and a PPIase (140). It facilitates the maturation of client proteins by stabilizing the closed conformation of Hsp90 (141). As a result, the ATP hydrolysis, which is indispensable for the release of the client protein (112,113), is partially inhibited in the presence of p23/Sba1 (142,143). Co-crystallization studies revealed that the contact sites are prominently located in the N-domain of Hsp90 (Fig. 7), but also with minor M-domain interaction (102). *In vivo* analysis in mice showed that p23 is necessary for perinatal survival, as the development of lungs functions is substantially impaired in p23/Sba1 knockout mouse embryos (144,145).

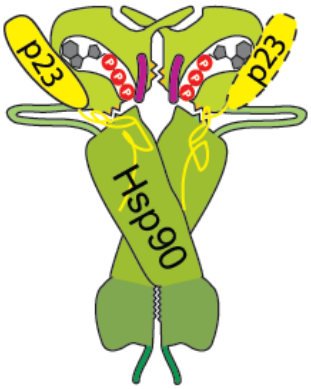

Figure 7. Interactions between Hsp90 and p23/sba1

p23/Sba1 associates with the N-domain of Hsp90, with minor contact in the M-domain.

Cdc37 is another co-chaperone which inhibits the ATPase activity of Hsp90 (146,147). Originally, Cdc37 was identified in *S.cerevisiae* as a gene essential for cell cycle progression (148,149). During the investigation of the oncoprotein v-Src, Cdc37 was found as part of the Hsp90-kinase complex (150,151). Further work in different organisms showed that Cdc37 is specific for chaperoning kinases (152). It interacts with kinases through its N-terminal domain and binds to the N-domain of Hsp90 via its C-terminal parts (Fig. 8). The ATPase arrest is mediated by the insertion of the Cdc37 R167 side chain into the nucleotide binding pocket of Hsp90. This directly inhibits the binding of ATP (102). Furthermore, the binding of the Hsp90 lid segment prevents its closing of the ATP binding site and blocks the access of catalytic residue of the Hsp90 M-domain to the ATP binding pocket. Finally, Cdc37 holds the N-domain in an open state and precludes its dimerization (153).

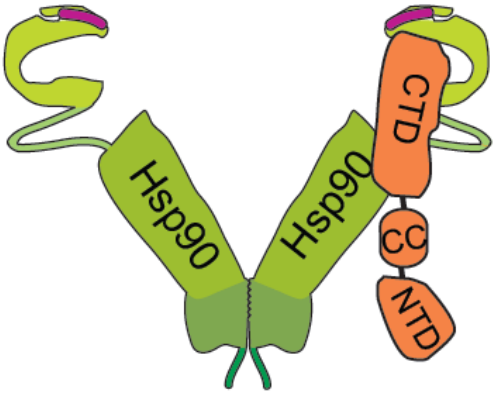

Figure 8. Interactions between Hsp90 and Cdc37

Cdc37 interacts through its C-domain with the N-domain of Hsp90.

Unlike the co-chaperones discussed above, Aha1 is so far the most potent ATPase activator of Hsp90. Biochemical and structural studies revealed that Aha1 binds the M-domain of Hsp90 (154,155). Recent experiment based on nuclear magnetic resonance (NMR) and mass spectrometry further suggests that the C-terminal domain of Aha1 interacts with the dimerized N-domain of Hsp90 (Fig. 9) (107,156). Retzlaff and co-workers further showed that one Aha1 molecule is sufficient to stimulate the ATPase activity of one Hsp90 dimer (107). Binding of Aha1 induces an Hsp90 domain orientation, where the N-domains are in a closed state, which accelerates the progression of the ATPase cycle (107,117). FRET measurements show that the presence of Aha1 enables Hsp90 to bypass the I1 state and to directly reach the I2 state in the ATPase cycle (117). Functional analysis indicated that both Aha1 and its homologue Hch1 are not essential in yeast (157). Nevertheless, the activation of specific clients such as v-Src and hormone receptors is severely affected in the double knockout cells (155). Interestingly, Aha1 seems to play an important role in the quality control pathway of the CFTR. Down-regulation of Aha1 could rescue the phenotype caused by misfolded CFTR (158).

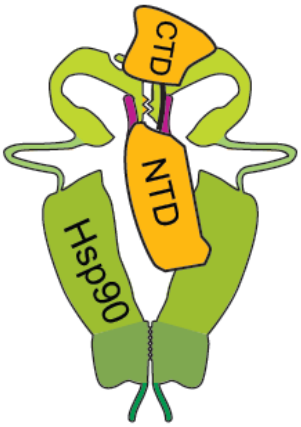

Figure 9. Interactions between Hsp90 and Aha1

Binding sites for Aha1 are located in the N- and the M-domain of Hsp90. Association with Aha1 induces a partially closed conformation of Hsp90.

Studies of steroid hormone receptor (SHR) complexes led to the identification of another subset of Hsp90 co-chaperones, the TPR-containing PPIases, such as Fkbp52, Fkbp51 and Cyp40 in mammals (123,125,159-161) and Cpr6, Cpr7 in yeast (162). These proteins contain a PPIase domain(s), which catalyzes the interconversion of the cis-trans isomerization of peptide bonds prior to proline residues (163), and a TPR domain(s) for the interaction with the C-terminal end of Hsp90 (Fig. 10). Most of these large PPIases show independent chaperone activity (123,164,165). However, the function of PPIases in SHR complexes is not well understood. They may be selected by specific client proteins. For example, Cyp40 is most abundant in estrogen receptor (ER) complexes (166) and Fkbp52 mediates potentiation of GR but not ER (127). Notably, TPR-containing PPIases are not only restricted to chaperoning SHRs but also influence the function of other proteins. For example, AIP was shown to be a negative regulator of PPAR α (Peroxisome proliferator-activated receptor family member, regulation of enzymes involved in fatty acid metabolism) (167). It also activates the AhR (Aryl-hydrocarbon Receptor, a transcription factor that belongs to the bHLH/PAS (basic helix-loop-helix/Per-Arnt-Sim) family) signaling pathway by preventing nucleo-cytoplasmic shuttling of the unliganded receptor (168-171). Fkbp38 affects neuronal apoptosis by inhibiting the anti-apoptotic function of Bcl-2 (172), and its isoform Fkbp8 plays a positive role in the RNA replication of Hepatitis C virus (173).

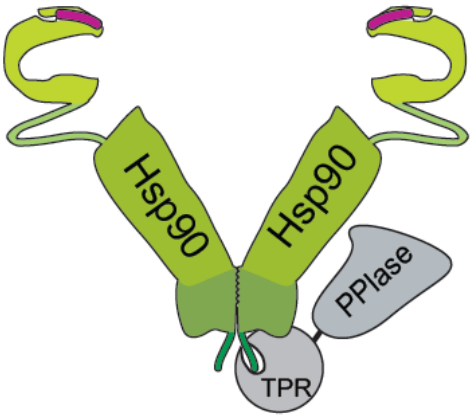

Figure 10. Interactions between Hsp90 and PPIase

Large PPIases bind to the C-terminal MEEVD motif of Hsp90 through their TPR domains

Pp5/Ppt1 is special among the co-chaperones as it is a protein phosphatase which associates with Hsp90 through its N-terminal TPR domain (Fig. 11). Binding to Hsp90 results in the abrogation of the intrinsic inhibition of Pp5/Ppt1 (174). In yeast, Ppt1 specifically dephosphorylates Hsp90 and Cdc37 (175,176). This influences the maturation of client proteins. In Ppt1 knockout strains, the activity of Hsp90-specific clients is significantly reduced, which implies that the tight regulation of the Hsp90 phosphorylation state is necessary for the efficient processing of client proteins (175).

Figure 11. Interactions between Hsp90 and PPIase

Pp5/Ppt1 is known to interact with the C-terminal MEEVD motif of Hsp90 through its TPR domain

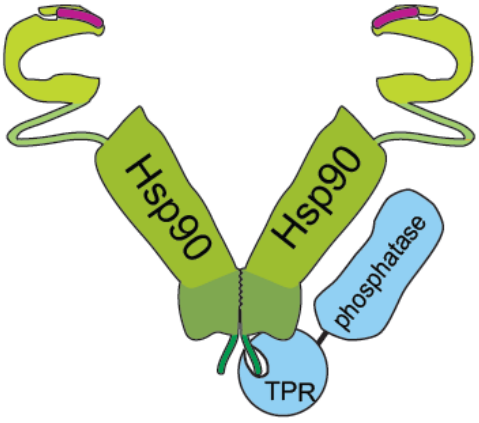

Sgt1 is a co-chaperone required for innate immunity in plants and animals (177). It interacts with the N-domain of Hsp90 through its CS domain, which is structurally similar to p23/Sba1 (Figure 7) (178,179). However, the binding surfaces are different and Sgt1 has no inherent Hsp90 ATPase regulatory activity (179). Interestingly,

although Sgt1 also contains a TPR domain, it is not involved in the interaction with Hsp90 (180). Functionally, Hsp90 and Sgt1 form a ternary complex with the co-chaperone Rar1 (Fig. 12), which acts as a core modulator in plant immunity (181). Recent co-crystallization studies provide a structural basis for the assembly of the Hsp90-Sgt1-Rar1 protein complex. Rar1 interacts with Hsp90 through the C-terminal lobe of its CHORD domain (cysteine and histidine-rich domain), opposite to the Sgt1-interacting region (182). This complex may be involved in the recruitment and activation of NLRs (nucleotide-binding leucine-rich repeat receptors) (181).

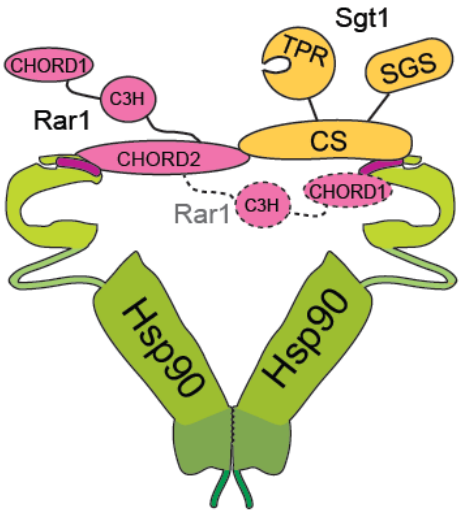

Figure 12. Interactions between Hsp90 and Sgt1/Rar1

Sgt1, Rar1 and Hsp90 form a ternary complex. Sgt1 binds to the N-domain of Hsp90 via its CS domain. The binding surface is different from that of p23/Sba1. The CHORD2 domain mediates the interaction with the N-domain of Hsp90 (The exact position of CHORD1 domain in the ternary complex is unknown, as indicated by the two positions in the cartoon).

Another ternary assembly, the Hsp90-Tah1-Pih1 complex, was recently discovered in chromatin remodeling and small nuclear RNP maturation. Tah1 interacts with Hsp90 through its TPR domain (Fig. 13) and its C-terminal region binds Pih1, an unstable non-TPR co-chaperone of Hsp90. The Hsp90-Tah1 complex stabilizes Pih1 *in vivo* and prevents its aggregation *in vitro* (183). Recent biochemical work points out that the Tah1-Pih1 heterodimer binds to Hsp90 with similar affinity as Tah1 alone and inhibits the ATPase activity of Hsp90 suggesting that the Pih1-Tah1 complex may act as a ‘client adaptor’ recruiting specific clients to the Hsp90 machinery (184).

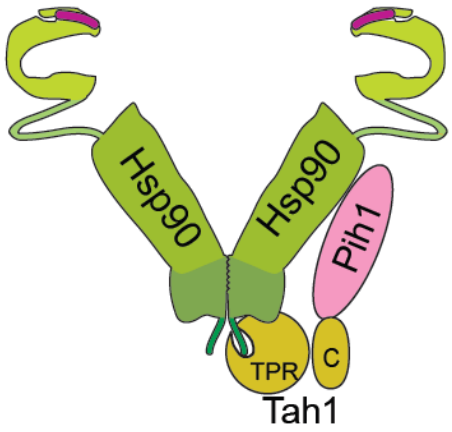

Figure 13. Interactions between Hsp90 and Tah1/Pih1

Tah1 binds to the C-terminal MEEVD motif of Hsp90 through its TPR domain. Pih1 interacts with the M-domain of Hsp90 and the C-domain of Tah1.

The above examples provide a glimpse on the gearings of the Hsp90 co-chaperone system. For some co-chaperones we have obtained a quite detailed picture on their structures and functions, for others we are beginning to understand their contributions to the Hsp90 system. Co-chaperones are also involved in other physiological processes not discussed here (Table 1), such as mitochondrial/chloroplast protein import (Tom70/Toc64) (185,186), nuclear migration (NudC) (187) and melanoma progression (TTC4) (188), Hsp90/Hsp70-dependent protein degradation (CHIP) (189,190). Thus, the picture will be expanding in the coming years.

Table 1. Summary of Hsp90 co-chaperones.

Co-chaperones				**Function**
TPR co-chaperones				
Mammals		**Yeast**	**Plant**	
protein	**Gene (human)**			
Hop	STIP1	Sti1	Hop	Scaffold for Hsp90/Hsp70 interaction; involved in client protein maturation; inhibition of Hsp90 ATPase
Fkbp52	FKBP4	None	AT5G48570*	Peptidy-prolyl-isomerase; chaperone; involved in client protein maturation
Fkbp51	FKBP5	None	ROF1	Peptidy-prolyl-isomerase; chaperone; involved in client protein maturation
Cyp40	PPID	Cpr6/ Cpr7	SQN	Peptidy-prolyl-isomerase; chaperone; involved in client protein maturation
AIP	AIP	None	None	Complex with AhR (aryl hydrocarbon receptor), PPARα (peroxisome proliferator-activated receptor α), Hbx (Hepatitis B virus X protein)
CHIP	STUB1	None	CHIP	Ubiquitin ligase, tagging protein for degradation
PP5	PPP5C	Ppt1	PP5.2	Phosphatase
Tpr2	DNAJC7	None	ATP58IPK*	Tpr2 recognizes both Hsp70 and Hsp90 through its TPR domains. It may mediates the retrograde transfer of substrates from Hsp90 onto Hsp70
Sgt1	SUGT1	Sgt1	SGT1B	Forms complex with Hsp90 and CHORD proteins; involved in the function of NLR receptors in plant and animal innate immunity
Unc45	UNC45B	She4	None	Assembly of myosin fibers

Ttc4	TTC4	Cns1	AT1G04130*	Nuclear transport protein; putative tumor suppressor involved in the transformation of melanocytes
Tom70	TOMM70A	Tom70p	None	Mitochondrial protein import
None		None	Toc64	Chloroplast protein import
Tah1	RPAP3/FLJ21908	Tah1	AT1G56440*	Forms complex with Pih1 and Hsp90
Non-TPR co-chaperones				
Aha1	AHSA1	Aha1	AT3G12050*	Stimulates ATPase activity; induces conformation changes in Hsp90
p23	PTGES3	Sba1	AT3G03773*	Involved in client protein maturation; inhibition of Hsp90 ATPase; chaperone
Cdc37	CDC37	Cdc37	None	Kinase-specific co-chaperone; inhibition of Hsp90 ATPase, chaperone
Chp1/ Melusin	CHORDC1	None	Rar1	Forms complex with Hsp90 and Sgt1; involved in the function of NLR receptors in plant and animal innate immunity
NudC	NUDC	NudC	AT4G27890*	CHORD domain-containing chaperone; dynein-associated nuclear migration protein; plays multiple roles in mitosis and cytokinesis

*Several homologues are uncharacterized in plants. The listed gene names are for *Arabidopsis thaliana.*

2.5.3 The chaperone cycle of Hsp90

During the maturation of the client protein such as steroid hormone receptors (SHRs) and kinases, Hsp90 functions in concert with a large well-defined set of co-chaperones (Table 1), which are essential to drive the cycle of Hsp90-client protein interactions (122-126,191). Co-chaperones such as Hop/Sti1 and PPIase have strong influences on the activation of the SHRs, most of which strictly depend on the interaction with the Hsp90 machinery (127,192). Research on the assembly of Hsp90 with SHRs has already shown that several distinct complexes could be formed during the maturation processes (Fig. 14) (140,160,193,194). According to reconstitution experiments, the assembly of SHRs is a chronological progression through three complexes with different co-chaperone compositions (160). Hsp70 and Hsp40 were identified as the partners in the ‘early complex’. After association with Hsp90, the 'intermediate complex' is formed (160). Hop/Sti1 is an important component in this process, it serves as an adaptor protein between Hsp70 and Hsp90 (128,130). In addition to the Hop/Sti1–Hsp90 complex, a third complex which contains a PPIase and the co-chaperone p23 has also been found to be the part of the cycle at a later stage (140-142,160,195,196), termed as ‘late complex’. Notably, similar heterocomplexes can be found from yeast to mammals.

This model provides us a first picture that how Hsp90 cooperates with different co-chaperones to assist the folding of its client proteins. However, the detailed mechanism remains to be further elucidated. For example, Hop has to leave from Hsp90 and be replaced by p23 and a PPIase to form the late complex, but the regulation of the progression of these complexes stays unclear. Moreover, more than 20 co-chaperones have been identified to regulate Hsp90 functions but only a few of them has been described in the current model of the chaperone cycle. What are the roles of other co-chaperones in the chaperone cycle? How do they work with these well studied co-chaperones? To address these questions, further research is required to explore the detail mechanism of the chaperone cycle.

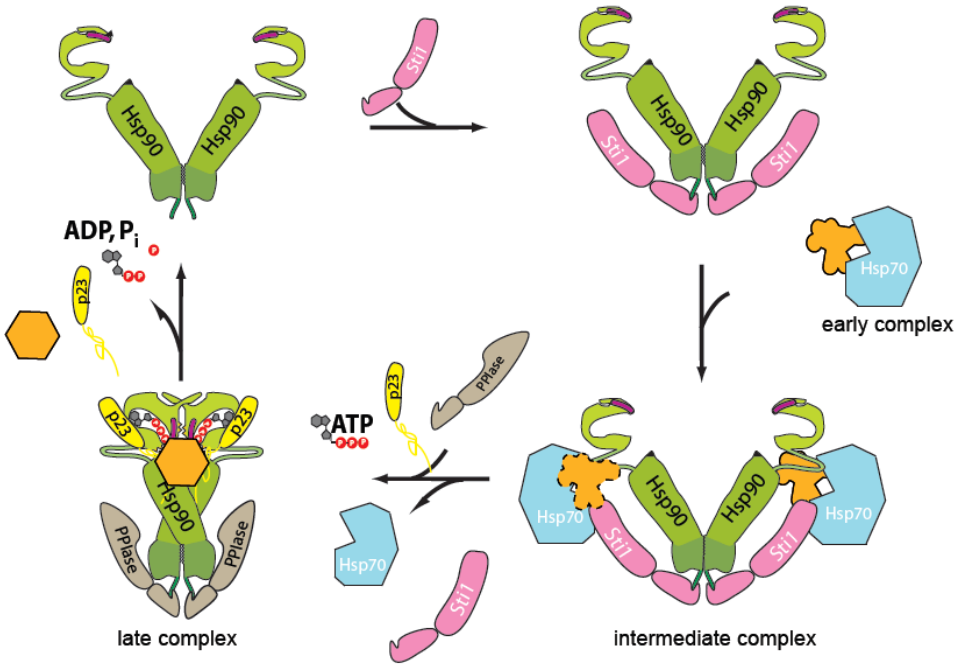

Figure 14. Chaperone cycle of Hsp90

Hsp70 forms an early complex with client protein. Hop/Sti1 binds to the open conformation of Hsp90 and acts as the attachment site for Hsp70 bound to client protein. For simplicity, Hsp70 is depicted to enter the cycle together with client protein after Hop/Sti1 is bound to Hsp90. It is reasonable to assume that this can also occur in complex with Hop/Sti1. Hop/Sti1 facilitates the transfer of the client protein from Hsp70 to Hsp90 and the intermediate complex was formed. Hsp90 converts to the closed conformation after binding of ATP and binding of p23. PPIase binds to Hsp90 and forms the late complex with p23. After hydrolysis of ATP, p23 and the folded client are released from Hsp90.

2.5.4 Regulation of Hsp90 cycle by posttranslational modifications

Extensive research on Hsp90 has revealed post-translational modifications as another level of regulation. Different post-translational modifications such as phosphorylation, acetylation, nitrosylation and methylation tightly control the function of Hsp90 and thus influence the maturation of the client proteins.

Phosphorylation

Phosphorylation is the most frequently detected posttranslational modification of Hsp90. A number of different tyrosine or serine phosphorylation sites have been identified and investigated for their impact on Hsp90's chaperone function (197). Also, client activation is tightly regulated by the phosphorylation states of Hsp90. For example, only phosphorylated Hsp90 stimulates the activity of Hsp90 client protein heme-regulated inhibitor kinase (HRI); dephosphorylation eliminated the ability of Hsp90 to activate this client protein (198). Interestingly, hyperphosphorylation also leads to a decreased Hsp90 activity. Buchner and co-workers showed that protein phosphatase Ppt1 dephosphorylates Hsp90 and Ppt1 deletion in yeast compromise the client activation (175). Therefore the phosphorylation states of Hsp90 must be precisely regulated in order to maintain the proper function of Hsp90.

A number of different kinases can phosphorylate Hsp90, such as Double-stranded DNA protein kinase, c-Src kinase, Protein kinase A (PKA), CK2 protein kinase and Swe1^{Wee1} kinase (199-202). Interestingly, many of them are at the same time Hsp90 client proteins. This indicates that the change of phosphorylation states of Hsp90 may influence the folding and activation of certain groups of client proteins.

Acetylation

Acetylation is a revisable modification mediated by opposing actions by acetyltransferase and deacetylase (203). Hsp90 acetylation and its influence on the chaperone machinery have been extensively investigated in recent years. In the case of Hsp90, p300 was reported to be the acetyltransferase and HDAC6 acts as a deacetylase which removes the acetyl group from the protein (204,205). The work by Yao and co-workers showed the direct interaction between HDAC6 and Hsp90,

which is important for regulating Hsp90 activity. Deacetylation of Hsp90 drives the formation of Hsp90 chaperone complexes and the maturation of the client protein GR. Hsp90 can be acetylated at different sites (206). A study from Necker's lab pointed out that K294, an acetylation site in the M-domain, strongly influences the binding between Hsp90 and its client protein. In general, acetylation weakens Hsp90-client interaction and thus Hsp90 fails to support the activation of the client protein (207).

Nitrosylation

S-nitrosyltaion is a reversible covalent modification of reactive cysteine thiols in proteins by nitric oxide (NO) (208,209). Hsp90 is also a target of S-nitrosylation medited by NO produced by its client protein, endothelial nitric oxide synthase (eNOS) (210,211). S-nitrosylation was reported as a negative regulator which inhibits the ATPase activity of Hsp90 (210). In addition, the activation of its client protein, eNOS, was also reduced. The authors propose a model in which Hsp90 acts as an NO sensor. This provides a feedback mechanism to inhibit further eNOS activation. To further investigate how S-nitrosylation regulate the function of Hsp90, Retzlaff and colleagues examined a number of different mutants and found that the nitrosylation on a C-terminal Cysteine residue led to a ATP-incompetent state in which the N-terminal domains are kept in the open conformation (211). The result indicates nitrosylatrion has a profound impact on the inter-domain communication in the Hsp90 dimer.

2.5.5 Hsp90 client protein recognition

In the past decades, more than 200 client proteins have been identified which show Hsp90 dependence (see http://www.picard.ch/downloads/Hsp90interactors.pdf). Early work on Hsp90 clients mainly focused on two classes: protein kinases and nuclear receptors (194,212). Besides those well-studied clients, many others related to e.g. viral infection, innate immunity and RNA modification have been discovered in recent years (183,213,214). To date, Hsp90 clients involve almost all physiological events such as signal transduction, cell cycle progression and transcriptional

regulation. The interaction with the Hsp90 machinery enables their correct folding, activation, transport and even degradation (185,215-217).

Hsf1 is the central player controlling the heat stress response. Under heat shock conditions it upregulates several hundred genes including Hsp90. Interestingly, the activation of Hsf1 is dependent on Hsp90 (218,219). Under normal condition, Hsf1 is kept in an inactive monomeric form through the transient interaction with Hsp90. During stress, Hsf1 is released from Hsp90 due to the competitive binding of unfolded protein. Upon dissociation from Hsp90, Hsf1 homotrimerizes, undergoes phosphorylation and translocates to the nucleus. Thus, Hsp90 functions as an Hsf1 regulator monitoring the cellular stress response (220).

Recent studies in plants and mammals revealed that Hsp90 is vital to stabilize NLR (nucleotide-binding domain and leucine-rich repeat containing) proteins, which are conserved immune sensors to recognize pathogens (214,221). Accumulating evidence indicates that Hsp90 and its co-chaperones Sgt1, Rar1 are involved in the maturation of these proteins (181,222).

Hsp90 is also known to chaperone nuclear proteins. The telomere protein system is a well-studied example. Freeman and co-workers found that Hsp90 facilitates telomere DNA maintenance by mediating the switch between its capping and extending structure (223). Latest studies show that the assembly of small nucleolar ribonucleoproteins and RNA polymerase as well requires Hsp90. The R2TP complex (consisting of Tah1, Pih1 and the AAA+ ATPase Rvb1 and Rvb2) is the client-specific co-chaperone system involved in RNA processing (183,224).

Interestingly, also viral proteins are Hsp90-dependent. Viral proteins, such as Picornavirus capsid proteins, hepatitis B virus (HBV) core proteins and hepatitis C virus (HCV) nonstructural protein NS3 have been identified as clients of Hsp90 as their folding and assembly requires the Hsp90 machinery (225-227). As well, Hsp90 was shown to facilitate the translocation of some toxins, such as diphtheria toxin and binary actin-ADP-ribosylating toxin (228,229). In consequence, inhibition of Hsp90 prevents cellular uptake and thus protects cells from intoxication.

A long standing open question is the molecular basis of client recognition by Hsp90. To date, no common sequence or motif has been identified among the numerous client proteins. The αC-β4 loop in the kinase domain was found to be an important region for the association with Hsp90 (230,231). However, it is not the only determinant for the interaction, since other regions near the kinase domain also have an influence on the binding to Hsp90 (232,233). Probably the association with Hsp90 is determined by the conformation or stability of the client protein instead of the primary structure. Prominent examples here are the Src kinases. Hsp90 is able to stably associate with viral Src kinase (v-Src), but it only transiently interacts with its normal cellular counterpart (c-Src) (234), although they are almost identical (95% sequence identity). Despite this high level of sequence identity, c-Src is more resistant to chemical and heat denaturation and v-Src is prone to aggregation (234). Moreover, also co-chaperones can contribute to the process of client selection and recognition. For example, Cdc37 seems to be a co-chaperone specific for kinases, while Sgt1 plays an important role in the processing of NLR proteins as discussed above.

Another challenging task is the structural analysis of the interaction of Hsp90 with client proteins, as most of them are highly unstable and aggregation-prone. The EM reconstruction of the Hsp90-Cdc37-Cdk4 complex provided a first view of a client-loaded Hsp90 complex. The model suggests that clients bind in an asymmetric manner to one N- and M-domain of Hsp90 (154). Recent structural studies using a model client protein showed that the Hsp90 M-domain preferentially binds a locally structured region in the intrinsically unfolded model protein (119). Binding induces a partially closed conformation of Hsp90 and enhances the ATPase activity (119,120).

The conformations of Hsp90-bound clients are yet to be answered, as the present results on this issue are controversial. Studies using the model client citrate synthase indicated that Hsp90 interacts with structured intermediates (235). This is consistent with the notion derived from the experiments with SHRs (193) and also the structure of a kinase in the cryo EM kinase complex (154). However, in the case of p53, the results from different groups are controversial. Biochemical experiments

suggest that p53 interacts with Hsp90 in a rather folded state (236,237). However, recent results imply that p53 may be destabilized by Hsp90 (238), and NMR-based approaches suggested that for heat-treated p53, Hsp90 bind the largely unfolded protein (239). Park et al. proposed that Hsp90 domains induce a molten globule state in p53 (240). In contrast, Hagn et al. reported a native like structure of bound p53 (241). Further analysis will be required to resolve this conundrum and to determine the folding states of different Hsp90-bound client proteins

2.5.6 Hsp90 and protein degradation

Although in general Hsp90 stabilizes and promotes the correct folding of its client proteins, Hsp90 is also found to facilitate protein degradation. Several reports have shown that Hsp90 is required for the degradation of ER membrane proteins such as cytochrome p450 2E1, mutant CFTRΔF508 and Apolipoprotein B (242-244). Another aspect which supports the idea that Hsp90 may be involved in the ubiquitin-proteasome pathway is the discovery of a protein called C-terminal of Hsp70-interacting protein (CHIP) (189). As an E3 ubiquitin ligase, CHIP can ubiquitinate unfolded proteins. It also interacts with the C-terminus of Hsp70 and Hsp90 through its TPR domain (190,245). The CHIP knockdown is known to stabilize some Hsp90 clients while the overexpression promotes their degradation (246-248). Interestingly, more E3 ligases have been found to be associated with Hsp90 such as Ubr1 and Cul5 involved in the quality control or degradation of different client proteins (249,250). However, the detailed mechanism such as the selection of different ligases remains to be further elucidated.

2.5.7 Hsp90, inhibitors and human diseases

As many proteins which control cell survival, proliferation and apoptosis are client proteins of Hsp90, Hsp90 function is closely related to human health. A number of reports have suggested that Hsp90 plays a crucial role in the progression of malignant diseases (251-254). For example, the expression of Hsp90 is two to tenfold higher in tumor cells than in the normal cells. Therefore targeting Hsp90 is considered to be a promising strategy for curing cancer. So far, many small

molecules have been identified as Hsp90 inhibitors, some of which exhibit excellent antitumor activities and have entered clinical trials.

Geldanamycin (GA), a benzoquinone ansamycin antibiotic (Fig. 15a), which is the first discovered Hsp90 inhibitor, as it competitively binds to the ATP binding sites in the N-terminal domain of Hsp90 and thus prevents ATP binding and the conformational change of Hsp90 (255,256). GA exhibits potent antitumor effects, however, due to the poor solubility and high toxicity GA cannot be used as a drug candidate (257). A number of different derivatives have been synthesized including 17-AAG, which is more hydrophilic and already show some success in the preclinical studies (258,259).

Radicicol is another commonly used Hsp90 inhibitor, which is a 14-membered macrolide originally isolated from *Monosporium bonorden* (Fig. 15b) (260). Similar to GA, Radicicol also acts as a nucleotide-mimicking compound and occupies the ATP binding pocket of Hsp90 but with a much higher affinity than ATP (260). Also, *in vitro* studies have shown that radicicol shows potent anti-proliferation effects. However, *in vivo* studies demonstrate that radicicol does not show anti-tumor activities which probably due to low stability and biological activity. For example, the inhibitory effects of radicicol against tyrosine kinases are eliminated by reducing agents such as DTT (261).

Besides these two, many new inhibitors are found and synthesized. For example, radanamycin amide (radamide) was designed based on the co-crystallization structures of the GA/Hsp90 N-domain and the Radiciol/Hsp90 N-domain (256,262). This chimeric compound contains both radicicol's resorcinol ring and the quinine ring from GA. It shows potent inhibition effects of Hsp90 in a low micromolar range in breast cancer cells (262). Novobiocin, a coumarin antibiotic was identified as an Hsp90 inhibitor (263). Interestingly, novobiocin targets the C-terminal domain of Hsp90 (264). More derivates with better inhibitory activity and less toxicity are currently designed and synthesized (265).

a **b**

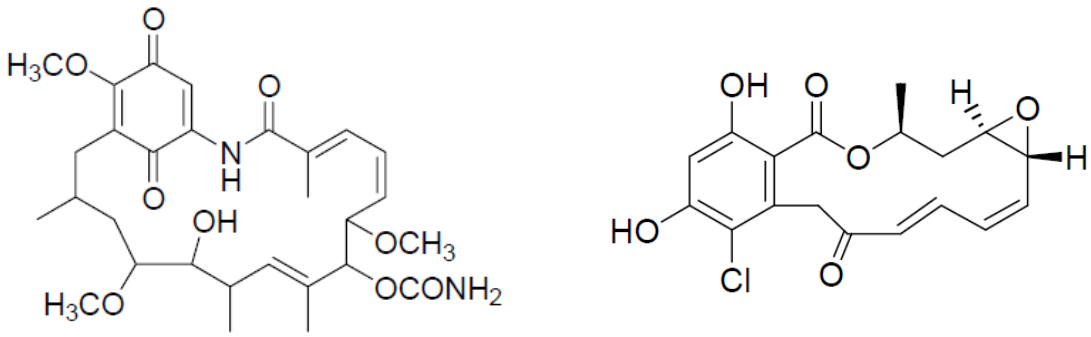

Figure 15. Structures of Hsp90 inhibitors: Geldanamycin (a) and Radicicol (b)

Currently, there are more than ten different Hsp90 inhibitors in various stages of clinical development, like 17-AAG, IPI504, NVP-AUY922, STA-9090 (266). Hsp90 is a promising target for the treatment of cancer, yet there are still several important questions still to be addressed. For example, what are the best clinical indications of Hsp90 inhibition? Whether the patients will benefit from the constant inhibition of the Hsp90 function as it is also essential for the normal cells is not clear. At present, the task is to increase drug specificity, lower the toxicity, search for better biomarkers and gain a deeper understanding on the Hsp90 machine machinery.

3. Objective

The objective of this thesis is to analyze the co-chaperone interactions with Hsp90 and further elucidates the mechanism on the progression of the Hsp90 chaperone cycle.

Hsp90 is known to interact with various different co-chaperones, which regulate the function of Hsp90 such as inhibition or activation of ATPase activity or recruitment of specific clients. In the early 1990s, a chaperone cycle of Hsp90 was proposed to explain how Hsp90 facilitates the maturation of its clients based on *in vitro* reconstitution experiments (160). The assembly of client proteins involves the progression of three different complexes containing different co-chaperones, named “early complex”, “intermediate complex” and “late complex”. The co-chaperone Hop is one component in the intermediate complex and it is important for the client transfer from Hsp70 to Hsp90 as it interacts with the two chaperone machineries simultaneously. Hop was reported to be a dimeric protein and to interact with the C-terminal MEEVD motif of Hsp90. Based on the model, dimeric Hop interacts with dimeric Hsp90 and facilitates the clients loading from Hsp70, after which it leaves the cycle. However, this “symmetric” model implies that two client proteins are transferred to the Hsp90 chaperone machinery at the same time since each Hop monomer contains one Hsp70 interacting domain. Moreover, how Hop exits from the Hsp90 chaperone cycle remained unclear. Another co-chaperone, Aha1, was identified as the most prominent ATPase activator of Hsp90. Similar to Hop and other co-chaperones, it also influences the maturation of Hsp90 client protein such as glucocorticoid receptor (GR). However, Aha1’s role has not been addressed in the model of chaperone cycle. How Aha1 interacts or cooperates with other co-chaperones during the progression of the chaperone cycle is also not clear.

Besides the well-established and investigated co-chaperones, there are some for which there is only little evidence. Sequence analysis suggests aryl-hydrocarbon receptor protein like-1 (AIPL1) is closely related to the Hsp90 co-chaperone AIP. Both could belong to the family of large PPIase. AIPL1 shows similar domain organization to AIP but with a unique C-terminal proline-rich region. The enzymatic

properties, chaperone activity and the interaction with Hsp90 of this potential new co-chaperone remain uncharacterized. Also, the role of the unique proline-rich domain in AIPL1 is to be investigated.

To address these issues and provide new insights on the mechanism of the Hsp90 chaperone machinery, a combination of biophysical, biochemical and in *vivo* methods was used. In this thesis, different FRET-based interaction assays were established to examine the binding and release of different co-chaperones. Also, analytical ultracentrifugation with fluorescence detection and pull-down assays were employed to dissect the Hsp90/co-chaperone complexes.

4. Results and discussion

4.1 Asymmetic Hsp90/co-chaperone complexes are important for the progression of the reaction cycle

4.1.1 Co-chaperone interaction in the yeast Hsp90 cycle

4.1.1.1 TPR co-chaperone interactions with Hsp90

Sti1 is the yeast homologue of Hop and serves as the adaptor protein between Hsp70 and Hsp90. It is known that Sti1 inhibits the ATPase activity of Hsp90, but the detailed mechanistic aspects remain to be elucidated. Cpr6 is the yeast homologue of Cyp40 and belongs to the PPIase family. It is known that both Sti1 and Cpr6 interact with Hsp90 through their TPR domains (111). We analyzed their interaction with Hsp90 by SPR spectrometry. Hsp90 was immobilized on the surface of a CM5 sensor chip as described in the methods section, and binding of Sti1 or Cpr6 was detected based on the change in resonance units (RU). The binding constant between these TPR co-chaperones and Hsp90 can be determined by the titrations of different concentrations of Sti1 or Cpr6. First we compared the binding and release kinetics of these TPR co-chaperones by a single injection of the same concentration of Sti1 or Cpr6. The sensogram revealed that Cpr6 binds to Hsp90 faster than Sti1 (Fig.16a). Also faster release kinetics was observed for Cpr6. Binding constants calculated from the titrations are 55 nM for Cpr6 and 53 nM for Sti1 (Fig.16b). The results indicate that Sti1 and Cpr6 have similar affinity for Hsp90. However, different interaction kinetics was observed for Sti1 and Cpr6, which implies that the interaction sites in Hsp90 for these two co-chaperones may be not exactly the same.

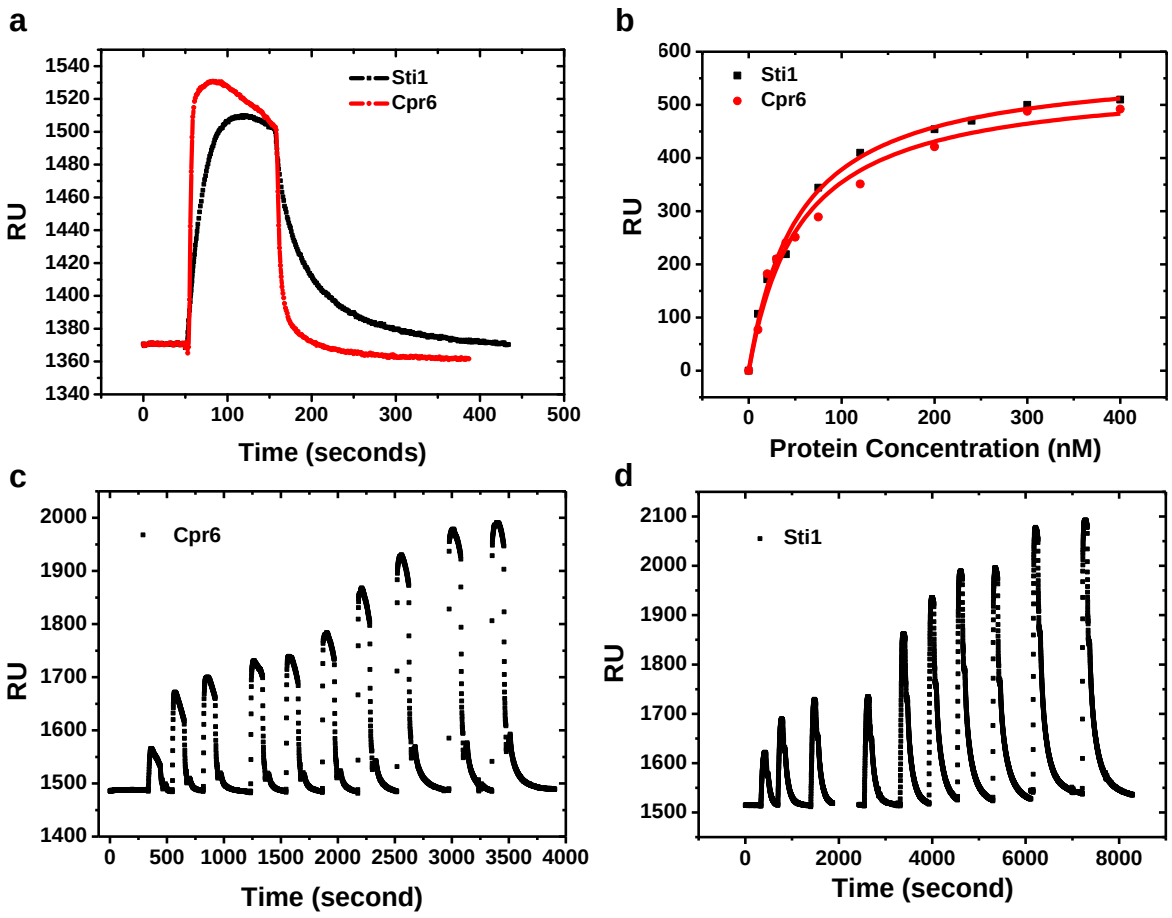

Figure 16. Binding of Sti1 and Cpr6 to Hsp90

Binding of Sti1 and Cpr6 was measured by SPR using a BiaCore X instrument. Injections of different concentrations of Sti1 and Cpr6 were made onto an yHsp90-coated CM5 chip. Binding kinetics of Sti1 (black) and Cpr6 (red) were measured by a single injection of 50 nM Sti1 or Cpr6 (a). The K_D for Sti1 (black squares) was calculated to be 53 nM, and the K_D for Cpr6 (red circles) was calculated to be 55 nM based on the plateau values of the individual injections (b). Sensograms of the injections are shown for Cpr6 (c) and Sti1 (d). Injections were performed at concentrations from 10 nM to 400 nM for both proteins.

4.1.1.2 Characterization of Sti1 inhibition on Hsp90 ATPase activity

Sti1 is a high-affinity TPR domain–containing inhibitor of the yeast Hsp90 ATPase activity (111,129). It inhibits the ATPase by preventing conformational changes required for Hsp90 to adopt the ATPase-active conformation (129). To determine whether one or two Sti1 molecules per Hsp90 dimer are required for inhibition, we added increasing amounts of Sti1 to Hsp90 and determined the remaining ATPase

activity. We were surprised to find that the addition of one molecule of Sti1 per Hsp90 dimer completely inhibited the Hsp90 ATPase activity (Fig.17), though we and others had previously determined that two molecules of Sti1 can bind simultaneously to an Hsp90 dimer (111,129).

As a control, we used the Sti1 mutant R341E in the ATPase assay. Based on previous results, this mutant affects the binding to Hsp90 as detected in an immunoprecipitation assay (267). The result indicated that the affinity of Sti1-R341E to Hsp90 is greatly reduced.

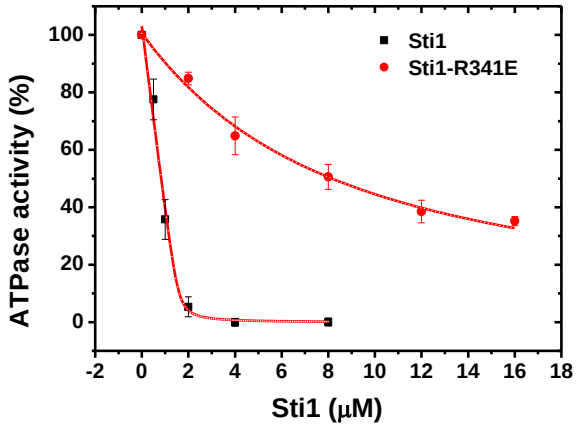

Figure 17. Inhibition of the ATPase activity of yeast Hsp90 by wtSti1 or mutant Sti1-R341E
Inhibition of the ATPase activity of yeast Hsp90 by Sti1 (black) or Sti1-R341E (red). Different concentrations of Sti1 or Sti1-R341E were added to 4 µM Hsp90 and the resulting ATPase activities were measured at 30 °C. Data were analyzed as described in the Methods section. The binding affinity of Sti1-R341E to Hsp90 is decreased by a factor of >20.

4.1.1.3 Interaction between Sti1, Hsp90 and Cpr6

In the ATPase assay, we found one Sti1 molecule is able to completely inhibit the ATPase activity of Hsp90. We wondered whether the second TPR-acceptor site of the Sti1-inhibited Hsp90 dimer can bind another TPR domain–containing protein. To test this, we added the yeast TPR-containing co-chaperone Cpr6 and performed a titration with Sti1. Notably, we were able to saturate one site of Hsp90 with Cpr6, and no substantial difference in Sti1 inhibition was observed (Fig. 18). At a high concentration of Cpr6, however, a reduction of Sti1 inhibition became evident (Fig. 18). This was unexpected, as the binding constants of the two TPR proteins are identical (see Fig. 16), in agreement with earlier studies (129). From the substoichiometric inhibition of Hsp90 by Sti1 and from the finding that Cpr6 could bind to the second Hsp90 subunit without disturbing Sti1 inhibition, we conclude that

the second TPR-acceptor site in the Sti1-inhibited state can be used by a different TPR domain–containing co-chaperone.

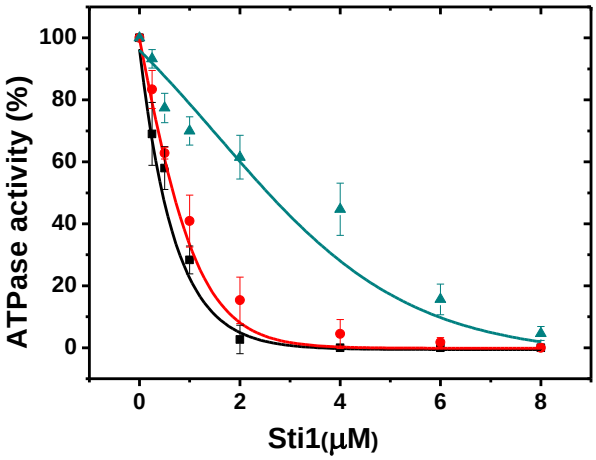

Figure 18. Inhibition of the ATPase activity of yeast Hsp90 by Sti1
Different concentrations of Sti1 were added to 4 μM Hsp90 and the resulting ATPase activities were measured at 30 °C (black). Identical experiments were performed in the presence of Cpr6 (red 2 μM Cpr6; turquoise 12 μM Cpr6).

4.1.1.4 Setting up a FRET system to study Hsp90–co-chaperone interaction

The co-chaperone Sti1 contains three cysteines, C49, C66 and C453. C453 is located in the TPR2B domain which potentially interacts with Hsp90 (Fig. 19). To set up a FRET system, we labeled the cysteines in Sti1 with donor dye Alexa Fluor 488 maleimide. Hsp90 was labeled at an engineered cysteine residue (S385C) in the M-domain (117) with the acceptor dye ATTO550 (*Hsp90 and *Sti1 denote the labeled molecules hereafter).

To study the interaction between Hsp90 and Sti1, we measured the emission spectra from 500 nm to 650 nm with exaction at 494 nm. Upon addition of *Hsp90 to *Sti1, we observed a concentration-dependent decrease of the donor emission and a concomitant increase in the acceptor emission (Fig. 20). To determine the specificity of the interaction, we added unlabeled Sti1 to preformed *Sti1–*Hsp90 FRET complexes and recorded the changes in the FRET signal. Unlabeled Sti1 disrupted the FRET and displaced the labeled *Sti1 fully from Hsp90 (Fig. 21). We further tested whether labeled *Sti1 could also be displaced by unlabeled Cpr6. We indeed observed displacement, but with a lower efficiency compared to the effect of Sti1 (Fig. 21), implying that full displacement of Sti1 is difficult to achieve with Cpr6.

Thus, the unexpected asymmetric behavior suggested by the results of ATPase-inhibition experiments was also visible in the FRET assay.

Figure 19. Cysteines location in Sti1
C49 and C66 are located in the TPR1 domain, and C453 is located in the TPR2B domain

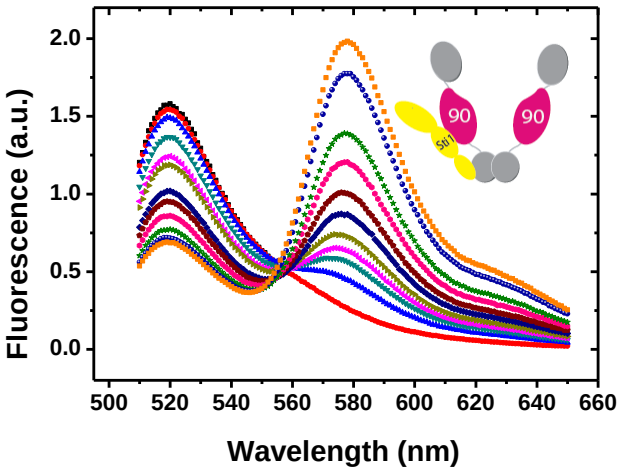

Figure 20. Titration of ATTO550-yHsp90 (*yHsp90, acceptor) to Alexa Fluor488-Sti1 (*Sti1, donor)

Different concentrations of *yHsp90 were added (0 nM, 25 nM, 50 nM, 75 nM, 100 nM, 150 nM, 200 nM, 300 nM, 400 nM, 600nM, 800 nM) to 300 nM *Sti1 and the emission spectra from 510 nm to 650 nm were recorded at 25 °C. The excitation wavelength was set to 494 nm.

Figure 21. Release of Sti1 from the Hsp90 complex.

300 nM *yHsp90 was added to 300 nM *Sti1, and the binding kinetics were monitored at 25 °C in standard assay buffer (black). Excess amount of unlabeled Sti1 (blue) or Cpr6 (red) were added to compete with the donor fluorophore (*Sti1) for the formation of Hsp90-complexes, and the kinetics were recorded at 25 °C. The arrow indicates the point of addition of proteins

.

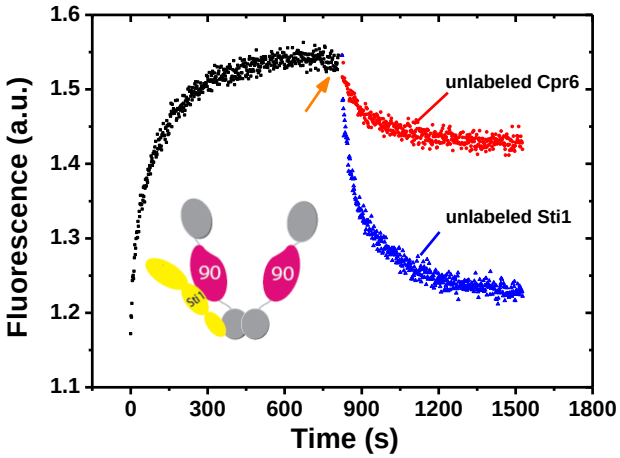

4.1.1.5 Sti1 and Cpr6 form a ternary complex in vivo

To examine the composition of Sti1-containing complexes *in vivo*, cell lysates from a yeast *Sti1*-deletion strain were analyzed using Sti1 immobilized on Ni-NTA beads (Fig. 22). Coprecipitated Hsp90 and Hsc70 (in yeast called Ssa1) were identified by western blotting. Analysis of the stoichiometry showed that we recovered one Hsc70 protein and a Hsp90 dimer per Sti1 monomer. Furthermore, about 7% of the pulled-down Sti1 complexes also contained Cpr6. Given that the concentration of Cpr6 is much lower than that of Hsp90 and Sti1 (1.86E+04 Cpr6 Molecules/Cell, 6.76E+04 Sti1 Molecules/Cell, 5.77E+05 Hsp90 Molecules/Cell) (268), this represents a notable enrichment. Thus, the coprecipitation results show that Sti1 and Cpr6 also bind to the same Hsp90 dimer in a cytosolic environment. As expected, we were unable to detect p23, an Hsp90 co-chaperone that binds specifically to the closed conformational state of Hsp90, in the Sti1 pull-down assays, as Sti1 keeps Hsp90 in the open state. We also could not detect Aha1, an activator of Hsp90 that binds to the M-domain and N-domain of Hsp90 and favors the closed conformation of Hsp90 (Fig. 22).

To further validate the existence of the Sti1–Hsp90–Cpr6 complex in the cytosolic environment, we performed a pull-down experiment using the cell lysate of a yeast *Cpr6*-deletion strain and His-tagged Cpr6. We detected Hsp90, Sti1 and Hsc70 in the Cpr6 complex, consistent with our analysis of the Sti1 complex. p23, which is part of the final complex together with Cpr6, was not detected, as a p23–Hsp90 interaction occurs only in the presence of 5’-adenylyl-β, γ-imidodiphosphate (AMP-PNP), as shown previously (269). A faint Aha1 band can be seen, which implies the potential existence of a Cpr6–Hsp90–Aha1 complex.

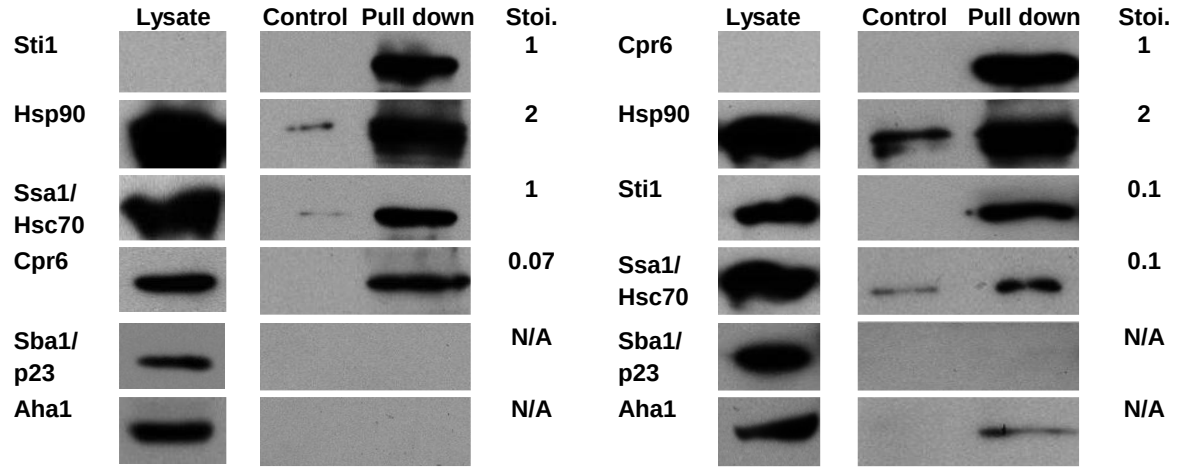

Figure 22. Affinity isolation of Sti1-containing and Cpr6-containing complexes from yeast cell lysates

Ni-NTA beads complexed with His-tagged Sti1 or Cpr6 were pulled down, and western blotting was performed with antibodies against the proteins indicated beside each row. The first column (Lysate) shows the presence of the proteins in the lysate. Control pull-down experiments were performed with beads to which a His-tagged *Escherichia coli protein* (YjiE) was coupled. The third column (Pull-down) shows the presence of the proteins in the Sti1 or Cpr6 complex. The stoichiometries (Stoi.) of the pulled-down proteins were calculated from a dilution standard of purified proteins. The left lanes show pull-downs of His-tagged Sti1. Sti1 was not present in the lysate because a *Sti1*-deletion strain was used. Right lanes show pull-down of His-tagged Cpr6. Cpr6 was not present in the lysate because a *Cpr6*-deletion strain was used.

4.1.1.6 Analysis of asymmetric Hsp90 complex by analytical ultracentrifugation

To further analyze the formation of hetero-oligomeric TPR co-chaperone–Hsp90 complexes, we used aUC coupled to fluorescence detection. Sti1 was labeled by Alexa Fluor 488 maleimide. As shown in the sedimentation profile, the sedimentation was accelerated by the addition of Hsp90 (Fig. 23).

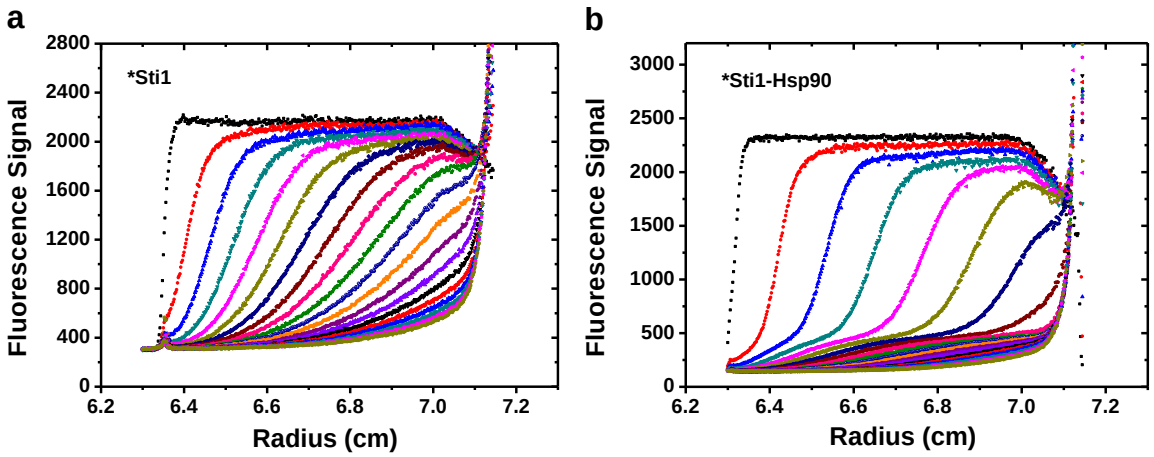

Figure 23. Sedimentation profiles for the Sti-Hsp90 complex formation in the aUC

Binding of Hsp90 to Sti1 was investigated using analytical ultracentrifugation. Shown are sedimentation profiles of *Sti1 (a) and *Sti1-Hsp90 (b). 500 nM of *Sti1 were subjected to analytical ultracentrifugation at 20 °C in 40 mM HEPES, 50 mM KCl, pH 7.5 in the absence or presence of 1 µM yHsp90. Centrifugation was performed at 42,000 r.p.m and fluorescence scans were performed every 90 seconds. Every 14th scan is shown.

After converting the sedimentation profile to a dc/dt plot, we could see that *Sti1 sedimented with an s value of 3.9 S, which indicates that Sti1, like its human homologue Hop (270), is a monomeric protein (Table 2). After addition of Hsp90 to *Sti1, the sedimentation coefficient of *Sti1 increased to 7.5 S owing to complex formation with Hsp90. We then added Cpr6 and obtained an s value of 8.2 S, which could represents the *Sti1–Hsp90–Cpr6 complex (Fig. 24 and Table 2).

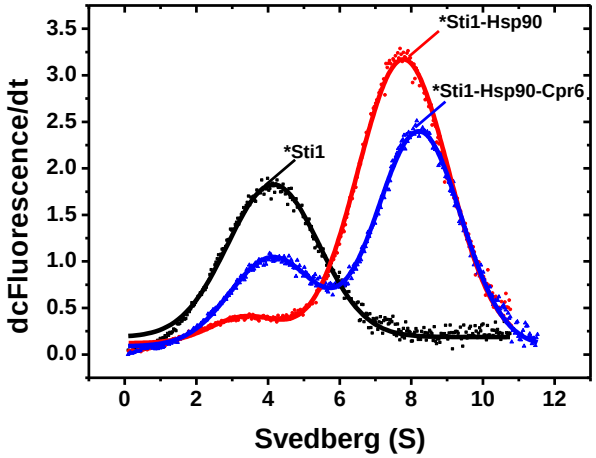

Figure 24. aUC analysis of the Sti1-Hsp90-Cpr6 interaction

Binding of Hsp90 to Sti1, investigated using aUC. dc/dt profiles (dc/dt represents the change in fluorescence signal intensity over time) are shown for 0.5 µM labeled *Sti1 alone (black), for *Sti1 mixed with 1 µM Hsp90 (red), and for *Sti1 mixed with 1 µM Hsp90 and 1 µM Cpr6 (blue).

To test this notion, we labeled Cpr6 (*Cpr6) and monitored the formation of *Cpr6–Hsp90 complexes (Fig. 25) *Cpr6 sedimented with an s value of 3.4 S, and the c(s) analysis using the UltraScan software package indicated that Cpr6 is a monomeric protein. After addition of Hsp90, the sedimentation coefficient of *Cpr6 increased to 7.1 S owing to interaction with Hsp90. Addition of unlabeled Sti1 to these *Cpr6–Hsp90 complexes resulted in a prominent shift to 8.2 S, consistent with the formation of *Cpr6–Hsp90–Sti1 complexes (Fig. 25 and Table 2). Cpr6 was not found to interact directly with Sti1 as analyzed by aUC (Table 2 and Fig. 26) and fluorescence anisotropy (data not shown).

Figure 25. aUC analysis of the Sti1-Hsp90-Cpr6 interaction.

Binding of Hsp90 to Cpr6, investigated using aUC. dc/dt profiles are shown for 0.5 µM labeled *Cpr6 alone (black), for *Cpr6 mixed with 1 µM yHsp90 (red), and for *Cpr6 mixed with 1 µM yHsp90 and 1 µM Sti1 (blue).

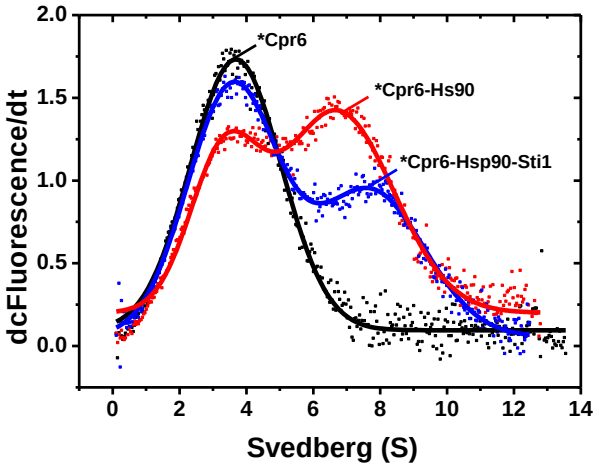

As a further control, we used the Sti1 mutant R341E in the aUC experiment. In contrast to Sti1, Sti1-R341E cannot shift either the *Sti1–Hsp90 complex or the *Cpr6–Hsp90 complex to larger s values (Table 2 and Fig. 26). Thus, the shift in the s value is due to the binding of a second TPR protein to the same Hsp90 dimer. Together, these data suggest that mixed complexes of Hsp90, Sti1 and another TPR protein are readily formed *in vivo* and *in vitro*.

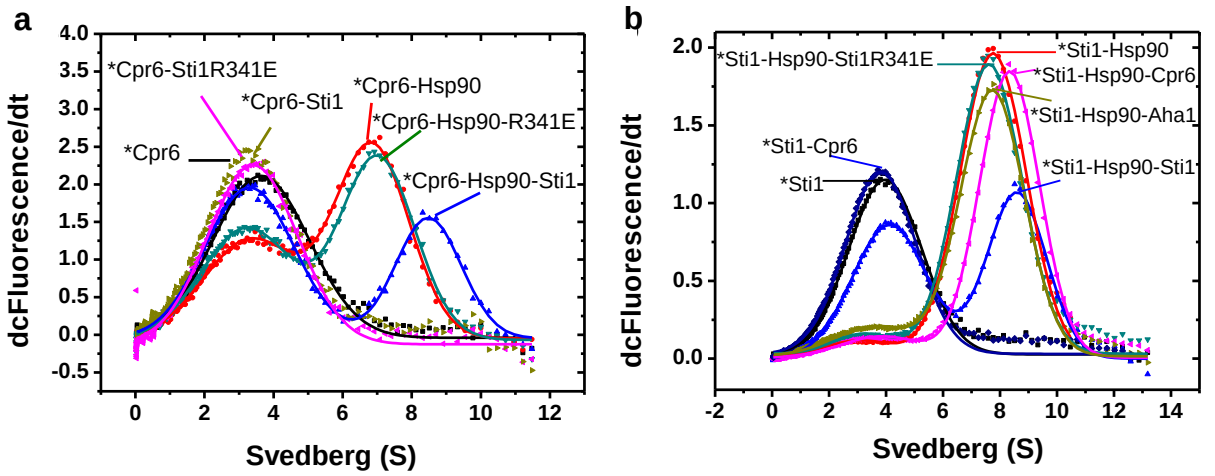

Figure 26. Ultracentrifugation analysis of the Sti1-yHsp90-Cpr6 interaction

a. Formation of Hsp90-Cpr6 complexes was investigated using analytical ultracentrifugation. 500 nM of *Cpr6 were subjected to aUC at 20 °C in 40 mM HEPES, 50 mM KCl, pH 7.5. dc/dt profiles are shown for labeled Cpr6 alone (black) and *Cpr6 mixed with 1 µM yHsp90 (red), and the further addition of 1 µM Sti1 (blue) or mutant Sti1-R341E (green). As a control, *Cpr6 and Sti1 or the mutant Sti1-R341E in the absence of Hsp90 are shown in pink or dark yellow. s values of different experiments are shown in table 2.
b. Formation of Hsp90-Sti1 complexes was investigated using analytical ultracentrifugation. 500 nM of *Sti1 were subjected to aUC at 20 °C in 40 mM HEPES, 50 mM KCl, pH 7.5. dc/dt profiles are shown for labeled Sti1 alone (black) and *Sti1 mixed with 1 µM yHsp90 (red), and the further addition of 1 µM Cpr6 (pink) or Aha1 (dark yellow) or unlabeled Sti1 (blue) or mutant Sti1-R341E (green). As a control, *Sti1 and Cpr6 in the absence of Hsp90 are shown in dark blue. s values of different experiments are shown in table 2.

Table 2. *s* values for Hsp90 complexes

Species	*s* value
*Sti1	3.9
Hsp90	6.1
*Sti1–Hsp90	7.5
*Sti1–Hsp90–Cpr6	8.2
*Sti1–Hsp90–Sti1	8.5
*Sti1–Hsp90–Sti1 R341E	7.5
*Sti1–Hsp90–Aha1	7.5
*Sti1–Cpr6	3.9
*Cpr6	3.4
*Cpr6–Hsp90	7.1
*Cpr6–Hsp90–Sti1	8.2
*Cpr6–Hsp90–Sti1 R341E	7.1

The *s*-values were obtained from the aUC experiments described in Figure 25 and Figure 26

4.1.1.7 Asymmetric complexes are disrupted by AMP-PNP and p23

The results obtained so far identify a new complex as a key intermediate in the Hsp90 chaperone cycle. This raised the question of how the progression from this complex to the late Hsp90–PPIase–p23 complex is regulated. As ATP binding influences the conformational status of Hsp90, we added the non-hydrolysable ATP analog AMP-PNP to *Sti1–Hsp90–PPIase complexes and monitored its effect by aUC. We observed a decrease in *Sti1 binding in these assemblies upon addition of AMP-PNP (Fig. 27), which was not evident upon addition of ADP (data not shown). This implies that the closing of the N-terminal domains induced by AMP-PNP (102,117) leads to a shift in the equilibrium binding constants that disfavors the presence of Sti1 in the asymmetric complexes.

It is known that nucleotides that induce the N-terminally closed state of Hsp90 are required for binding of the co-chaperone p23 (136). We therefore sought to understand how the addition of p23 influences the asymmetric complex, using the aUC assay with *Sti1. We added p23 and observed a further decrease of Sti1 in the complexes when AMP-PNP was present (Fig. 27). In the absence of AMP-PNP, p23 did not bind; no effect on the asymmetric complexes was therefore expected, and none was observed (Fig. 27). These data show that the asymmetric complex of the two TPR proteins can be dissolved by the addition of cofactors characteristic of late stages of the chaperone cycle.

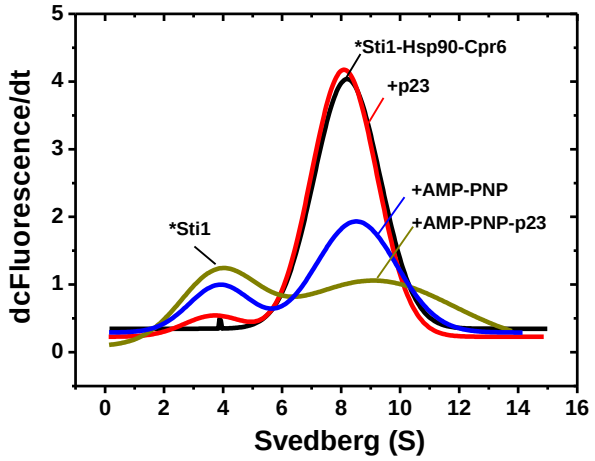

Figure 27. Regulation of the asymmetric complex by nucleotides and p23 analyzed by aUC

aUC d*c*/d*t* profiles are shown for the ***Sti1–Hsp90–Cpr6 asymmetric complex in the absence (black) or presence (blue) of AMP-PNP, and for the asymmetric complex with 2 µM p23 and 2 mM AMP-PNP (dark yellow). No effect of p23 was observed in the absence of AMP-PNP (red).

To analyze the transition kinetically, we performed FRET experiments in which the influence of the non-hydrolysable ATP analog AMP-PNP and p23 on *Sti1–*Hsp90 complexes was monitored. We first added Cpr6 and observed a slight decrease in the amount of the *Sti1–*Hsp90 complex (Fig. 28), whereas addition of p23 or AMP-PNP alone had no substantial effect. An efficient displacement of Sti1 from Hsp90 complexes could be observed if AMP-PNP and p23 were added together (Fig. 28) and an even more efficient one if Cpr6 was added together with p23 and AMP-PNP.

Figure 28. Regulation of the asymmetric complex by nucleotides and p23 analyzed by FRET

We added 300 nM *Hsp90 (acceptor) to 300 nM *Sti1 (donor), and the binding kinetics (black) were monitored at 25 °C in standard reaction buffer. We added Cpr6 alone (red) Cpr6 and AMP-PNP (light blue), Cpr6, AMP-PNP and p23 (turquoise), or AMP-PNP and p23 (dark blue) to the *Sti1–*Hsp90 complex to trace the kinetics of *Sti1 release. As controls, AMP-PNP (pink) and p23 (dark yellow) were added alone. The orange arrow indicates the addition of nucleotide or protein. a.u, arbitrary units.

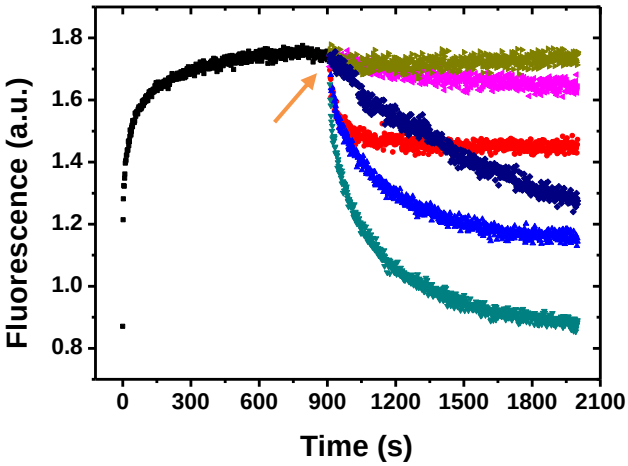

When we added p23 first to *Hsp90–*Sti1 complexes, we saw an effect on the *Sti1–*Hsp90 complex only in the presence of AMP-PNP (Fig. 29). Again, Cpr6 was required to displace *Sti1, suggesting that the order of addition is not important for the effects observed. Thus, the components that are found together in the late complex displace Sti1 synergistically and support the closing of the N-domains. Notably, the kinetics of Sti1 displacement also differed depending on the added proteins. In particular, the slow kinetics observed after addition of AMP-PNP implies that the AMP-PNP–induced closing reaction at the N-domains contributes greatly to the displacement of Sti1 from Hsp90 complexes (Fig. 29).

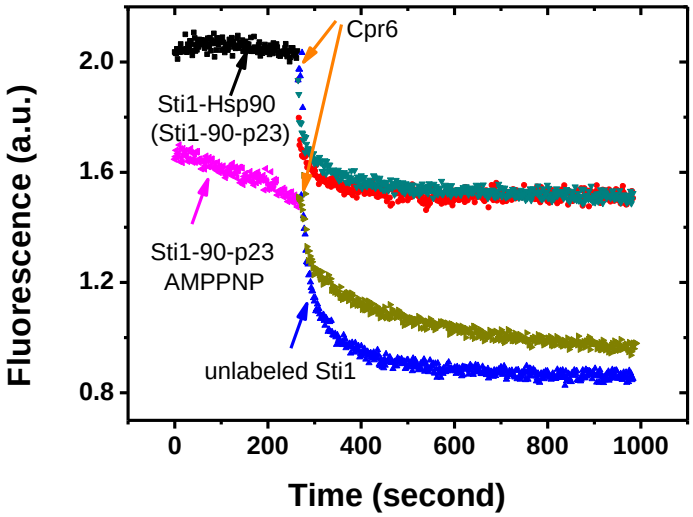

Figure 29. Effect of Cpr6, p23/Sba1 and AMP-PNP on the release of Sti1 from Hsp90

A *Sti1-*Hsp90 FRET-complex was assembled either alone (black) or in the presence of p23 with AMP-PNP being absent (black) or present (pink). Without AMP-PNP, the FRET values of *Sti1-*Hsp90 in the presence or absence of p23/Sba1 are identical. The initial plateau values were lower in the presence of p23/Sba1 and AMP-PNP, indicating a significant influence of p23/AMP-PNP on the complex. 1.5 µM Cpr6 was added to the preformed complexes in the absence (turquoise) or presence of p23/Sba1 (red) at the time point indicated in the figure. Similarly, 1.5µM Cpr6 was added to Sti1-Hsp90 complexes in the presence of p23/AMP-PNP (dark yellow). For comparison, 1.5 µM of Sti1 were added to Sti1-Hsp90 complexes to fully dissociate the FRET-complex (blue).

4.1.2 Asymmetric complexes are conserved in the Hsp90 cycle

4.1.2.1 Co-chaperone interaction in human Hsp90 cycle

Having observed the asymmetric PPIase–Hsp90–Hop complex in the yeast Hsp90 cycle, we wondered whether it is conserved in the mammalian Hsp90 chaperone system. We therefore started to characterize the interaction between TPR co-chaperones with human Hsp90. We set up a SPR measurement to determine the binding constants between TPR co-chaperones and Hsp90. The results show that Hop, the human homologue of Sti1, binds to Hsp90 with an affinity of 0.8 µM while the binding constant of AIP/Xap2, a TPR containing PPIase (168), is 2.28 µM (Fig. 30).

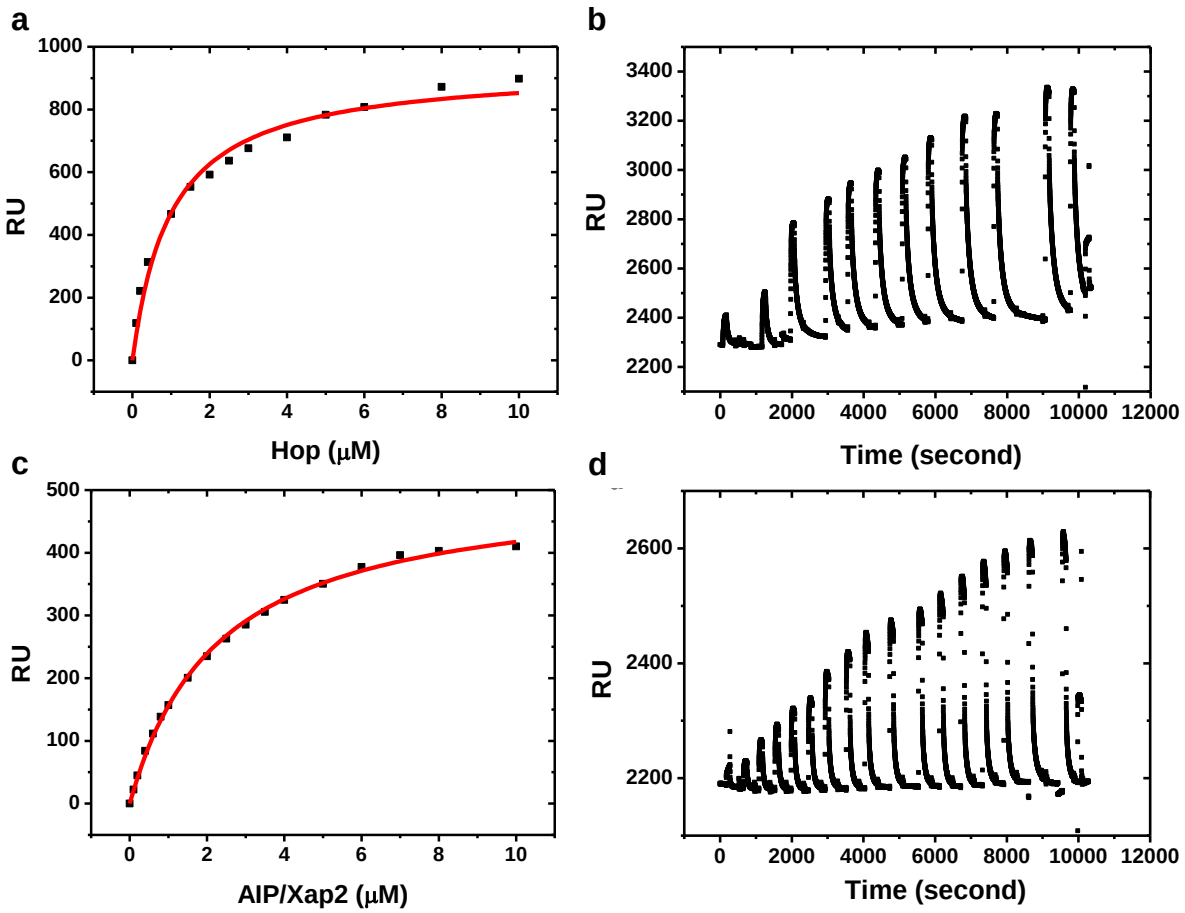

Figure 30. Binding of Hop and AIP/Xap2 to Hsp90

a. Determination of the affinity of Hop to Hsp90 by SPR. The K_D of Hop to hHsp90 was calculated to be 0.8 μM based on injections with different concentration of Hop onto a human Hsp90-coated CM5 chip

b. Determination of the affinity of AIP/Xap2 to Hsp90 by SPR. The K_D of AIP/Xap2 to hHsp90 was calculated to be 2.28 μM based on injections with different concentrations of AIP/Xap2 onto a human Hsp90-coated CM5 chip. Sensograms of the titration are shown for Hop (c) and for AIP/Xap2 (d). The injected protein concentrations were in the range of 100 nM to 10 μM for both proteins.

To verify the results from SPR experiments, we set up isothermal titration calorimetry (ITC) to measure the binding between TPR co-chaperones and human Hsp90. Binding constants calculated from the titration curves were 1.3 μM for Hop and 2.3 μM for AIP/Xap2 (Fig. 31). Although the affinities of both AIP/Xap2 and Hop are in the micro molar range, the binding reactions are characterized by very different contributions of enthalpy and entropy. In the case of AIP/Xap2, the change in enthalpy approximates to the free energy of the reaction (ΔG= -7.6kcal/mol; ΔH=-

6.1kcal/mol), indicating that the entropic contributions to binding are very small. In contrast, the binding of Hop to Hsp90 displays a large favorable enthalpy contribution (ΔH=-18kcal/mol) offset by a large unfavorable change in entropy (TΔS=-11kcal/mol), which indicates conformational changes of one or both components during the binding reaction.

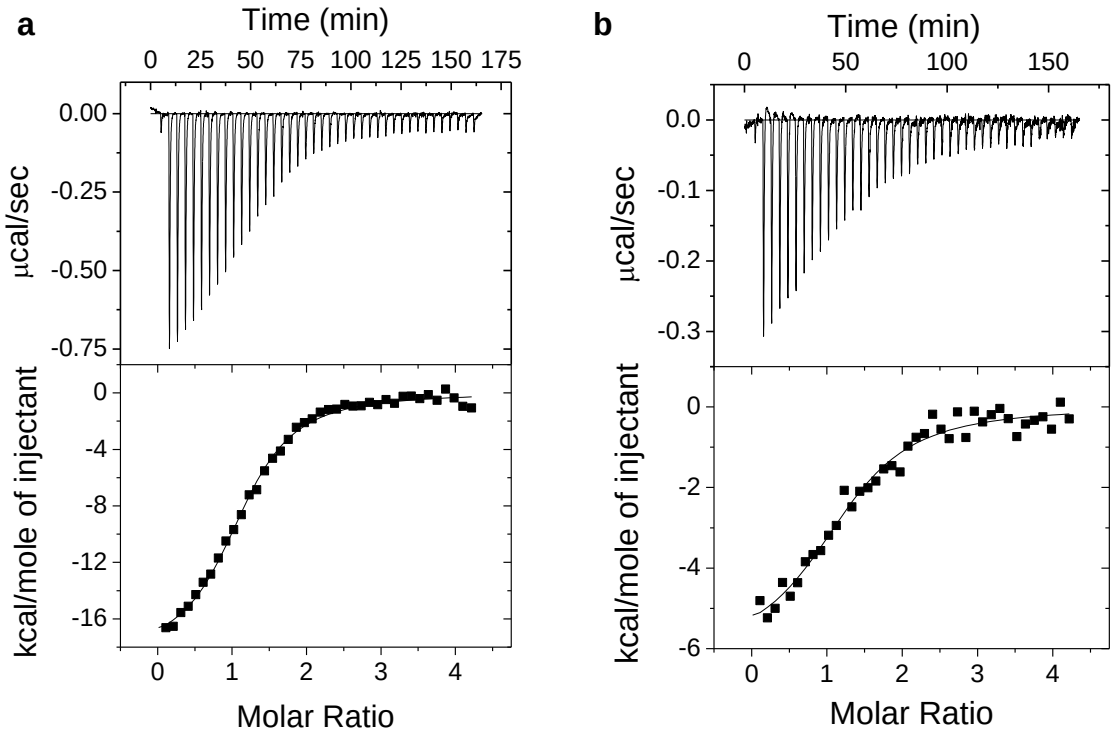

Figure 31. Calorimetric analysis of co-chaperone binding to Hsp90

Isothermal titration calorimetry experiments were performed at 25 °C in standard buffer. The Hsp90 concentration was 15 µM in both experiments. Titrations were performed with 35 injections of 8 µl each and a concentration of 300 µM Hop (a) or AIP/Xap2 (b) in the injection syringe. The data analysis was performed with the Origin package included in the instrument software.

4.1.2.2 Asymmetric co-chaperone complex is covserved in human hsp90 cycle

To further clarify whether the asymmetric complex of Hsp90 cofactor is conserved in the human system, we therefore used aUC to test the ability of the human PPIases AIP/Xap2 and also the well-studied Fkbp51 (271) to form complexes with Hop and human Hsp90. Using labeled PPIases (*PPIase), we observed *PPIase–Hsp90–Hop complexes with s values larger than those of the *PPIase–Hsp90 complexes for both

PPIases (Fig. 32a,b). In particular, for Fkbp51, the addition of Hop increased the amount of PPIase in complexes and decreased the free PPIase (Fig. 32a). Thus, the formation of Hsp90 complexes simultaneously containing Sti1 (or Hop) and a PPIase seems to be conserved between yeast and man, and the preference for mixed complexes seems to be more pronounced in the human system than in yeast.

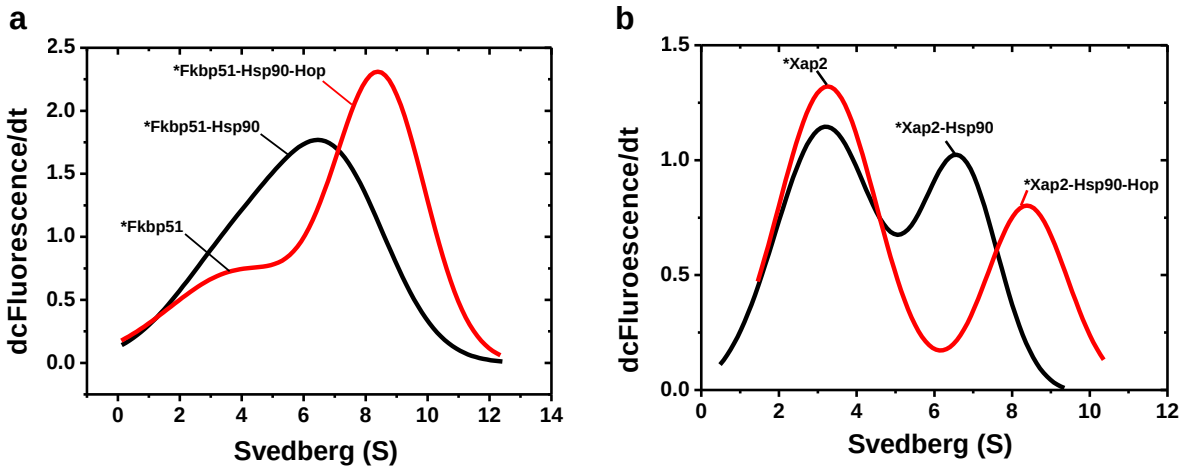

Figure 32. Asymmetric complex formation in the human hsp90 system

a. Generation of the Fkbp51-Hsp90-Hop asymmetric complex. Binding of human Hsp90β to Fkbp51 was investigated using analytical ultracentrifugation. 1 µM of labeled Fkbp51 and 2 µM Hsp90 in standard buffer were subjected to analytical ultracentrifugation at 20 °C. dc/dt profiles are shown for Fkbp51 with Hsp90 (black) and with further addition of Hop (red)

b. Generation of the AIP/Xap2-Hsp90-Hop asymmetric complex. Binding of human Hsp90β to AIP/Xap2 was investigated using analytical ultracentrifugation. 1 µM of labeled AIP/Xap2 and 2 µM Hsp90 in standard buffer were subjected to analytical ultracentrifugation at 20 °C. dc/dt profiles are shown for AIP/Xap2 with Hsp90 alone (black) and with the further addition of Hop (red)

To determine whether asymmetric complexes form more often than would be expected by chance, we statistically simulated the complexes formed between human Hop, AIP/Xap2 and Hsp90, assuming random association (Fig. 33a), and we determined experimentally the amount of labeled *AIP/Xap2 in these complexes at different Hop concentrations. In the experiments, we observed that the asymmetric complex formed, and then, at higher concentrations of Hop, *AIP/Xap2 was displaced by Hop at the second TPR-acceptor site (Fig. 33a, b). Notably, *AIP/Xap2 was not completely displaced, even at high concentrations of Hop. This was

unexpected, as Hop binds more strongly to Hsp90 than does AIP/Xap2 (Fig. 30, 31), and the simulation of complex formation suggested that full displacement of Hop should be achievable (Fig. 33a). Moreover, Fkbp51 and unlabeled AIP/Xap2 were both capable of displacing *AIP/Xap2 from these complexes in control experiments. This demonstrates that in the human system, mixed complexes are preferentially formed and are not generated randomly.

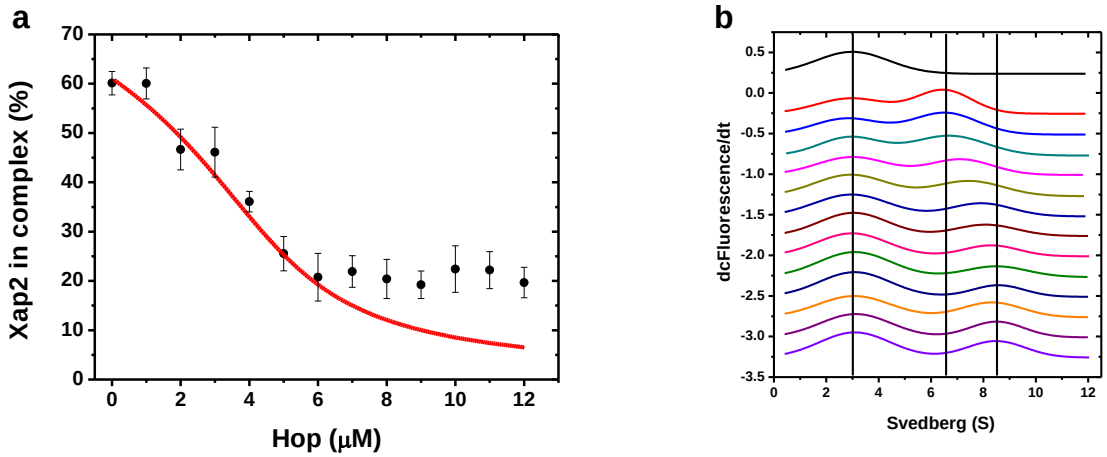

Figure 33. Quantitative evaluation of Hop- AIP/Xap2-Hsp90 complex formation

a. Raw sedimentation velocity runs were evaluated by UltraScan to obtain the complexed and free concentrations of AIP/Xap2 in the presence of Hsp90 at different concentrations of Hop. The data for the complexed fraction of AIP/Xap2 were plotted and a simulation of the behavior was performed for plain statistical binding. To simulate the behavior, the binding constant for Hop was used, which best matched the initial decrease in the “complexed” AIP/Xap2-fraction (red line).

b. Different concentrations of Hop were added to a constant AIP/Xap2-Hsp90 mixture to monitor the formation of the asymmetric complex. dc/dt profiles are shown for labeled AIP/Xap2 alone (black), AIP/Xap2 with Hsp90 (red) and the addition of different concentration of Hop (1 μM to 12 μM, various colors). Vertical lines represent the position of the free AIP/Xap2 peak (left, 3.1 S), the position of the Xap2-Hsp90 complex (middle, 6.5 S) and the position of the Hop-Hsp90-Xap2 peak (right, 8.3 S)

To determine whether human p23 influences the association of Hop and AIP/Xap2 with Hsp90, we added p23 to *Hop–Hsp90–AIP/Xap2 complexes in the presence of AMP-PNP and subjected them to sedimentation-velocity experiments. We observed a marked decrease in the amount of asymmetric complex (Fig. 34), suggesting that Hop exits the complex when p23 and AMP-PNP are present. As in the yeast system (see Fig. 27), the addition of AMP-PNP alone led to a smaller decrease in the amount of Hsp90 complexes containing Hop, whereas the addition of p23 had only

minor effects on complex composition. Thus, regulation of the progression of the co-chaperone cycle is fully conserved between the yeast and human Hsp90 systems.

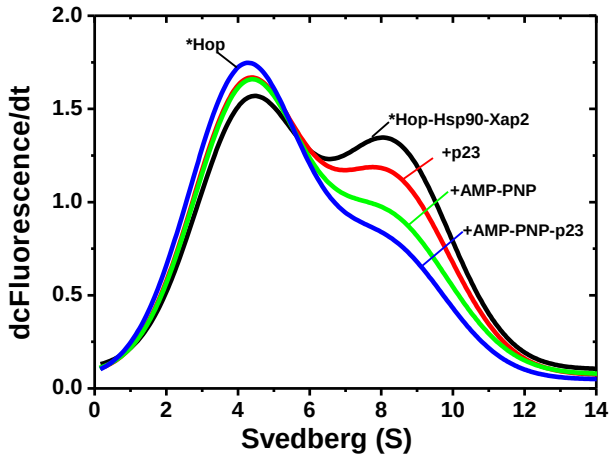

Figure 34. Regulation of asymmetric complex in human Hsp90 cycle

The regulation of the asymmetric AIP/Xap2-containing complex was investigated using aUC. 1 µM of labeled Hop, 2 µM Hsp90β and 2 µM AIP/Xap2 in 40 mM HEPES, 50 mM KCl and 5 mM $MgCl_2$ at pH 7.5 were subjected to aUC at 20 °C. dc/dt profiles are shown for the AIP/Xap2-Hsp90-Hop asymmetric complex (black) and the addition of p23 (2µM) in absence (red) or presence of 2 mM AMP-PNP (blue). Addition of AMP-PNP alone is depicted in green.

4.1.3 Discussion: the Hsp90 co-chaperone cycle

In the last decade, a large number of different co-chaperones have been identified to be associated with Hsp90 during the chaperone cycle (75). In the cell, the maturation of client proteins involves the succession of at least two different complexes containing Hsp90 and specific co-chaperones (160). It implies that there must be factors determining which co-chaperone interacts with Hsp90 at a specific stage. It becomes clear that the conformational state of Hsp90 plays a role in this process. For example, Hop/Sti1 binds and stabilizes the open conformation of Hsp90 (128) while p23 specifically interacts with the closed conformation of Hsp90 (143,196,272). The extensive research on Hsp90/co-chaperone binary complex provides us with a detailed mechanism on how one co-chaperone interacts with Hsp90. However, these results still do not solve the central issue in understanding the Hsp90 cycle as they only provide static pictures on this dynamic process. For example, the progression from the intermediate complex to the late complex remains unclear. During this process, the inhibitory co-chaperone Hop/Sti1 has to exit from Hsp90 and is replaced by p23 and a PPIase (160). It was not clear how this can be achieved since Hop/Sti1 and the large PPIase interact with Hsp90 with similar affinity.

The results of this study suggest that one Sti1 molecule is sufficient to stabilize the open conformation and inhibit the ATPase activity of the Hsp90 dimer. It is reasonable to assume that only one Sti1 is bound per Hsp90 dimer given the fact that the concentration of Sti1 *in vivo* is only around 10% of Hsp90 (268). Since Sti1 only occupied one TPR binding sites, the second subunit is free to interact with another co-chaperone. In our study, the asymmetric PPIase-Hsp90-Hop complex is favored as shown by the comparison of complex formation with the statistical expectations. This is probably due to the binding of the second Sti1 being sterically unfavorable. Or the binding of Sti1 induces a conformational change in Hsp90 which favors the binding of different TPR co-chaperones.

Several studies have addressed the composition of Hop/Sti1-containg complexes by immunoprecipitation from cell lysate (273,274). It is clear that Hsp90 and Hsp90

were involved while p23 was absent. However, the situation was less clear for the PPIase co-chaperones probably owing to the low abundance in the cell as only low amount of PPIase co-chapeones was detected in our study. Interestingly, under heat shock conditions, only three proteins in the Hsp90 chaperone machine, Hsp90, Sti1 and Cpr6 were upregulated (275,276), exactly matching the asymmetric complex we reported here. Compared to the situation where two Hop/Sti1 molecules were bound to Hsp90, these complexes are more readily transformed to the late complex. To completely expel Hop/Sti1 from Hsp90, the concerted action and nucleotides and p23 is required (Fig.35). It is known that p23 interacts with the N- and M-domains of Hsp90, and therefore it is reasonable to assume that Sti1 may have a second interaction sites located in the N- or M-domain of Hsp90. The conformational changes induced by nucleotide binding may weaken the interaction of Sti1 with the second binding sites and the competition with p23 resulted in the complete release of Sti1 from Hsp90.

Thus, two different co-chaperones have to act in a coordinated manner together to promote the formation of the late complex and to simultaneously displace Sti1. This stringent regulation suggests that the transition from the asymmetric Sti1-complex to the late complex is the key step in the chaperone cycle of Hsp90.

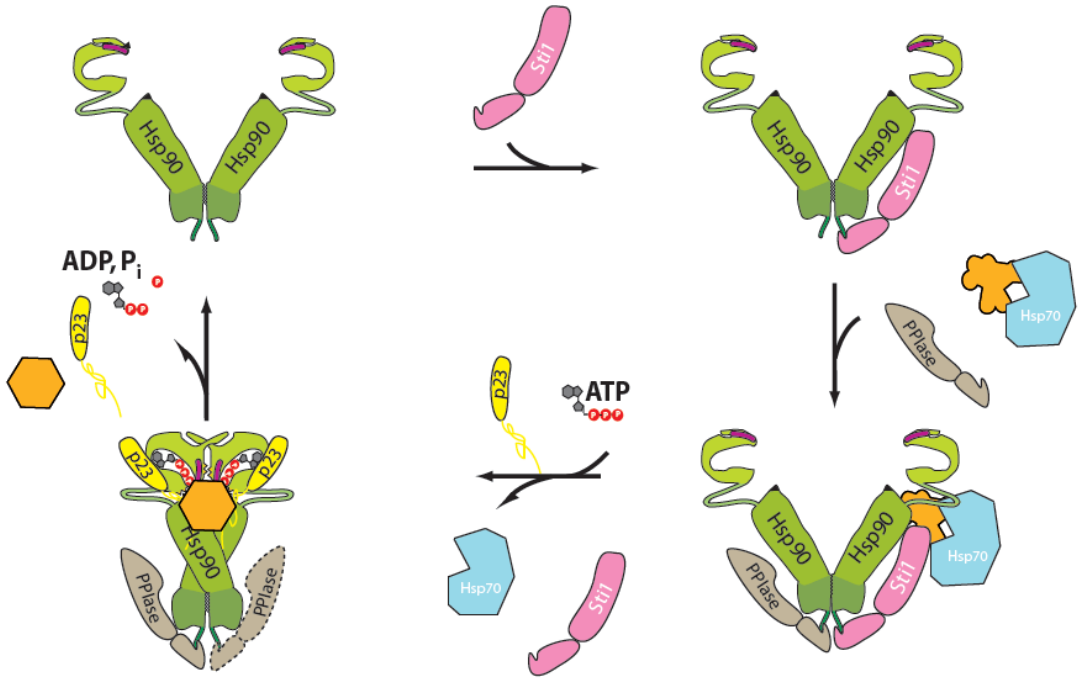

Figure 35. Model of the Hsp90 co-chaperone cycle

Hop/Sti1 binds to the open conformation of Hsp90 and acts as the attachment site for Hsp70 bound to client protein. One Sti1 molecule bound is sufficient to inhibit the Hsp90 ATPase activity. For simplicity, Hsc70/Ssa1 is depicted to enter the cycle together with client protein after Sti1 is bound to Hsp90. It is reasonable to assume that this can also occur in complex with Sti1. The other TPR-acceptor site is preferentially occupied by a PPIase, leading to an asymmetric Hsp90 complex. Hsp90 converts to the closed conformation after binding of ATP. This reaction weakens the binding of Sti1 and therefore promotes its exit from the complex. Potentially, another PPIase (dashed line) binds to form the late complex together with Hsp90 and p23. After hydrolysis of ATP, p23 and the folded client are released from Hsp90.

4.2 Synergistic binding of Aha1 and Cpr6 to Hsp90 promotes the progression of chaperone cycle

4.2.1 Aha1/Hch1 and Cpr6 prefer the closed conformation of Hsp90

Aha1 is an ATPase activator of Hsp90, which plays an important role in the regulation of Hsp90's function (121,277). Previous studies showed that Aha1 led to the closed conformation of Hsp90 even without nucleotides (117). To assess the role of Aha1 in the Hsp90 chaperone cycle, we first investigated the interaction between Aha1 and Hsp90 using aUC in the absence and presence of nucleotides. The dc/dt plot clearly showed that the interaction between Aha1 and Hsp90 was greatly enhanced by adding AMP-PNP, which led to the closed conformation of Hsp90 (Fig.36).

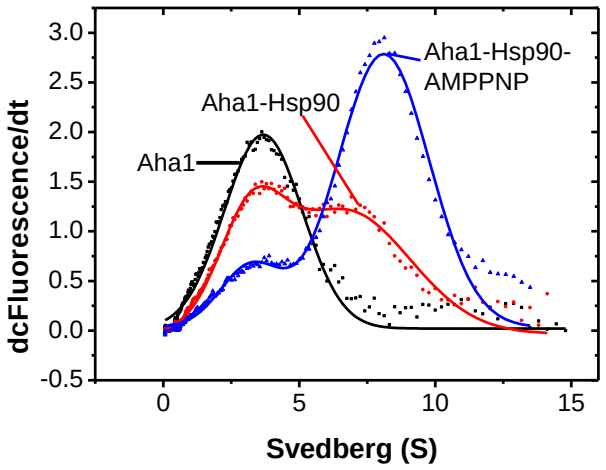

Figure 36. Aha1 has higher binding affinity for the closed conformation of Hsp90

Binding of Hsp90 to Aha1, investigated using aUC. dc/dt profiles (dc/dt represents the change in fluorescence signal intensity over time) are shown for 0.5 µM labeled *Aha1 alone (black), for *Aha1 mixed with 1 µM Hsp90 (red), and for *Aha1 mixed with 1 µM Hsp90 in the presence of AMP-PNP (blue).

To determine the binding constants between Aha1 and Hsp90, we performed SPR titrations using "open" Hsp90 (in the absence of AMP-PNP) and "closed" Hsp90 (pre-incubated with AMP-PNP). Interestingly, the binding affinity increased from 1.2 µM to 160 nM when Hsp90 adopted the closed conformation (Fig.37a,b). The change in the binding affinity implies that the binding sites may be different when Hsp90 is in the "closed" conformation. Hch1 is a homologous protein to Aha1 that shows 36% sequence identity to the N-terminal domain of Aha1 (121). We also determined the binding constant between Hch1 and Hsp90 and found that similar to

Aha1, Hch1 also showed higher affinity for the “closed” Hsp90. The binding constant changed from 1.8 µM to 0.9 µM (Fig. 37c, d).

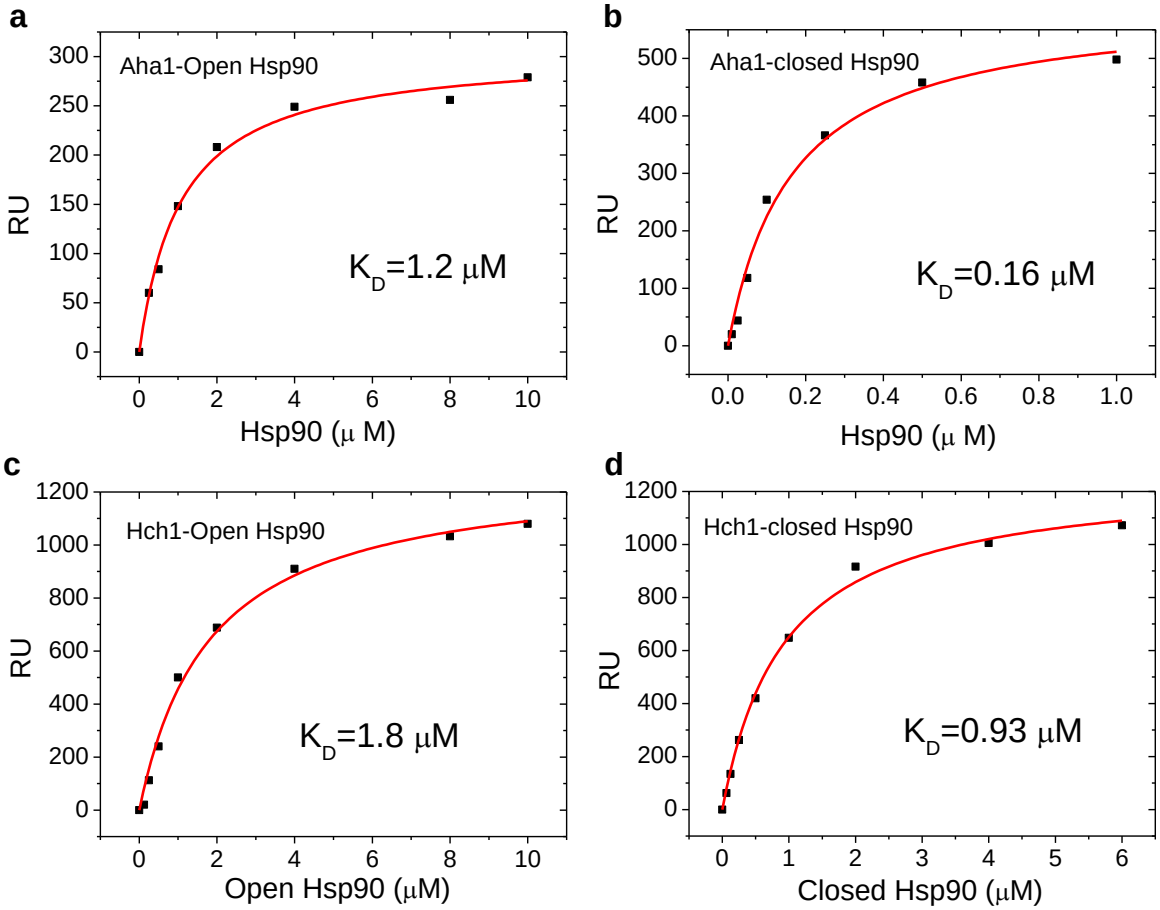

Figure 37. Different affinities of Aha1 and Hch1 for different conformations of Hsp90

Binding of Aha1 (a, b) and Hch1(c, d) was measured using SPR spectrometry. Injections of different concentrations of open (a, c) and closed (b, d) conformations of Hsp90 (pre-incubation with AMP-PNP) were made onto a yAha1-coated or yHch1-coated CM5 chip. For Aha1, the K_D for open conformation of Hsp90 was calculated to be 1.2 µM, and the K_D for closed conformation of Hsp90 was calculated to be 160 nM based on the plateau values of the individual injections. For Hch1, The K_D for open conformation of Hsp90 was calculated to be 1.8 µM, and the K_D for closed conformation of Hsp90 was calculated to be 930 nM based on the plateau values of the individual injections.

We also investigated the nucleotide dependency of the Cpr6 interaction with Hsp90 using aUC. The experiments showed that the interaction between Cpr6 and Hsp90 was greatly enhanced by the presence of AMP-PNP, which indicates that Cpr6 bound to the closed conformation Hsp90 with higher affinity (Fig. 38). After

converting the sedimentation profile to a dc/dt plot, it could be seen that the *Cpr6–Hsp90 complex sedimented with an s value of 7.1 S in the absence of AMP-PNP. After addition of AMP-PNP, the sedimentation coefficient of *Cpr6 increased to 7.6 S owing to conformational changes of Hsp90 (Fig. 38).

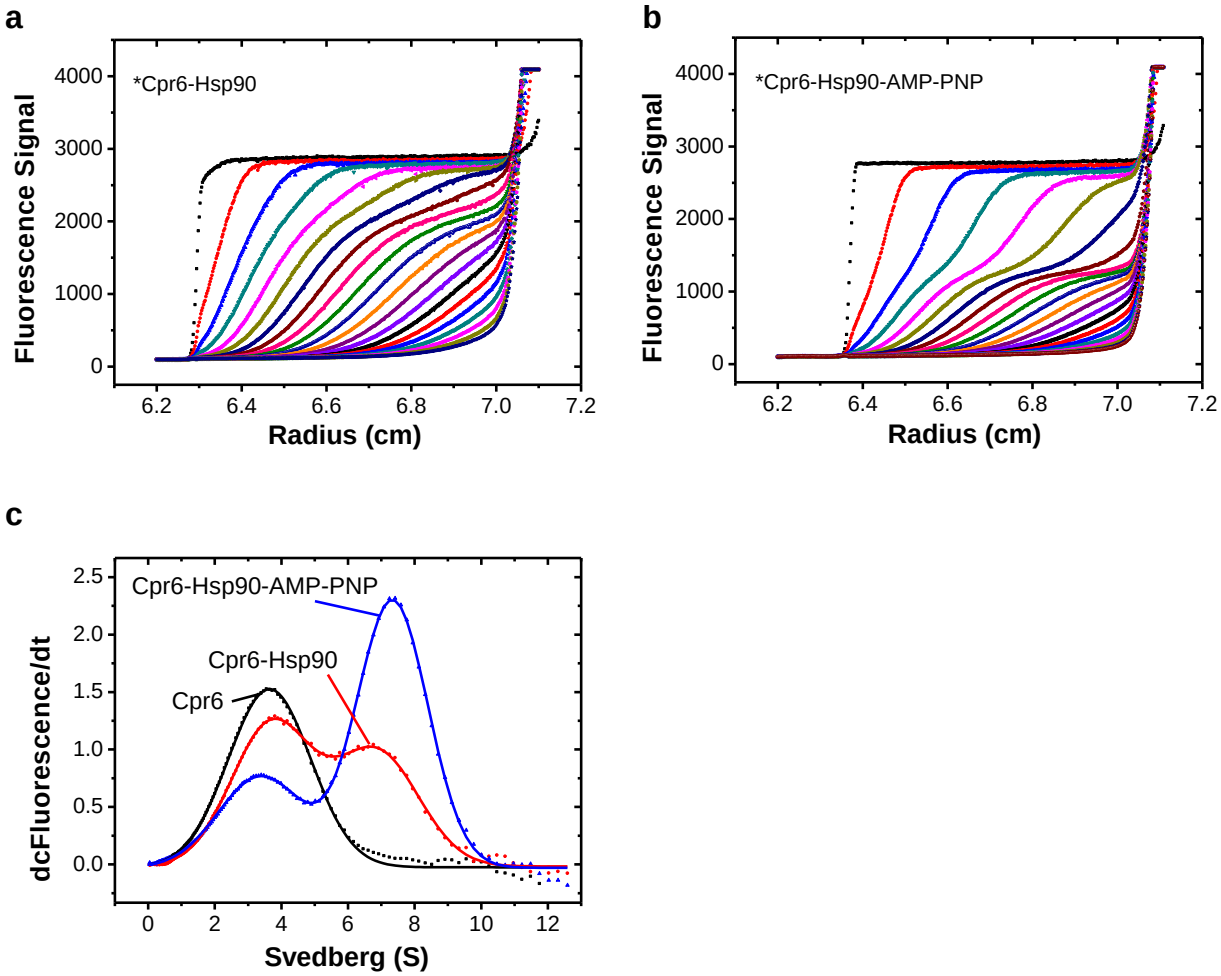

Figure 38. Cpr6 prefers to bind the closed conformation of Hsp90

Binding of Hsp90 to Cpr6 investigated by aUC. Shown are sedimentation profiles of *Cpr6 (a) and *Cpr6-Hsp90 (b). dc/dt profiles (c) are shown for 0.5 µM labeled *Cpr6 alone (black), for *Cpr6 mixed with 1 µM Hsp90 (red), and for *Cpr6 mixed with 1 µM Hsp90 in the presence of AMP-PNP (blue).

We also tested whether Cpr7, a close homologue of Cpr6 in yeast, has a similar nucleotide dependency. Cpr7 was also labeled with Alexa 488 and subjected to aUC

to examine the interaction with Hsp90. *Cpr7 sedimented with an s-value of 3.4 S, which indicates that Cpr7 is also a monomeric protein. Upon adding Hsp90, the s-value increased to 6.8 S owing to the formation of a *Cpr7–Hsp90 complex. In the presence of AMP-PNP, the sedimentation coefficient increased to 7.4 S due to the conformational change of Hsp90. However, different from Cpr6, we didn't observe any nucleotide dependency in the interaction between Cpr7 and Hsp90 (Fig. 39).

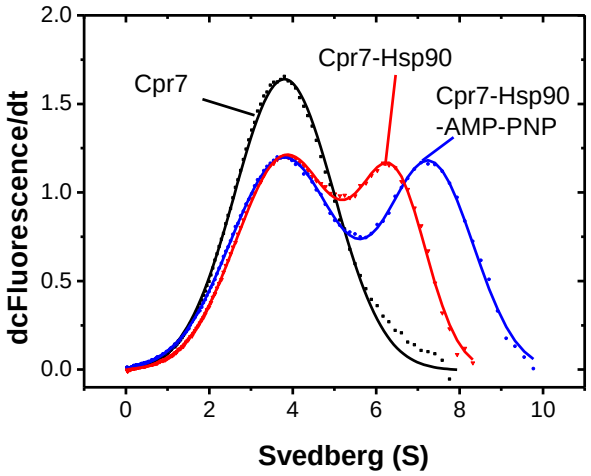

Figure 39. Binding of Cpr7 to Hsp90 is not influenced by AMP-PNP

Binding of Hsp90 to Cpr7 investigated using aUC. dc/dt profiles are shown for 0.5 µM labeled *Cpr7 alone (black), for *Cpr7 mixed with 1 µM Hsp90 (red), and for *Cpr7 mixed with 1 µM Hsp90 in the presence of AMP-PNP (blue).

4.2.2 Aha1 and Cpr6 form ternary complex with Hsp90

Since both Aha1 and Cpr6 preferentially bind to the closed conformation of Hsp90. Therefore we wondered whether these two proteins could form a ternary complex with Hsp90. To test this hypothesis, we added Cpr6 to the *Aha1–Hsp90 complex in the absence and presence of nucleotide. In both cases, as shown in the dc/dt plot, the shift of the sedimentation coefficient indicates that Cpr6 forms a ternary complex with *Aha1 and Hsp90 (Fig. 40a,b). Interestingly, the presence of Cpr6 increased the binding between Aha1 and Hsp90 especially when AMP-PNP is absent. Although Cpr7 can also form a ternary complex with Hsp90 and Aha1, the affinity between Aha1 and Hsp90 remained the same in the absence and presence of Cpr7 (Fig. 40c,d). To elucidate the interaction between these three proteins, we determined the binding constants of Aha1 for the Hsp90/Cpr6 complex in absence and presence of nucleotides. SPR titrations revealed that Aha1 binds to "open" Hsp90/Cpr6 complex with the an affinity of 420 nM and with 130 nM to the "closed" Hsp90/Cpr6 complex (Fig.41a,b). Notably, in the "open" conformation, the presence of Cpr6 increased the

binding affinity around three-fold compared to that of Hsp90 alone (see Fig.37a), which suggests a cooperative binding. Similarly, the presence of Cpr6 also promoted the binding of Hch1 to Hsp90 (Fig. 41 c,d and Fig.37c,d).

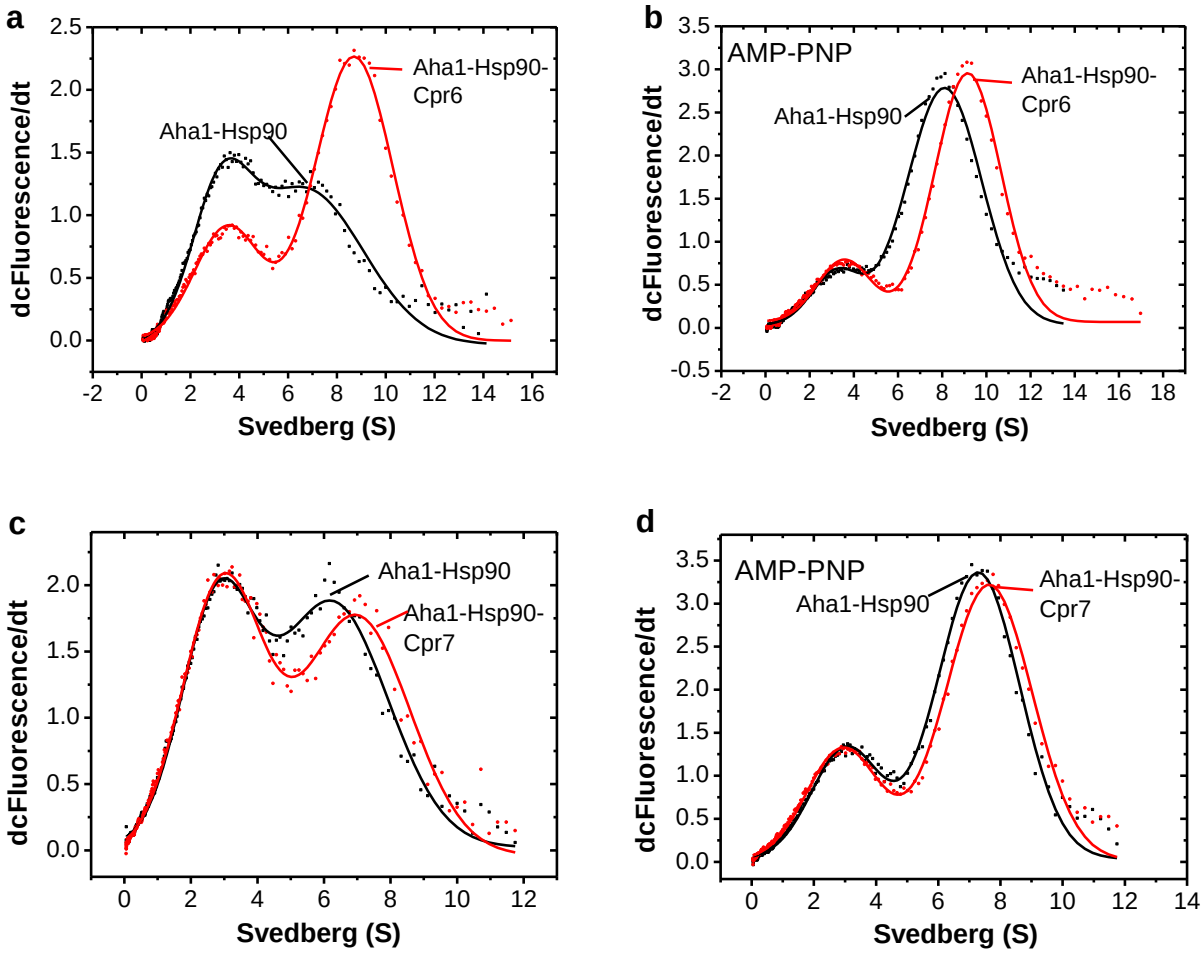

Figure 40. Aha1 froms a ternary complex with Hsp90 and Cpr6 or Cpr7

Binding of Aha1 and Cpr6 to Hsp90 in the absence (a) and presence (b) of AMP-PNP, investigated by aUC. dc/dt profiles are shown for 0.5 µM labeled *Aha1 mixed with 1 µM Hsp90 (black), and for *Aha1 mixed with 1 µM Hsp90 in the presence of Cpr6 (red). For comparison, binding of Aha1 and Cpr7 to Hsp90 was also investigated in the absence (c) or presence (d) of AMP-PNP. dc/dt profiles are shown for 0.5 µM labeled *Aha1 mixed with 1 µM Hsp90 (black), and for *Aha1 mixed with 1 µM Hsp90 in the presence of Cpr7 (red).

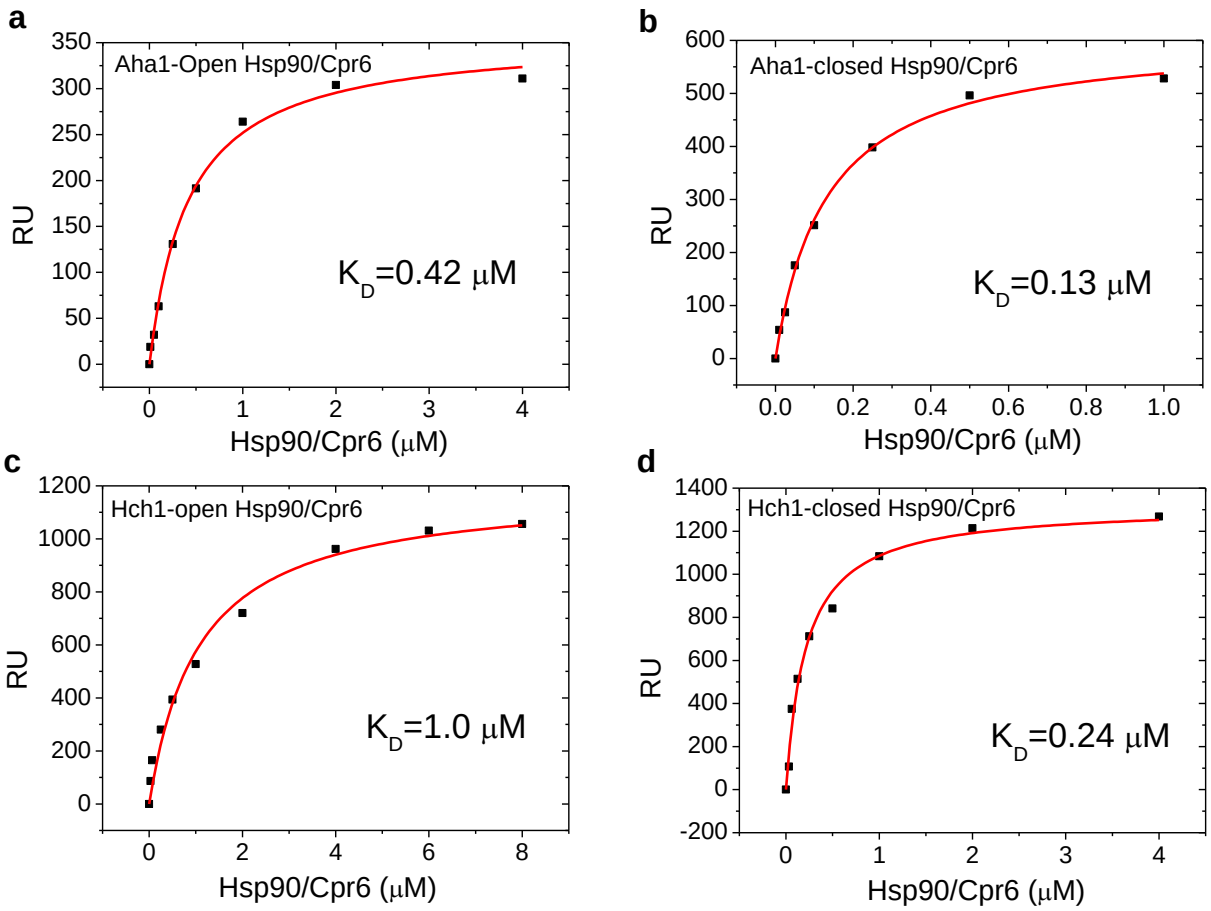

Figure 41. The binding affinity between Hch1 to Hsp90 is increased by Cpr6

Binding of Aha1 (a,b) or Hch1(c,d) to Hsp90 was measured in the presence of Cpr6 using SPR spectrometry. Injections of different concentrations of open and closed conformation of the Hsp90/Cpr6 complex (pre-incubation with AMP-PNP) were made onto a yAha1-coated or yHch1-coated CM5 chip. For Aha1, the K_D for the open conformation of Hsp90/Cpr6 was calculated to be 420 nM (a), and the K_D for the closed conformation of Hsp90/Cpr6 was calculated to be 130 nM (b) based on the plateau values of the individual injections. For Hch1, the K_D for the open conformation of Hsp90/Cpr6 was calculated to be 1.0 μM (c), and the K_D for the closed conformation of Hsp90/Cpr6 was calculated to be 240 nM (d) based on the plateau values of the individual injections.

To further verify the cooperative binding between Aha1 and the Hsp90/Cpr6 complex, we set up an *Aha1–*Hsp90 FRET system. Addition of an excess amount of unlabeled Aha1 led to the release of *Aha1 from Hsp90 (Fig.42a). Addition of Cpr6 did not interrupt the binding kinetics but resulted in a new binding kinetics, which revealed that Cpr6 binds to Hsp90 in addition to Aha1 (Fig.42b). The results

also showed that nucleotides, which led to the closed conformation of Hsp90, enhanced the binding of Aha1 as we observed in the aUC experiments. Moreover, we observed that Cpr6 promotes the binding of Aha1 to Hsp90 in the FRET system (Fig.42c), which confirms the cooperative binding model for the Aha1–Hsp90/Cpr6 interaction.

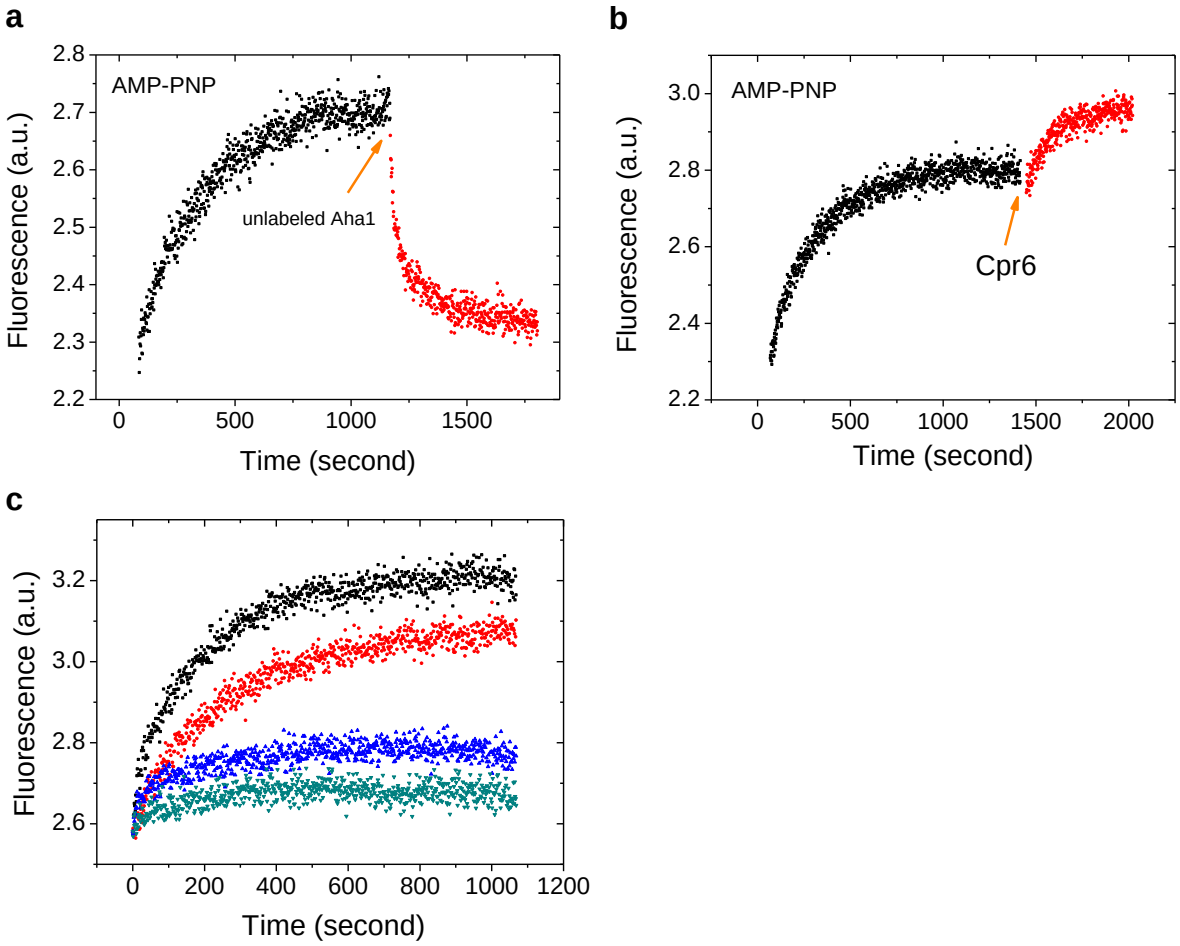

Figure 42. Cpr6 promotes Aha1/Hsp90 interaction

The effect of Cpr6 and AMP-PNP on the interaction between Aha1 and Hsp90 was investigated by FRET. We added 300 nM *Hsp90 (acceptor) to 300 nM *Aha1 (donor) in the presence of AMP-PNP (a, b), and the binding kinetics (black) were monitored at 25 °C in standard reaction buffer. We added unlabeled Aha1 (a) or unlabeled Cpr6 (b) to the *Aha1–*Hsp90 complex to trace the kinetics change. The orange arrow indicates the addition of protein (a,b). To compare the binding kinetics of *Aha1 to different Hsp90/Co-chaperones, we added 300 nM *Hsp90 (turquoise), 300 nM *Hsp90/Cpr6 complex (blue), 300 nM *Hsp90 in the presence of AMP-PNP (red) or 300 nM *Hsp90/Cpr6 complex in the presence of AMP-PNP (black) to 300 nM *Aha1 (donor), respectively (c). The binding kinetics were monitored at 25 °C in standard reaction buffer. a.u, arbitrary units.

4.2.3 Aha1 provides additional driving forces for the progression of the Hsp90 cycle

Previous studies showed that Cpr6 could partially displace Sti1 from the Hsp90 complex, and therefore we tested whether Aha1 also contributes to the exit of Sti1. aUC experiments showed that Aha1 could also release Sti1 to some extent from the Hsp90 complex, and more Sti1 was expelled from the complex upon adding Cpr6. Moreover, Sti1 exits from Hsp90 completely when Aha1, Cpr6 and nucleotide were present together (Fig.43a).

To analyze this transition kinetically, FRET experiments were performed to examine the influence of Aha1 on the exit of Sti1 in combination with other cofactors (Fig. 43b). We bound donor-labeled *Sti1 to acceptor-labeled *Hsp90 and then added an excess amount of unlabeled Aha1. The decreased fluorescence signal showed that Aha1 could displace Sti1 from Hsp90, which confirms the notion that Aha1 competes with Sti1 for the interaction with Hsp90. Since previous studies have shown that the interaction of Aha1 with Hsp90 involved the N- and M-domain of Hsp90, this result also indicates that Sti1 may interact with the same region besides binding to the C-terminal MEEVD motif. An efficient displacement of Sti1 could be observed only when Aha1 and Cpr6 were added together. For complete release of Sti1, AMP-PNP need to be added together with Aha1 and Cpr6 (Fig.43b). Taken together, the results suggest that in the Hsp90 chaperone cycle, Sti1 can be released from Hsp90 before p23 binding due to the cooperative binding of Aha1 and Cpr6.

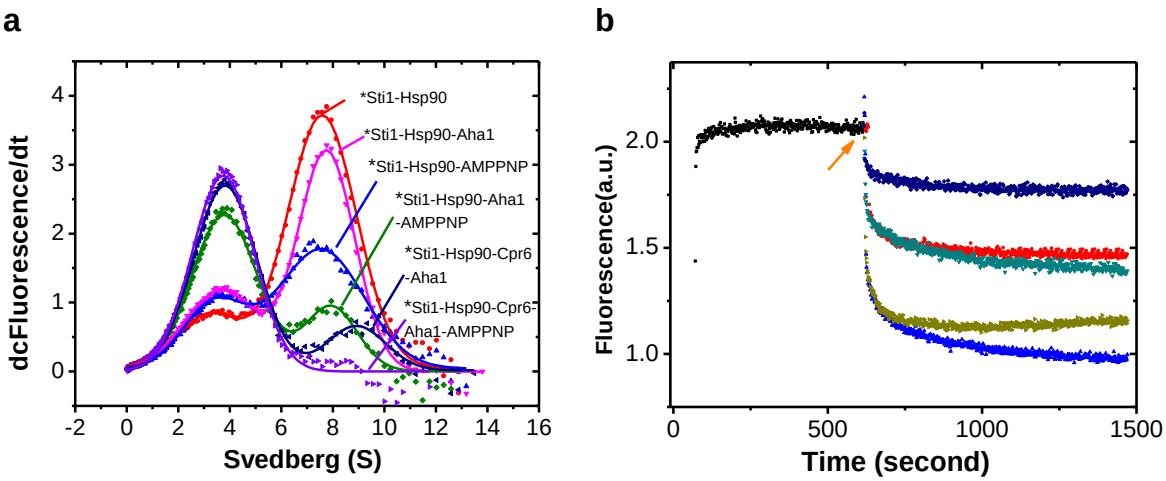

Figure 43. Aha1, Cpr6 and nucleotides release Sti1 from Hsp90

a. The release of Sti1 from the Hsp90 complex, investigated using aUC. d*c*/d*t* profiles are shown for the *****Sti1–Hsp90 complex in the absence (red) of AMP-PNP. We added Aha1 alone (pink), AMP-PNP alone (blue), Aha1 and Cpr6 (dark blue), Aha1 and AMP-PNP (green) or Cpr6, Aha1 and AMP-PNP (purple) to the *Sti1-*Hsp90 complex to follow the release of *Sti1.

b. The release of Sti1 from the Hsp90 complex, investigated by FRET. We added 300 nM *Hsp90 (acceptor) to 300 nM *Sti1 (donor), and the binding kinetics (black) were monitored at 25 °C in standard reaction buffer. We added Aha1 alone (red), Aha1 and AMP-PNP (turquoise), Aha1 and Cpr6 (dark yellow), AMP-PNP alone (dark blue) or Aha1, Cpr6 and AMP-PNP (bright blue) to the *Sti1–*Hsp90 complex to trace the kinetics of *Sti1 release. The orange arrow indicates the addition of nucleotide or protein. a.u., arbitrary units.

4.2.4 Aha1 and Cpr6 stimulate the ATPase activity of Hsp90

To evaluate the influence of Cpr6 on the ATPase activity of Hsp90, we performed the ATPase assay in the absence and presence of Cpr6. The results indicate that Cpr6 could stimulate the ATPase activity of Hsp90 around 1.5 fold while Cpr7 did not influence it (Fig. 44a). Interestingly, at sub-stoichiometric concentrations, Aha1 and Cpr6 stimulated the ATPase activity synergistically.

To further investigate the mechanism of the ATPase stimulation by Aha1, we studied the ATPase activation using different concentration of Hsp90 (Fig.44b). The result showed that the stimulation effect is limited by the amount of Aha1, which indicates that Aha1 may not be released from Hsp90 after ATP hydrolysis.

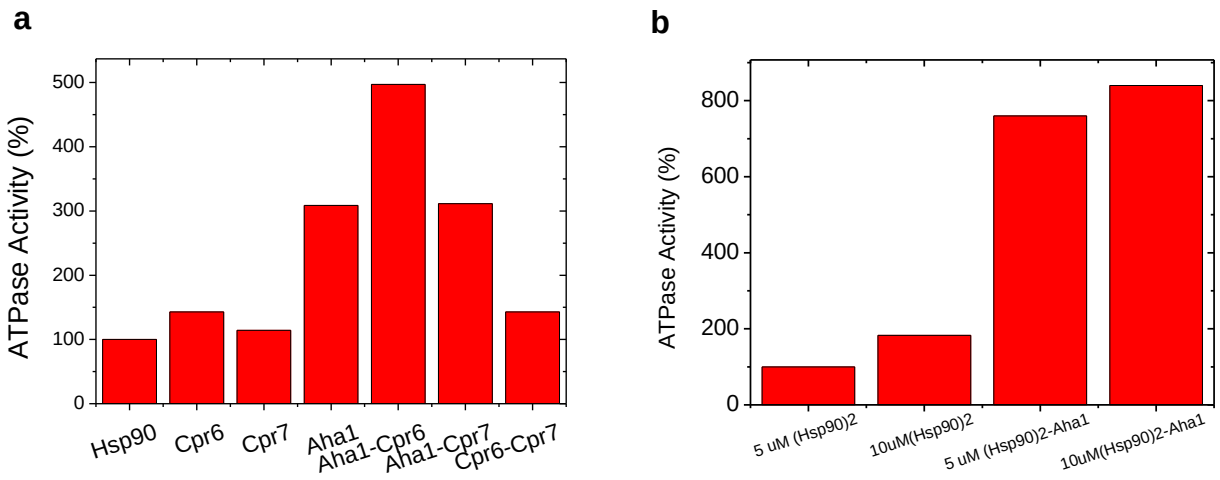

Figure 44. Stimulation of ATPase activity of Hsp90 by Aha1 and Cpr6

a. Different co-chaperones or mixtures were added to Hsp90 to examine the activation of the ATPase activity of yHsp90. The resulting ATPase activities were measured at 30 °C.
b. 5 µM Aha1 was added to 5 µM Hsp90 dimer or to 10 µM Hsp90 dimer to examine the activation of the ATPase activity of yHsp90. The resulting ATPase activities were measured at 20 °C.

4.2.5 p23 releases Aha1 from Hsp90

The results of the ATPase experiments imply that the exit of Aha1 may require the competition with other co-chaperones. To test this notion, we investigated the effects of p23 and Aha1 on complex formation with Hsp90 by aUC. As shown in the dc/dt plot, p23 could completely displace Aha1 from Hsp90 in the presence of AMP-PNP (Fig. 45a). To confirm this finding, we measured the release of Aha1 by p23 in the *Aha1–*Hsp90 FRET system (Fig. 45b). The results showed that addition of p23 results in the exit of Aha1 from Hsp90.

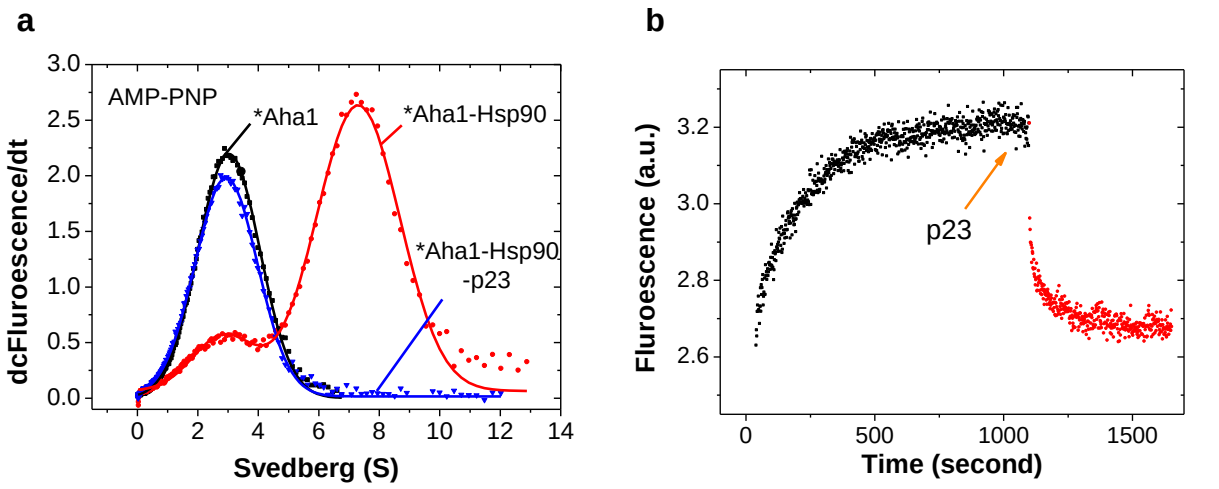

Figure 45. p23 releases Aha1 from Hsp90

a. The release of Aha1 from the Hsp90 complex was investigated using aUC. d*c*/d*t* profiles are shown for the *****Aha1 alone (black) or the *Aha1–Hsp90 complex in the presence of AMP-PNP (red). We added unlabeled p23 to the *Aha1–Hsp90 complex to follow the release of *Aha1 (blue).

b. The release of Aha1 from the Hsp90 complex was investigated by FRET. We added 300 nM *Hsp90 (acceptor) to 300 nM *Aha1 (donor) in the presence of AMP-PNP, and the binding kinetics (black) were monitored at 25 °C in standard reaction buffer. We added p23 (red) to the *Aha1–*Hsp90 complex to trace the kinetics of *Aha1 release. The orange arrow indicates the addition of protein. a.u., arbitrary units.

4.2.6 Discussion: Aha1 in the co-chaperone cycle of Hsp90

As the most potent ATPase activator of Hsp90 (121), Aha1 exerts a strong influence on the Hsp90 chaperone machinery. For example, Aha1 induces a conformational change in Hsp90 in the absence of nucleotides (117). It is also known that the knockout of Aha1 in yeast severely affected the maturation of several different Hsp90 clients such as GR (277). Previous studies demonstrated that co-chaperones such as Hop and p23 are also crucial for the activation of GR, which has to pass through different Hsp90 co-chaperone complexes to achieve the functional conformation (160). However, how Aha1 cooperates with other co-chaperones in chaperoning client proteins remained unclear. Thus role of Aha1 in the progression of the chaperone cycle needed to be elucidated.

Compared to other Hsp90 co-chaperones such as Sti1 and Cpr6, Aha1 binds weaker to Hsp90, as the binding constant is in the micro molar range. In this work, we determined the binding constants between Aha1 and different conformation of Hsp90. A six fold increase in the binding affinity showed that Aha1 strongly prefers the closed conformation of Hsp90. This result also implies that Aha1 might have different binding sites in the open and closed conformation of Hsp90. We also observed the synergistic binding between Aha1, Cpr6 and Hsp90, as Cpr6 promotes more Aha1 to interact with Hsp90. Moreover, these two co-chaperones stimulate the ATPase activity of Hsp90 in a cooperative way. With the concerted action of nucleotides, Aha1 and Cpr6 could completely expel Sti1 from Hsp90. Interestingly, a number of studies have shown that p23 stabilized the closed conformation of Hsp90 and contributed to the exit of Hop/Sti1 from the chaperone cycle (143,196,272,278). It seems that the function of p23 might be partially substituted by Aha1 at least in the progression of the chaperone cycle. It is clear that Aha1 interacts with the N- and M-domain of Hsp90 (107,155). Therefore our results also imply that Sti1 may have a second interaction site located in the N- or M-domain and the competition with Aha1 contributes to the full exit of Sti1 from Hsp90 (Fig. 46). Taken together, these findings support the idea that Aha1 may be involved in the late stage of the Hsp90 chaperone cycle.

Cpr6 was shown to slightly activate the ATPase activity of Hsp90 in previous research (121). However, the influence of Cpr7, a closely related TPR-containing PPIase of Cpr6 in yeast, was unclear. In this work, we found that these two proteins are different in many aspects such as the nucleotide dependency, stimulation of the ATPase activity and the cooperativity with other co-chaperones. Early studies indicated that these two co-chaperones differ in some biochemical properties (122). For example Cpr6 has a 100-fold higher PPIase activity but much lower chaperone activity than Cpr7. These results strongly suggest that Cpr6 and Cpr7 perform partially overlapping but not identical tasks in the Hsp90 chaperone cycle.

To date, the stimulation mechanism of Aha1 for the ATPase activity of Hsp90 is well documented (106,107,156). In contrast, little is known on the exit of Aha1 from the Hsp90 complex. Here we tested the hypothesis that Aha1 may act as a catalyst to stimulate the ATPase activity. It may leave the complex spontaneously afterwards and catalyze other Hsp90 molecules. This may explain how Aha1 works on the tremendous amount of Hsp90 molecules in the cell, since the cellular concentration of Aha1 is only around 3% of that of Hsp90 (268). The results obtained do not support this idea as we observed that the stimulation of ATPase activity is strictly limited by the amount of Aha1 presents. This also indicates that the exit of Aha1 may require the competition with other cofactors. In this work, it is shown that an excess amount of p23 could fully displace Aha1 from Hsp90, which sheds light on the mechanism of Aha1's disassociation from the Hsp90 chaperone cycle (Fig. 46).

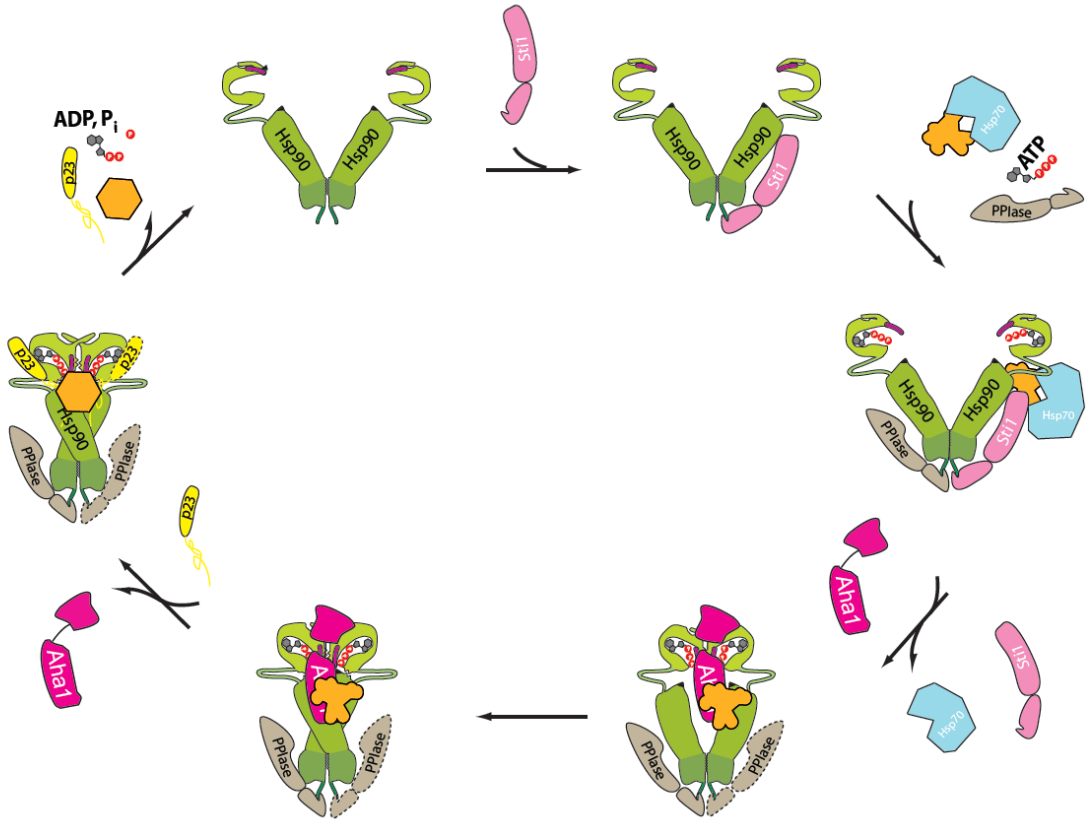

Figure 46. Aha1 in the Hsp90 chaperone cycle.

Hop/Sti1 binds to the open conformation of Hsp90 and acts as the attachment site for Hsp70 bound to client protein. One Sti1 molecule bound is sufficient to inhibit the Hsp90 ATPase activity. The other TPR-acceptor site is preferentially occupied by a PPIase, leading to an asymmetric Hsp90 complex. The synergistic interaction of Aha1 weakens the binding of Sti1 and therefore contributes to its exit from the chaperone cycle together with the concerted action of nucleotides. Aha1 further promotes changes in the domain orientation and accelerates the nucleotide-induced transition of Hsp90 conformation. The binding of p23 stabilizes the closed conformation of Hsp90, expels Aha1 from the chaperone cycle and leads to the formation of the late complex including a PPIase. After hydrolysis of ATP, p23 and the folded client are released from Hsp90.

4.3 Comparative studies of AIP/Xap2 and AIPL1

4.3.1 AIP and AIPL1 show high sequence and structural similarity but distinct differences in the C-terminal region

Hsp90 and its co-chaperones are essential for maintaining the activatable state or conformation of its client proteins (193,194,216). In the case of the aryl hydrocarbon receptor (AHR), the co-chaperone AIP/Xap2 was reported to play an important role in the regulation of AHR activity together with Hsp90 (168). On the sequence level, AIP is closest related to the AIP-like protein (AIPL1), which was originally identified by genetic analysis of patients with the autosomal recessive eye disease, leber's congenital amaurosis (LCA) (279). LCA is the most rapid and severe form of congenital blindness and AIPL1 mutations result in clinically severe forms of LCA (280).

AIP and its homologue AIPL1 shares 49% sequence identity (Fig.47). Both proteins have an N-terminal Fkbp-like domain, which indicates that AIP and AIPL1 might possess PPIase activity, like Fkbp52. Moreover, the three conserved TPR domains, which are modules for protein protein interaction (109), may have a role in Hsp90 interaction. However, the C-terminal regions of AIP and AIPL1 are significantly different. AIPL1 contains a unique proline-rich domain with XXPP repeats in its very C-terminal region (Fig.47). This proline-rich region is thought to be present only in primates and shows considerable sequence variation (281), suggesting that the proline-rich domain might have a unique function.

a

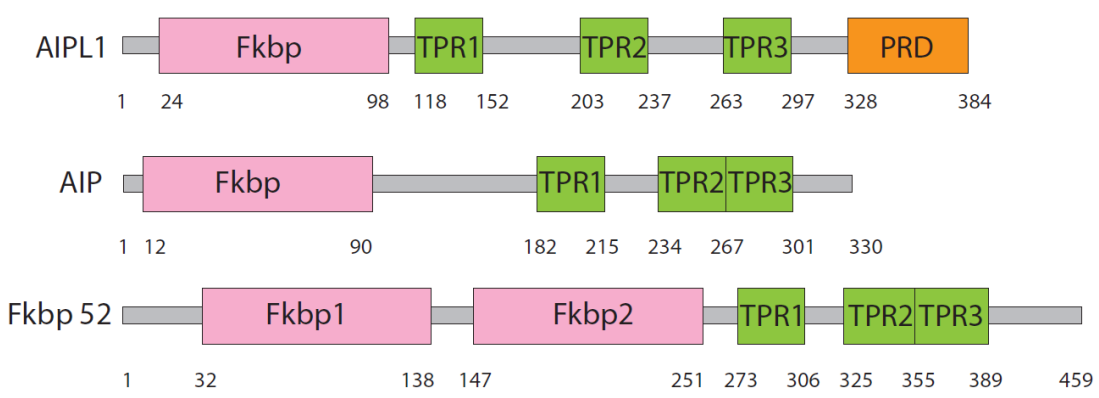

b

```
AIP       MADIIARLREDGIQKRVIQEGRGELPDFQDGTKATFHYRTLHSDDEGTVLDDSRARGKPM
AIPL1     -MDAALLLNVEGVKKTILHGGTGELPNFITGSRVIFHFRTMKCDEERTVIDDSRQVGQPM
            *    *. :*::* ::: * ****:*  *::. **:**::.*:* **:****  *:**

AIP       ELIIGKKFKLPVWETIVCTMREGEIAQFLCDIKHVVLYPLVAKSLRNIAVGKDPLEGQRH
AIPL1     HIIIGNMFKLEVWEILLTSMRVHEVAEFWCDTIHTGVYPILSRSLRQMAQGKDPTEWHVH
          .:***: *** *** :: :**  *:*:* **  *. :**::::***::* **** * : *

AIP       CCGVAQMREHSSLGHADLDALQQNPQPLIFHMEMLKVESPGTYQQDPWAMTDEEKAKAVP
AIPL1     TCGLANMFAYHTLGYEDLDELQKEPQPLVFVIELLQVDAPSDYQRETWNLSNHEKMKAVP
           **:*:*  : :**: *** **::****:* :*:*:*::*. **::.* :::.** ****

AIP       LIHQEGNRLYREGHVKEAAAKYYDAIACLKNLQMKEQPGSPEWIQLDQQITPLLLNYCQC
AIPL1     VLHGEGNRLFKLGRYEEASSKYQEAIICLRNLQTKEKPWEVQWLKLEKMINTLILNYCQC
          ::* *****:: *: :**::** :** **:*** **:* . :*::*:: *..*:******

AIP       KLVVEEYYEVLDHCSSILNKYDDNVKAYFKRGKAHAAVWNAQEAQADFAKVLELDPALAP
AIPL1     LLKKEEYYEVLEHTSDILRHHPGIVKAYYVRARAHAEVWNEAEAKADLQKVLELEPSMQK
           *  *******:* *.**.:: . ****: *.:*** ***  **:**: *****:*::

AIP       VVSRELQALEARIRQKDEEDKARFRGIFSH-----------------------------
AIPL1     AVRRELRLLENRMAEKQEEERLRCRNMLSQGATQPPAEPPTEPPAQSSTEPPAEPPTAPS
          .* ***: ** *: :*:**:: * *.::*:

AIP       -------------------------
AIPL1     AELSAGPPAEPATEPPPSPGHSLQH
```

Figure 47. Domain architecture and Sequence alignment of AIP and AIPL1

a. Domain organization of AIPL1, AIP and FKbp52. AIPL1 contains one Fkbp-like domain, followed by three TPR domains and a unique C-terminal proline-rich domain (PRD). AIP contains one Fkbp-like domain and three TPR domains. Fkbp52 contains two Fkbp domains and three TPR domains. The amino acid positions are indicated by numbers.

b. Sequence alignment of AIP and AIPL1 was performed by means of Clustalw software at: http://www.ebi.ac.uk/clustalw/. * indicates identical or conserved residues in all sequences in the alignment; :, conserved substitutions; and., semiconserved substitutions.

We expressed AIP and AIPL1 in *E.coli* and purified it from the soluble fraction of the lysate. As shown by far UV CD spectroscopy, AIP and AIPL1 have an ordered structure with strong signals at 208 nm and 222 nm, indicative of a high α-helical content (Fig. 48a). We used thermal transitions in order to estimate the stability of AIP and AIPL1. The midpoint of the thermal transitions as measured by CD spectroscopy was around 50°C for both proteins (Fig. 48b,c). To elucidate the effects of the unique proline-rich domain on the structural features of AIPL1, we created an AIPL1 variant lacking the proline-rich domain (AIPL1-ΔPRD). In addition, to further clarify the functions of proline-rich domain, a chimeric protein consisting of wild type AIP and the proline-rich domain from AIPL1 (AIP-PRD) was constructed and purified as well. The far UV CD spectrum of AIPL1-ΔPRD is typical for an alpha-helix protein with a local minimum at 222 nm and 208 nm (Fig. 48a). Next, we compared the stability of AIPL1-ΔPRD to that of human AIPL1 by monitoring the CD signals of both proteins at 220 nm during constant heating. For both proteins, the CD signal starts to decrease above 40°C and the unfolding process is completed at around 65°C, with Tms of 45°C and 48°C for AIPL1-ΔPRD and AIP-PRD, respectively (Fig. 48d,e). Based on these experiments, we conclude that removal of the proline-rich domain does not influence the thermal stability of AIPL1 significantly.

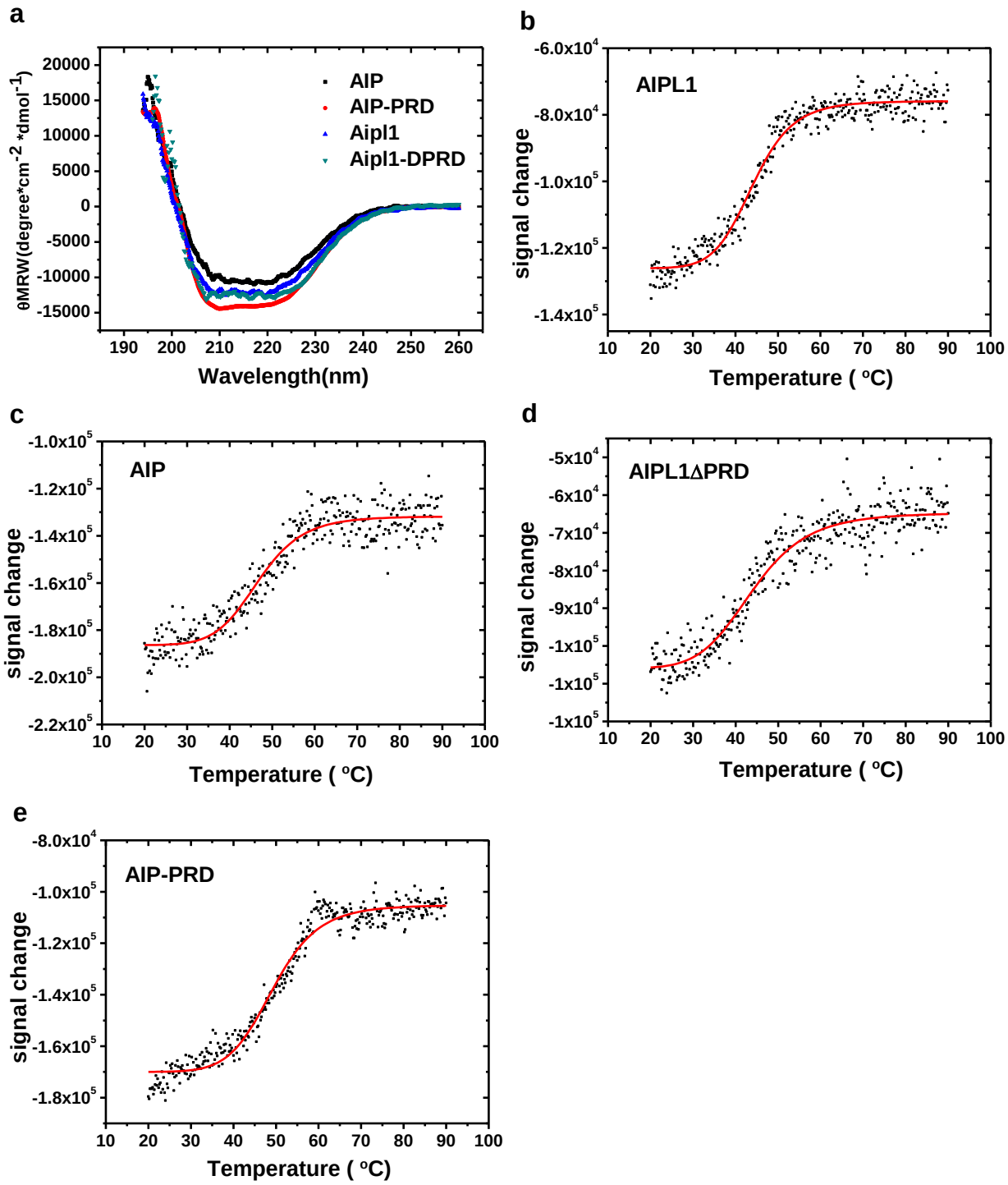

Figure 48. Structure and stability of AIP, AIPL1, AIP-PRD and AIPL1ΔPRD

Far UV CD spectra of AIP (black), AIPL1 (blue), AIP-PRD (turquoise) and AIPL1ΔPRD (red) measured at 20°C (a). To assess the stability of the different proteins, temperature-induced unfolding experiments were performed (b-e). Temperature-induced unfolding was monitored by far UV-CD spectroscopy at a fixed wavelength with a heating rate of 20 °C h^{-1}. Data were fitted to a Boltzmann function to obtain transition midpoints.

4.3.2 AIP and AIPL1 are inactive PPIase with altered function

AIP and AIPL1 share homology to the PPIase domain of Fkbps. To test whether AIP and AIPL1 catalyze peptidyl-prolyl isomerisation *in vitro*, we performed a fluorescence-based PPIase assay (282). As a control, we used Fkbp51 and Fkbp52, Hsp90 associated PPIases with prolyl-isomerisation activity (123). First, PPIase activities were measured using an aminobenzoyl-Ala-Tyr-Pro-Phe-4-nitroanilide model peptide, in agreement with previous results, Fkbp51 and Fkbp52 accelerated the cis/trans isomerization of our model peptides (Fig. 49 a). No influence on the isomerization of the model peptide was observed in the presence of AIP or AIPL1 (Fig. 49 a). We further investigated whether AIP or AIPL1 catalyze the isomerization of other proline-containing peptides. However, the results indicated that both AIP and AIPL1 are inactive PPIases (Fig. 49 b). Therefore it is reasonable to assume that the PPIase-function of either AIP or AIPL1 is strongly diminished compared to the more active Fkbp51 and Fkbp52.

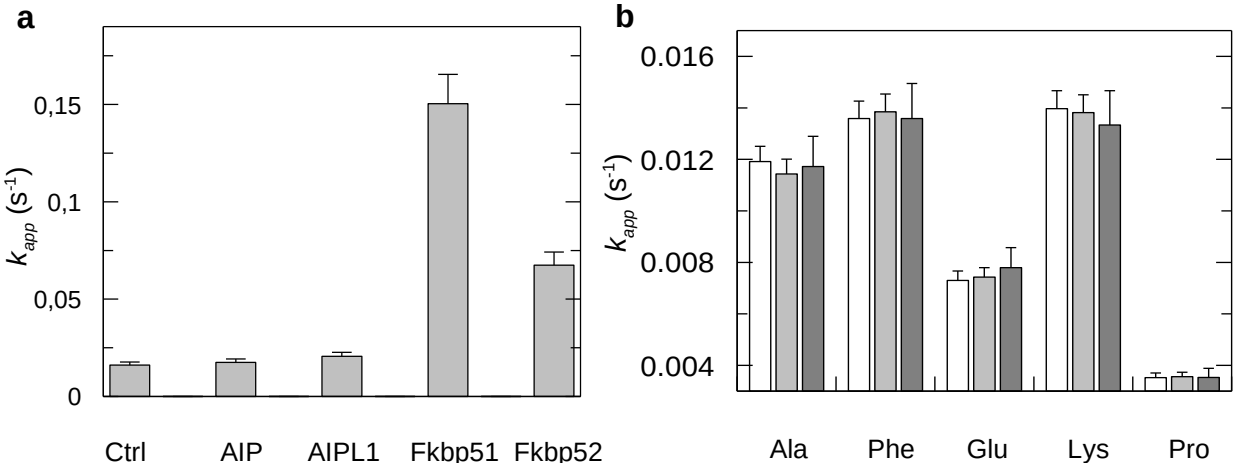

Figure 49. Catalysis of cis/trans isomerisation of the model peptides aminobenzoyl-Ala-Xaa-Pro-Phe-4-nitroanilide (Abz-Ala-Xaa-Pro-Phe-pNA) by AIP and AlLP1

PPIase activity was measured using a fluorescent peptide-based method (282). 2 μM Tyr (Xaa) peptides were use in the assays. The measurements were performed at 15 °C in a buffer containing 40 mM HEPES, 100 mM KCl, 1 mM DTT, pH 7.5 in the presence of 1μM different proteins. As a control, the peptide in the absence of any additional components was measured (a). To further examine the PPIase activity of AIP and AIPL1, the isomerization of different peptides were measured in the absence (white) or presence of 1μM AIP (light grey) /AIPL1(dark grey) (b). The measurements were performed by Dr. Gabriel Zoldak at the University of Bayreuth.

4.3.3 AIPL1 but not AIP shows molecular chaperone activity

In addition to its PPIase activity, FKBP52 also exhibits chaperone activity (164). To analyze whether AIP and AIPL1 interact with an unfolding protein, we performed the well-established citrate synthase (CS) aggregation and inactivation assays (235). CS loses its activity and aggregates rapidly when incubated at 43 ^{o}C, which can be visualized by monitoring the turbidity of the protein solution. In these experiments, AIP did not influence the temperature-induced aggregation of CS, even in experiments, where AIP was added in large excess (Fig. 50a). Surprisingly, AIPL1 shows strong chaperone activity compared to AIP. A three-fold excess of AIPL1 could suppress the thermal aggregation of CS completely and for half-maximum suppression on equal molar ratio was sufficient (Fig. 50a). SDS-PAGE analysis of the insoluble pellet fraction and the soluble supernatant fraction following centrifugation of the samples supports the light-scattering results (Fig. 50b). In the presence of increasing concentrations of AIPL1, increasing amounts of CS remained soluble at 43 ^{o}C.

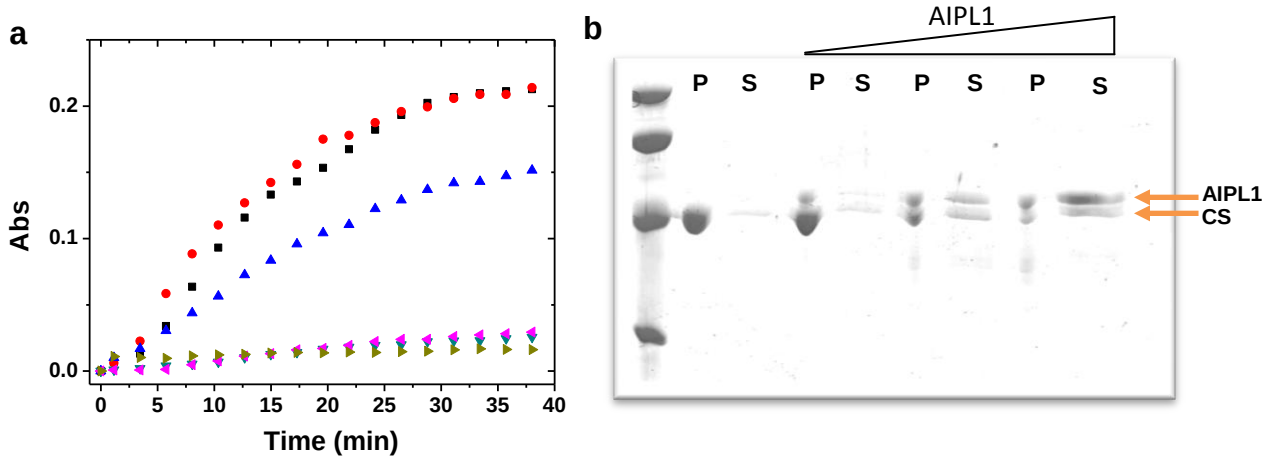

Figure 50. AIPL1 suppress the thermal aggregation of CS

a. Influence of AIP and AIPL1 on the aggregation of thermally denatured CS. 0.5 µM CS (monomer) were incubated at 43 °C in 40 mM Hepes (pH 7.5). CS aggregation was monitored by measuring the absorption at 360 nm in the absence of additional components (black) or in the presence of an equal molar amount (blue), a three-fold molar excess (pink), a fivefold molar excess (green) or a tenfold molar excess (dark yellow) of AIPL1. As a control, a tenfold molar excess of AIP was added to CS (red).
b. AIP prevents the thermal aggregation of CS. CS (0.15 µM monomer) was incubated alone or together with different concentration (1:1, 3:1 and 5:1) of AIPL1 at 43 °C for 30 min. The soluble supernatant and the aggregates were subjected to SDS analysis. The orange arrows indicate the size of CS and AIPL1. P. pellet; S. supernatant

Next, we aimed to determine whether AIPL1 protects CS from thermal inactivation at denatured temperature. To this end, we performed CS activity assays after different time points of incubation at elevated temperature. The results indicate that AIPL1 slows down the thermal inactivation of CS while AIP show no effect (Fig.51). However, after 30 minutes heat shock, the remaining activity of CS is less than 10% of wild type protein, although CS remained in a soluble form as shown in the light scattering experiment above (Fig. 51). To further elucidate the chaperone activity of AIPL1, a CS refolding assay was performed to examine whether AIPL1 accelerates the refolding of heat denatured CS. However, no significant increase of CS activity was detected in the presence of excess amount AIPL1 (date not shown). Taken together, AIPL1 acts as a holdase which is capable to keep the CS in a soluble intermediate form.

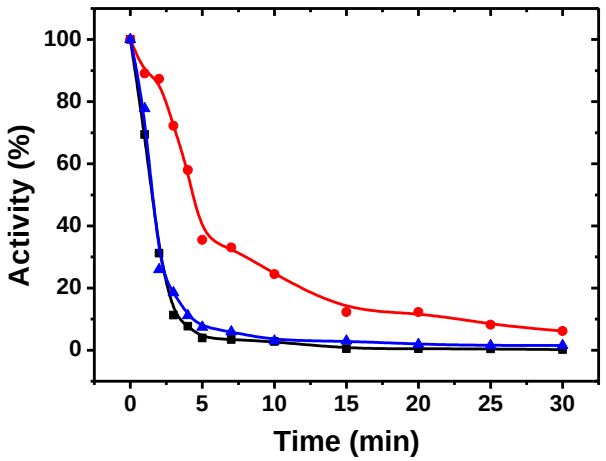

Figure 51. AIPL1 slows down the thermal inactivation of a model client protein

Inactivation kinetics of citrate synthase (0.15 µM monomer) was recorded following incubation at 43°C (black). The effect of AIP (blue) and AIPL1 (red) on the inactivation kinetics was measured in the presence of a fivefold molar excess of AIP or AIPL1 over CS.

4.3.4 The Proline-rich domain is critical for the chaperone activity of AIPL1

As AIPL1 but not AIP binds specially to non-native proteins, we tested whether the C-terminal proline-rich domain alters the behavior of AIPL1 towards non-native proteins. In contrast to wild type AIPL1, the presence of the C-terminal truncated mutant AIPL1-ΔPRD did not have any influence on the aggregation behavior of CS, even if present in huge excess (Fig. 52a). Similarly, no effects could be detected in the inactivation assay in the presence of AIPL1-ΔPRD (Fig. 52b), which suggests that the C-terminal proline-rich region is required for the chaperone function of AIPL1.

Next, we asked whether the function of the proline-rich domain could be transfered to AIP by creating the chimeric protein AIP-PRD in which this domain was fused to AIP. Indeed, a slight suppression of CS aggregation was achieved in the presence of an excess of AIP-PRD (Fig. 52a). However, compared to the wild type AIPL1, AIP-PRD showed only weak chaperone activity. In addition, AIP-PRD is not capable to protect CS from thermal inactivation (Fig. 52b). Taken together, the C-terminal proline-rich region is necessary, but not sufficient for the chaperone function of AIPL1.

Since the interaction between chaperones and client protein often involves hydrophobic interactions, we tested the presence of accessible hydrophobic patches by the probe bis-ANS. This dye bound to AIPL1 much better than to AIP, suggesting more hydrophobic surfaces on AIPL1 (Fig. 53). Deletion of the proline-rich domain results in a dramatic decrease of the fluorescence intensity. This observation parallels the results that AIPL1 exhibits more chaperone activity compared to AIPL1-ΔPRD.

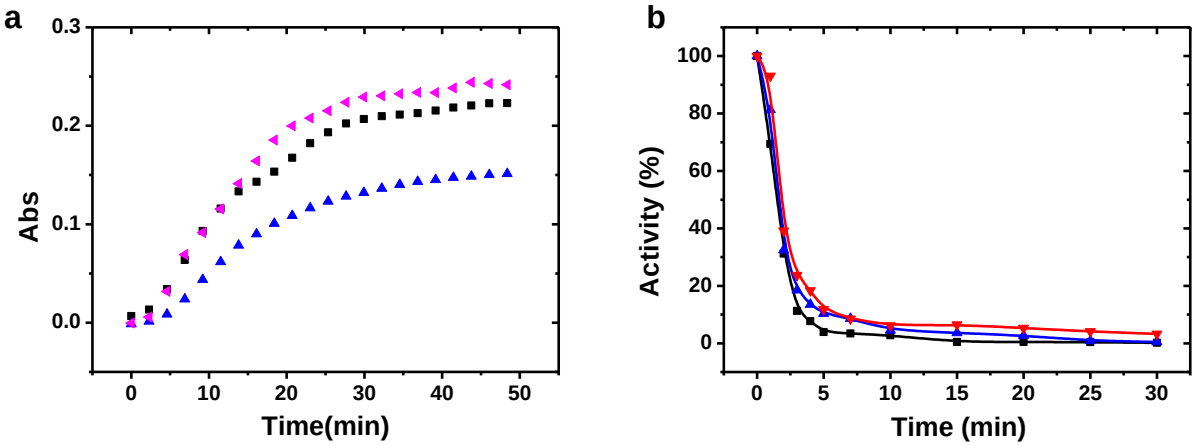

Figure 52. The Proline-rich domain is necessary but not sufficient for the chaperone activity.

a. Influence of AIP-PRD (blue) and AIPL1ΔPRD (pink) on aggregation of thermally denatured CS. A 0.5 µM CS (monomer) sample was incubated at 43 °C in 40 mM Hepes (pH 7.5). CS aggregation was monitored by measuring the absorption at 360 nm in the absence of additional components (black) or in the presence of a fivefold molar excess AIP-PRD (blue) or AIPL1ΔPRD (pink) of AIPL1.

b. Inactivation kinetics of CS (0.15 µM monomer) (black) was recorded following incubation at 43°C. The effect of AIP-PRD (blue) and AIPL1ΔPRD (red) on the inactivation kinetics was measured with fivefold molar excess of AIP-PRD or AIPL1 ΔPRD over CS.

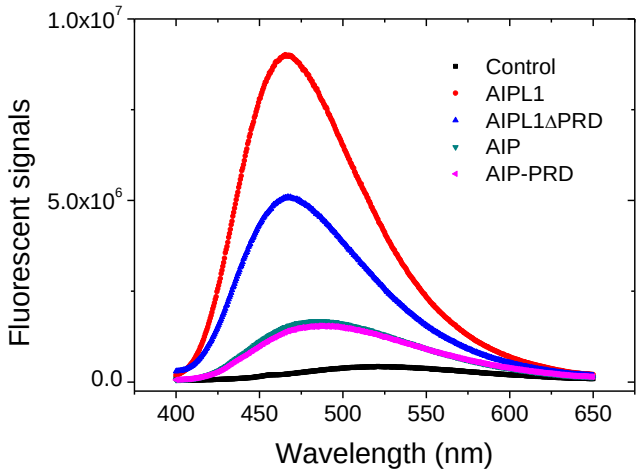

Figure 53. Bis-ANS binding to AIP, AIPL1 and their variants

Fluorescence emission spectra of ANS (100 µm, in HEPES buffer of pH 7.5 with 50 mM KCl) were measured in the presence of AIP (turquoise), AIPL1 (red), AIP-PRD (pink) or AIPL1ΔPRD (blue). As a control, fluorescence spectra for ANS were recorded for the dye alone (black) after excitation at 395 nm.

4.3.5 The Proline-rich domain is a negative regulator of Hsp90 interaction

AIP was known to form a ternary complex with Hsp90 and AHR (169), and recently, AIPL1 was shown to be part of chaperone heterocomplex together with Hsp70/Hsp90 (283), consistent with the notion that both proteins are potential Hsp90 co-chaperones. However, the binding of either AIP or AIPL1 to Hsp90 has not been characterized *in vitro*. We were interested in determining the relative affinities of these proteins for Hsp90 by SPR. Human Hsp90 was covalently coupled to the chip surface. In addition to AIP and AIPL1, we included the Hsp90 co-chaperone Hop in this analysis. We found that these partner proteins bind to Hsp90 with similar affinites between 0.9 µM and 2.6 µM (Fig. 54). Surprisingly, the K_D of AIPL1-ΔPRD was increased to 0.9 µM compared to 2.6 µM for AIPL1 (Fig. 54). In addition, the K_D of AIP-PRD drops to 6.9 µM compared to 2.3 µM for the wild type protein (Fig. 54). Thus, the C-terminal proline-rich region influences the association with Hsp90. We therefore propose that proline-rich domain acts as a negative regulator of Hsp90 interaction.

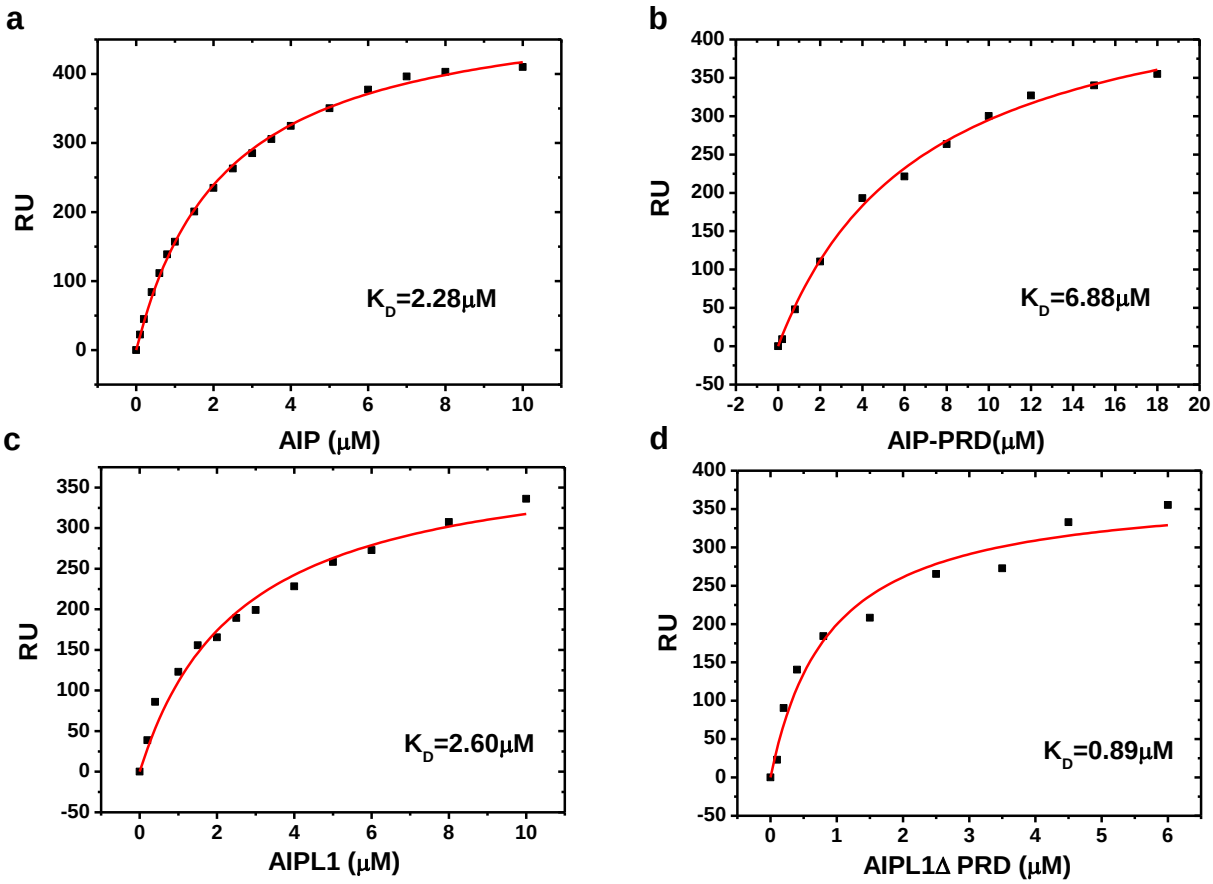

Figure 54. The proline-rich domain is a negative regulator of Hsp90 interaction.

a. Determination of the affinity of AIP to Hsp90 by SPR. The K_D of AIP to hHsp90 was calculated to be 2.28 μM based on injections with different concentration of AIP onto a human Hsp90-coated CM5 chip

b. Determination of the affinity of AIP-PRD to Hsp90 by SPR. The K_D of AIP-PRD to hHsp90 was calculated to be 6.88 μM based on injections with different concentrations of AIP-PRD onto a human Hsp90-coated CM5 chip.

c. Determination of the affinity of AIPL1 to Hsp90 by SPR. The K_D of AIPL1 to hHsp90 was calculated to be 2.60 μM based on injections with different concentration of AIPL1 onto a human Hsp90-coated CM5 chip

d. Determination of the affinity of AIPL1ΔPRD to Hsp90 by SPR. The K_D of AIPL1ΔPRD to hHsp90 was calculated to be 0.89 μM based on injections with different concentrations of AIPL1ΔPRD onto a human Hsp90-coated CM5 chip.

4.3.6 Discussion: Chaperone function of AIP and AIPL1

AIP and AIPL1 have highly similar primary structure but distinct biological functions. AIP is ubiquitously expressed in almost all tissues and its mutations are associated with familial pituitary adenomas (284,285). It has also been shown that AIP is essential in cardiac development (286). Moreover, AIP was reported to interact and regulate the functions of viral protein, transcription factors and nuclear receptors (167,169,287). In contrast, AIPL1 is expressed specifically in adult rod photoreceptor cells, where its function is essential but not well understood. The mutation of AIPL1 is related to an inherited eye disease, Leber congenital amaurosis (LCA) (288-290).

Except a unique proline-rich domain in the C-terminal of AIPL1, both proteins have similar domain organization, an N-terminal PPIase-like domain, followed by three consecutive TPR domains. In this study we demonstrate that both AIP and AIPL1 are inactive PPIases as they cannot catalyze the cis-trans isomerazation of proline-containing peptide *in vitro*. However, AIPL1 is an active chaperone. It protects a model client from thermal aggregation effectively. This result indicates that AIPL1 could act as a molecular chaperone for retinal protein folding. The TPR domain is a repeat motif found in many proteins and functions as a protein-protein interaction domain. AIP was reported to form ternary complexes containing Hsp90 and aryl-hydrocarbon receptor (168). However, the binding affinity between AIP and Hsp90 is unknown. In this study, we measured the binding constants between AIP or AIPL1 and Hsp90. Both proteins interact with Hsp90 in the micro molar range. This implies that both proteins are a part of the Hsp90 chaperone machinery.

The proline-rich region is also a common module mediating protein-protein interactions especially with signaling proteins and thus many proteins with proline-rich motifs are important in the signaling transduction pathways, such as p53 (291). A number of different consensus motif sequences have been described (292). However, the pattern of the proline-rich domain in AIPL1 is novel and unique. To examine the possible role of this unique proline-rich domain, we created a deletion mutant and also a chimeric protein containing AIP and the proline-rich domain. Interestingly, the unique proline-rich domain in AIPL1 is essential for the chaperone function. It also acts as a negative regulator in the interaction with Hsp90.

The results from this study suggest a role of AIPL1 as a molecular chaperone and a regulatory function of the unique proline-rich domain. However, further experiments need to be performed to uncover the physiological function of AIPL1 *in vivo.* For example, it is important to identify the interacting partners specifically for the proline-rich domain. AIPL1 may be involved in the signaling transduction pathways through interactions mediated by this region. Also, the key question which needs to be answered is what is the physiological client of AIPL1 as a molecular chaperone? Studies on the physiological clients will lead to a deeper understanding of the *in vivo* function of this unique retina-specific molecular chaperone.

5. Material and methods

5.1 Material

5.1.1 Chemicals

Acrylamide solution (38% with 2% bisacrylamide)	Roth, Karlsruhe, Germany
Adenosyl-imidodiphosphate (AMP-PNP)	Roche, Mannheim, Germany
Adenosin-5´-diphosphate (ADP), disodium salt	Roche, Mannheim, Germany
Adenosin-5´-triphosphate (ATP), disodium salt	Roche, Mannheim, Germany
Agarose, ultra-pure	Roth, Karlsruhe, Germany
Albumin from bovine serum	Sigma, St. Louis, USA
Ammoniumperoxodisulfate (APS)	Roche, Mannheim, Germany
Ammoniumsulfate	Merck, Darmstadt, Germany
Ampicillin	Roth, Karlsruhe, Germany
Bacto Peptone	Difco, Detroit, USA
Bacto Tryptone	Difco, Detroit, USA
Bromphenol blue S	Serva, Heidelberg, Germany
Coomassie Brilliant Blue G-250	Serva, Heidelberg, Germany
Coomassie Protein Assay Reagent	Pierce, Rockford, USA
Dithiothreitol	Roth, Karlsruhe, Germany
ECL+plus Western Blotting Detection System	Amersham, Uppsala, Sweden
Ethanol, p.a.	Roth, Karlsruhe, Germany
Ethidiumbromide	Sigma, St. Louis, USA
Glycerine, 99%	ICN, Irvine, USA
Guanidinium hydrochloride, p.a.	ICN, Irvine, USA
Kanamycin	Roth, Karlsruhe, Germany
2-Mercaptoethanol, pure	Sigma, St. Louis, USA
N-(2-Hydroxyethyl)-piperazine-N'-2-ethansulfonic	ICN, Irvine, USA

acid (Hepes)	
N,N,N',N'-Tetramethylethylendiamin (TEMED)	Roth, Karlsruhe, Germany
Protease inhibitor mix G	Serva, Heidelberg, Germany
Protease inhibitor mix HP	Serva, Heidelberg, Germany
Sodiumdodecylsulfate (SDS)	Roth, Karlsruhe, Germany
Tris-(hydroxymethyl)-aminomethan (Tris)	ICN, Irvine, USA
Titriplex (EDTA)	Serva, Heidelberg, Germany
Isopropyl β-D-1-thiogalactopyranoside (IPTG)	Merck, Darmstadt, Germany

All other chemicals were purchased from the company Merck (Darmstadt, Germany) and were of grade p.a. if not stated otherwise. For the preparation of buffers double distillated water was used.

5.1.2 Fluorophors

Name	**Ex_{max} (nm)**	**Em_{max} (nm)**	**ε ($M^{-1} cm^{-1}$)**	**Origin**
Alexa Fluor 488 maleimide	490	520	71,000	Invitrogen (Carlsbad, USA)
ATTO488-maleimid	501	523	90,000	ATTO-TEC (Siegen, Germany)
ATTO550-maleimid	554	576	120,000	ATTO-TEC (Siegen, Germany)
5-iodoacetamidoflurescein	494	518	78,000	Invitrogen, (Karlsruhe,Germany)

5.1.3 Size and molecular mass standard kits

BiaCore amine coupling kit	BiaCore Inc., Uppsala, Sweden
1 kb DNA ladder molecular weight standard	New England Biolabs, Beverly, USA
1 kb DNA ladder molecular weight standard	Peqlab, Erlangen, Germany
Calibration proteins for HPLC	Serva, Heidelberg, Germany
Wizard® Plus SV Mini-Preps DNA purification kit	Promega, Madison, USA
High Pure PCR Product Purification Kit	Promega, Madison, USA
High-Range-molecular weight marker (HMW for SDS-PAGE)	BioRad, München, Germany
Low-Range-molecular weight marker (LMW for SDS-PAGE)	BioRad, München, Germany
Rainbow marker for SDS-PAGE	Amersham, Uppsala,Sweden

5.1.4 Protein and antibodies

Alkaline phosphatase	Roche, Mannheim, Germany
Citrate Synthase from pig heart	Roche, Mannheim, Germany
Monoclonal IgG-POD conjugate against rabbit-IgG (sheep)	Sigma, St. Louis, USA
Polyclonal serum against Sti1 (rabbit)	Dr. J. Pineda Antibody Service, Berlin, Germany
Polyclonal serum against Aha1 (rabbit)	Dr. J. Pineda Antibody Service, Berlin, Germany
Polyclonal serum against Hsp90 (rabbit)	Dr. J. Pineda Antibody Service, Berlin, Germany
Polyclonal serum against Ssa1 (rabbit)	Dr. J. Pineda Antibody Service, Berlin, Germany
Polyclonal serum against Sba1	Dr. J. Pineda Antibody

	Service, Berlin, Germany
Pwo-DNA polymerase	Roche, Mannheim, Germany
Pfu-DNA polymerase	Roche, Mannheim, Germany
Restriction enzymes	Promega, Madison, USA
T4-Ligase	Promega, Madison, USA

5.1.5 Chromatographic material

Amylose-Resin (15 ml)	New England BioLabs, (Hitchin, UK)
Ni-NTA (5 ml)	GE Healthcare, (Freiburg Germany)
Resource-Q (6 ml)	GE Healthcare, (Freiburg Germany)
Superdex 75 Prep Grade (320 ml)	GE Healthcare, (Freiburg Germany)
Superdex 200 Prep Grade (320 ml)	GE Healthcare, (Freiburg Germany)

5.1.6 Miscellaneous material

Amicon-Ultrafiltration Membrane YM10/30/100	Millipore (Bedford, USA)
Centricon 10/30/100- microconcentrators	Millipore (Bedford, USA)
Dialysis tubes Spectra/Por (6-8 kDa)	Spectrum (Houston, USA)
Cuvettes 1.5 ml	Zefa (Munich, Germany)
Cuvettes	Starna GmbH (Pfungstadt, Germany)
Filterpaper	Whatman (Maidstone, England)
Immobilon-P(PVDF)-Membrane	Millipore (Bedford, USA)
pH-Indicator paper	Roth (Karlsruhe, Germany)
Polyacrylamide gels (10-20 % Tricine)	Novex (Frankfurt, Germany)
Sterile filter 0.2µm	Zefa, München, Germany
X-ray films X-OMAT AR	Eastman Kodak, Rochester, USA

5.1.7 Equipment

Balance	
Analysis balance BP 121 S	Sartorius, Göttingen, Germany
Halfmicro balance BL 310	Sartorius, Göttingen, Germany
Centrifuges	
Avanti J 25 with JA-10 and JA-25.50 rotors	Beckman, Wien, Austria
Beckman XL-I analytical ultracentrifuge	Beckman, Wien, Austria
Eppendorf table-top centrifuge 5415 C	Eppendorf, Hamburg, Germany
Rotina 46 R coolable centrifuge	Hettich, Tuttlingen, Germany
Universal 32 R coolable centrifuge	Hettich, Tuttlingen, Germany
Chromatographic machines	
Äkta FPLC machine	Amersham, Uppsala, Sweden
FP-1520 fluorescence detector	Jasco, Groß-Umstadt, Germany
GradiFrac system	Amersham, Uppsala, Sweden
HighLoad system	Amersham, Uppsala, Sweden
LG-980-02S gradient unit	Jasco, Groß-Umstadt, Germany
PU-1580 HPLC Pump	Jasco, Groß-Umstadt, Germany
Super loop 150 ml	Amersham, Uppsala, Sweden
UV-1575 UV-VIS detector	Jasco, Groß-Umstadt, Germany
Fluorescence detection devices	
AVIV-FIS fluorescence detection system	AVIV Biomedical, Lakewood, USA
Gelelectrophoresis and blotting devices	
Fast Blot B44 apparatus	Biometra, Göttingen, Germany
Hoefer Mighty Small II gelelectrophoresis unit	Amersham, Uppsala,Sweden
RHU10X	Roth, Karlsruhe, Germany

Microcalorimeter	
VP-ITC MicroCalorimeter	MicroCal Inc., Northampton, USA
spectrophotometer	
Varian Cary 50 Bio UV-Vis-Spectrophotometer	Varian, Palo Alto, USA
Varian Cary 100 Bio UV-Vis-Spectrophotometer	Varian, Palo Alto, USA
Jasco J715 including PTC 343 Peltier temperature device	Jasco, Groß-Umstadt, Germany
Spectrofluorometer: Fluoromax I, II and III (with autopolarizers) with temperature adjustable cuvette holder	Spex: Edison, USA
Surface plasmon resonance instrument	
BiaCore X	BiaCore, Uppsala, Sweden
Voltage sources	
LKB-GPS 200/400	Amersham, Uppsala, Sweden
EPS 3500, 301 und 1001	Amersham, Uppsala, Sweden
Additional equipment	
Air circulation incubator	New Brunswick Scientific, Nürtingen, Germany
Cell disruption machine Basic Z	Constant Systems, Warwick, England
Culture shaker Certomat S	Braun Biotech, Melsungen, Germany
Digital thermometer with thermosensor	Keithley, Cleveland, USA
Eppendorf thermomixer	Eppendorf, Hamburg, Germany
Icemachine	Ziegra, Isernhagen, Germany
Magnetic stirrer Heidolph MR 2000	Heidolph, Kelheim, Germany
Metal thermo block TB 1	Biometra, Göttingen, Germany
pH-meter	WTW, Weilheim, Germany

Thermocycler Primus	MWG, Ebersberg, Germa
Test tube roller	Heidolph, Kelheim, Germany
Sonic cell disruption device Sonifier B-12	Branson, Danbury, USA
Sonic water bath Sonsorex RK 100H	Bandelin, Berlin, Germany
Varioklav steam autoclave EP-Z	H+P, Oberschleißheim, Germany
Water bath Haake F6-K	Haake, Karlsruhe, Germany

5.1.8 Computer software

Adobe Photoshop CS5	Adobe Inc., San Jose, USA
Adobe Illustrator CS5	Adobe Inc., San Jose, USA
Adobe Acrobat Reader 7.0	Adobe Inc., San Jose, USA
Biacore X Control Software	Biacore, Uppsala, Sweden
Borwin	Jasco, Groß-Umstadt, Germany
ClustalW	Swiss EMBnet, http://www.ch.embnet.org/software/ClustalW.html
ImageJ 1.42	National Institutes of Health, USA
Microsoft Office 2007	Microsoft, Unterschleißheim, Germany
ProtParamTool	ExPasy, http://expasy.hcuge.ch/
ProtScale Tool	ExPasy , http://expasy.hcuge.ch/
OligoCalculator 3.26	Northwestern University, Chicago
Origin 8.0	OriginLab Corp.,Northampton, USA
Reference Manager 12	ISI, Philadelphia, USA
Sedview	Hayes DB and Stafford WF, 2010
UCSF Chimera 1.4.1.	Resource for Biocomputing, Visualization, and Informatics at the University of California, San Francisco, USA
Ultrascan	Dr. Borries Demeler, The Univ. of Texas Health Science Center, Texas, USA

5.2 Organisms and cultivation

5.2.1 Strains

***E.coli* Strain**	**Geno-/Phenotype**	**Origin/Company**
E. coli DH10B	F-*ara*D 139Δ(*ara leu*) 7697Δ*lac*X74 *gal*U *gal*K *mcr*A Δ(*mrr- hsd*RMS- *mcr*BC) *rps*L *dec*R 380 Δ*lac*Z ΔM15 *end*A1 *nup*G *rec*A1	Berthesda Research Laboratories, Berthesda, USA
E. coli XL1 Blue	Δ(*mcr*A) 183 Δ (*mcr*CB-hsdSMRmrr) 173 *end*A1 supE44 thi-1 *rec*A1 *gyr*A96 *rel*A1 *lac*[F`*pro*AB *lac*IqZΔM15 Tn10 (Tetr)] Su-	Stratagene, La Jolla, USA
E. coli BL21 (DE3) Codon Plus	F- *omp*T *hsdSB* (rB-mB-) gal *endA* The [argU ileY leuW CamR	Stratagene, La Jolla, USA
E. coli One-Shot BL21 Star (DE3)	F- ompT hsdSB (rB-mB-)gal dcm rne131 (DE3)	Invitrogen, Groningen, Netherlands

***S. cerevisiae* strains Acc. No. (Euroscarf)**	**Strain/genotype**	**Origin/Company**
Y00000 (wild-type)	BY4741; MATa; his3Δ1; leu2Δ0; met15Δ0; ura3Δ0	Euroscarf, Frankfurt, Germany
Y01803 (sti1Δ)	BY4741; Mat a; his3Δ1; leu2Δ0; met15Δ0; ura3Δ0; YOR027w::kanMX4	Euroscarf, Frankfurt, Germany
Y04165 (cpr6Δ)	BY4741; Mat a; his3Δ1; leu2Δ0; met15Δ0; ura3Δ0; YLR216c::kanMX4	Euroscarf, Frankfurt, Germany

5.2.2 Media and antibiotics

The following media were used for growth of *E.coli:*

LB_0	*20 g/l LB-powder*
LB_0 plates	*20 g/l LB-powder, 15 g Bacto-Agar*

Antibiotic concentrations used for growth of *E. coli*:

Ampicillin	100 µg/ml
Kanamycin	35 µg/ml
Chloramphenicol	50µg/ml

Following media were used for growth of yeast strains:

YPD	*Yeast Extract*	*5 g*
	Bacto Pepton	*10 g*
	Glucose	*20 g*
	H_2O	*ad 1 l*
YPD plates	*YPD*	
	Bacto Agar	*20 g*

5.2.3 Growth and storage of *E. coli*

Streaked cultures of *E. coli* on agar plates were incubated at 37 °C overnight and kept at 4 °C in the fridge for short-time storage. Growth of *E. coli* liquid cultures in LB media was performed upon addition of the according antibiotic in order to select for the respective plasmid. Small volumes were inoculated with a single colony from the plate, larger volumes with an overnight culture. Volumes up to 10 ml were incubated in a test tube roller, volumes larger than 10 ml were incubated in a culture shaker.
Growth of *E. coli* was monitored photometrically at a wavelength of 600 nm. An OD_{600}~ 1 roughly represents 8 x 10^8 cells. For long-term storage of bacterial strains,

700 µl of an exponentially growing culture were mixed with 300 µl of 50% sterile glycerol, shock-frozen in liquid nitrogen and stored at -80 °C.

5.2.4 Growth and storage of yeast cells

Streaked cultures of *S. cerevisiae* were incubated on YPD or CSM plates at 30 °C for two to three days. Growth in liquid cultures was performed in test tube rollers for small volumes and for large volumes in a culture shaker at 30 °C. Small volumes were inoculated with single colonies and large volumes were inoculated with stationary overnight cultures. Growth of cells was monitored photometrically at a wavelength of 600 nm. An OD_{600} of one roughly equates to $2x10^7$ cells.

For short-time storage, yeast cells were kept on the respective plates or in respective liquid medium at 4 °C. For long-term storage, 700 µl of an exponentially growing liquid culture was mixed with 300 µl of 50 % sterile glycerol and stored at -80 °C.

5.3 Methods in molecular biology

5.3.1 Plasmids and constructs

For the purification of recombinant proteins the expression vector pET28a and pET28b was used. The vector exhibits a kanamycin resistance and allows the expression of a His_6-tag at the N- or C-terminus of the protein. The expression of the recombinant protein is under the control of a lac-promotor. The constructs were sequenced at GATC (Konstanz, Germany) with T7 and pET-RP primers prior to purification. In this thesis, the following constructs were generated/used and expressed:

	Protein	Gene name	Description
1	yHsp90 yHsp90(S385C) yHsp90(S61C)	HSP82	Yeast Hsp90 and its single cysteine mutants
2	hHsp90	HSP90AB1	Human Hsp90
3	Hop	STIP1	Human Hsc70/Hsp90‐organizing protein, binds to the open conformation of Hsp90 and inhibits the ATPase activity
4	Fkbp51	FKBP4	TPR-containing PPIase, chaperoene
5	Fkbp52	FKBP5	TPR-containing PPIase, chaperoene
6	AIP/Xap2	AIP	Complex with AhR (aryl hydrocarbon receptor), PPARα (peroxisome proliferator-activated receptor α), Hbx (Hepatitis B virus X protein)
	AIP-PRD		AIP with proline rich domain from AIPL1
7	AIPL1	AIPL1	AIP like protein 1, 49% sequence identity to AIP
	AIPL1ΔPRD		AIPL1 with deletion of proline rich domain
8	p23	PTGES3	Inhibitor of Hsp90 ATPase
9	Sti1	STI1	Yeast homologue of Hop
10	Cpr6	CPR6	TPR-containing PPIase
11	Cpr7	CPR7	Homologue of Cpr6, TPR-containing PPIase
12	Aha1	AHA1	ATPase activator of Hsp90
13	Hch1	HCH1	Homologue of Aha1
14	Sba1 Sba1(S2C)	SBA1	Yeast p23 homologue and its single cysteine mutant

5.3.2 Molecular biological solutions

TAE (50×):	Tris/Acetate pH 8,0	2 M
	EDTA pH 8,0	50 mM
Gel loading buffer (10×):	Glycerin	50% (v/v)
	EDTA pH 8,0	10 mM
	Bromphenole blue	0,2% (w/v)
	Xylencyanole	0,2% (w/v)
1% Agarose solution:	Agarose	1 g
	TAE (1×)	100 ml
	Ethidiumbromide solution	1 µl
dNTP-Mix	dATP	10 mM
	dGTP	10 mM
	dCTP	10 mM
	dTTP	10 mM
Solution A	1 M CaCl2	100 ml
	2.8 M MnCl2	25 ml
	H_2O	862 ml
	sterile filtered	
Solution A - Glycerin	Glycerin (87%)	69 ml
	Solution A	331 ml

For the growth microorganisms and for molecular biological work sterile hollow-ware and solutions were used all the time. If not stated otherwise, work was performed at room temperature.

5.3.3 Preparation of plasmid DNA from *E. coli*

Plasmid DNA for analytical and preparative purposes was prepped and purified from 4 ml overnight cultures with the Wizard® Plus SV Mini-Prep kit according to the protocol of the manufacturer (Promega, Madison, USA).

5.3.4 Separation of DNA by agarose gel electrophoresis

The analytical and preparative separation of DNA was performed in 1% (w/v) agarose gels which contained 0.4 µg/ml ethidium bromide. Electrophoresis was carried out in 1x TAE running buffer with a constant voltage of 120 V. After approx. 25 min gelelectrophoresis was stopped and DNA was detected with a Bio Doc II system. 1 kb or 100 bp DNA-ladder (Peqlab, Erlangen, Germany) was used as molecular weight standard.

5.3.5 DNA isolation from agarose gels

DNA bands were excised from the gel with a scalpel and the DNA was extracted from the agarose piece using the PCR Product Purification kit (Promega, Madison, USA) according to the manufacturer's protocol. Purified DNA was stored at -20 °C.

5.3.6 Purification of PCR products and plasmids

PCR products and plasmids were purified with the PCR Product Purification kit (Promega, Madison, USA) according to the manufacturer's protocol. Purified DNA was stored at -20 °C.

5.3.7 DNA sequencing analysis

Plasmid was sequenced prior to further use. For sequencing, 15 µl DNA derived from a standard mini-prep were mixed with 15 µl of sterile H_2O_{dd} (concentration 30 ng/µl to 100 ng/µl) in an Eppendorfd cup and sent to GATC Biotech (Konstanz, Germany).

5.3.8 Transformation of *E. coli*

For the transformation of *E. coli* the respective strains were made chemically competent. Briefly, 2 ml of sterile 1 M $MgCl_2$ were added to a fresh, exponentially growing 100 ml culture of *E. coli* (OD_{600} ~ 0.5-0.8) and incubated for further 10 min at 37 °C. Subsequently, the culture was chilled on ice for 60 min and centrifuged with 4500 g at 4 °C for 5 minutes. The cell was resuspended in 20 ml Solution A and incubated on ice for further 60 min. After an additional centrifugation step at 4 °C for five minutes, the sediment was resuspended in 2 ml of Solution A-glycerol and

divided into 100 µl aliquots. Aliquots were either directly transformed with plasmid DNA or frozen in liquid nitrogen and stored at -80 °C until further use.

For transformation, 100 µl of competent cells were incubated with the transforming DNA (usually 0.5-1.0 µl of Mini-prepped plasmid DNA or 10 µl of a typical ligation reaction, respectively) and incubated on ice for 15 min. Afterwards, the cells were heat-shocked at 42 °C for 60 sec, cooled on ice for 2 min and incubated at 37 °C for 40 min in a shaking incubator after addition of 800 µl of LB_0 media. Cells were centrifuged at 1000 g for 3 min, the supernatant was discarded and the cell pellet was resuspended in the remaining media. Subsequently, the suspension was plated on the respective selection plates.

5.3.9 PCR amplification

PCR was used to selectively amplify coding regions of plasmids for further subcloning of the DNA fragments into other plasmids. To reduce the error rate in the PCR reaction, proof-reading polymerase, such as *Pwo* or *Pfu* polymerase, were used. The melting temperature of the primers was designed to be similar for both primers and was between 65 and 72 °C. The calculation of the melting temperature was performed by the internet-based program Oligo Calculator. For selective cloning, restrictions sites for restriction enzymes were attached at the ends of the primers. In general, PCR amplification reactions were carried out using the following standard mixture:

Template DNA	*1 µl (ca. 50 ng)*
10 x reaction buffer	*10 µl*
dNTP-mix	*2 µl*
Primer (50 pmol/µl)	*1 µl each*
Polymerase (5 U/µl)	*0.5 µl*
H2O $_{dd}$	*85 µl*

If PCR amplification was not successful, the so-called *hot start* method was carried out. In this case, the polymerase is added to the reaction mixture after the

temperature has reached 95 °C. This procedure prevents the formation of unspecific amplification products and increases the PCR yield.

The amplification was carried out in a Primus thermocycler (MWG Biotech, Ebersberg, Germany). The settings were adjusted according to the length of the desired PCR product and the type of polymerase. Principially, 35 cycles of the following program were operated:

Denaturation	*95 °C 30 s*
Annealing	*45-55 °C 30 s*
Synthesis	*68 °C (or 72 °C) 1 min per 1 kb of product*

5.3.10 DNA digestion by restriction endonucleases

Restriction digests were performed both for analytical control of a plasmid and for preparative extraction of cutted DNA fragments. Depending on the purpose different volume were chosen. For an analytical digest, 1 µl of 10 x reaction buffer and 0.5 µl of one or two restriction enzyme(s) were added to 8 µl of plasmid DNA from a typical Mini prep and incubated at 37 °C for three hours. Subsequently, the digest was verified by agarose gel electrophoresis. For the preparative digest of DNA, 24µl of water, 5 µl of 10 x reaction buffer and 1 µl of one or two restriction enzymes were added to 20 µl of a typical plasmid Mini prep or purified PCR-DNA and the mixture incubated for three hours at 37 °C. Subsequently, DNA fragment was analyzed by agarose gel electrophoresis and purified with the Promega PCR Product Purification kit.

5.3.11 Dephosphorylation of DNA ends

In order to prevent self-ligation, digested vectors were treated with shrimp alkaline phosphatase after the restriction digest. For this purpose 5 µl of alkaline phosphatase (0.5 U) and 5 µl of 10 x reaction buffer were added to 40 µl of digested vector and the mixture incubated at 37 °C for one hour. Afterwards, the plasmid was purified by agarose gel electrophoresis and the Promega PCR product purification kit.

5.3.12 Ligation of DNA fragments

Generally, 600 ng of fragment DNA was ligated with 200 ng of vector DNA. For this purpose, the respective volume of DNA were mixed with 2 µl of 10 x ligation buffer, 2 µl of T4 DNA ligase (approx. 2 U) and incubated at 4 °C over-night.

5.4 Preparative methods

5.4.1 Expression kinetics

Expression kinetics was performed with new *E. coli* expression construct before large scale expression for optimizing the culture conditions. 250 µl of LB media with the respective antibiotic were inoculated with 1 ml of an overnight culture in stationary phase and incubated at different temperatures. The IPTG concentration was held constant at 1 mM because it was observed that changing the IPTG concentrations had only minor effects on solubility of the target proteins. Every hour 1 ml samples were taken and the OD_{600} was determined. For expression analysis the pellet of a 1 ml sample was resuspended in 100 µl 1x Laemmli buffer x OD_{600}. This allowed evaluation if there is an expression of target protein independent of the cell density at any time point. At the end of the expression kinetics, the remaining cells were centrifuged and the pellet resuspended in lysis buffer. Subsequently, the cells were lysed in a Basic Z model cell disruption system (Constant Systems, Warwick, UK) at a pressure of 1.8 kbar and centrifuged at 18,000 r.p.m. for 45 min. A sample was taken from the supernatant, the supernatant discarded, the pellet resuspended in the same volume of lysis buffer and a sample taken from the resuspended pellet. Both samples were mixed with 4x Laemmli buffer and loaded on an SDS-PAGE gel together with the other samples. This procedure allowed estimation of how much of the expressed protein was soluble.

5.4.2 Growth and storage of *E.coli* cells

E. coli strain BL21 (DE3) Codon Plus was used to express protein. For a large expression, a flask of 100 ml of an overnight culture were mixed with four flasks of 2 l of fresh LB media containing the respective antibiotic. The flasks were shaken at 37 °C till an OD_{600} of 0.6 to 0.8 and induced with 1 mM IPTG. Cells were grown for

an additional 5-6 hours at 37 °C or overnight at 30 °C. Cells were harvested by centrifugation with 6000 r.p.m. at 8 °C for 10 min.

5.4.3 Cell disruption

In order to access the recombinantly produced proteins, cells had to be lysed. The pellets of the harvested *E. coli* or *S. cerevisiae* cells were resuspended in lysis buffer. Lysis buffer usually was Buffer 1 of the first chromatography step including a small amount of DNAse I and Serva HP protease inhibitor mix. The resuspended cells were lysed in a Basic Z model cell disruption system (Constant Systems, Warwick, England) at a pressure of 1.8 kbar *(E.coli)* or 2.6 kbar (*S. cerevisiae)*. In this system, the cell suspension is accelerated with high pressure through a cone against a metal plate. The shearing forces that develop at the exit point of the cone and the intensive turbulence at the metal plate destroys the cell integrity. To clear the lysate it was centrifuged at 8 °C and 18.000 r.p.m. for 45 min.

5.5 Methods in protein purification

The following chromatographic methods were applied for protein purification in this work. The quality of purification was controlled with SDS-PAGE after each step.

5.5.1 Affinity chromatography

Affinity chromatography is suitable to purify a particular protein from a mixed sample. It is based on a specific and reversible interaction of a molecule to a matrix-bound binding partner. The interaction with the ligand is used to selectively bind the target molecule from a complex mixture. The elution of the target molecule is either achieved by competitive displacement or by a conformational change induced by the change of pH. The Ni-affinity chromatography used in this work is based on an interaction between a nickel matrix and a His_6-tag (six histadine amino acids) that is fused to the protein of interest. The Ni^{2+}-ion is bound to an agarose bead by chelation using nitroloacetic acid (NTA) beads. Elution is achieved by increasing the concentration of imidazole in the running buffer which competes with the His_6-tag for binding to the Ni-NTA matrix.

5.5.2 Ion exchange chromatography

Ion exchange chromatography is a popular method for the purification of proteins or other charged molecules. The principle is based on the attraction of oppositely charged particles. In cation exchange chromatography, the positively charged molecules are attracted to a negatively charged matrix. On the contrary, in anion exchange chromatography, negatively charged molecules are attracted to a positively charged matrix. Proteins have either a positive or negative net charge depending on their side-chains as well as the carboxyl- and amino-termini. This characteristic enables them to bind to an oppositely charged carrier material. Elution of a bound protein occurs by a gradually increase in ionic strength of the running buffer. Thereby electrostatic interactions between the protein and the column material are weakened and bound proteins dissociate from the matrix. Proteins carry a net positive charge below the isoelectric point and a negative charge above it. Therefore both the column material and the running buffer are chosen in dependence of the amino acid composition of the protein.

5.5.3 Gel filtration chromatography

Proteins can be separated from each other by their hydrodynamic radius with gel filtration chromatography. The matrix of these columns is composed of a three-dimensional network of defined pore size. Proteins that have a larger diameter than the pore size are not capable to penetrate the pores of the material and hence elute with the void volume of the column. However, smaller particles can penetrate the pores and therefore have a larger way to travel and elute later compared to bigger molecules. Consequently, the separation range of a gel filtration column is determined by the pore size of the carrier material. Generally, buffers with higher ionic strength are used as running buffers to suppress unspecific ionic interactions between proteins and the matrix. In this work, precast columns of the type Superdex 75 Prep Grade and Superdex 200 Prep Grade were used depending on the required separation range.

5.5.4 Concentration of proteins

To concentrate protein solutions with less than 15 ml volume Millipore Ultra-15 concentrators were used. The solution was concentrated by centrifugation at 3500 r.p.m and 4 °C until the desired concentration was reached. In principle, the protein solution is pressed through a membrane with a defined pore size and molecular weight cut-off and the proteins are concentrated above the membrane. Depending on the size of the proteins, 10 kDa or 30 kDa molecular weight cut-offs were used in this work. For larger volumina Amicon cells were used that press protein solutions through filters with a defined molecular weight cut-off with nitrogen gas pressure at 3 bar. Essentially, the same cut-offs like with the Ultra-15 devices were used.

5.5.5 Protein dialysis

To change the buffer composition the protein was dialyzed in a dialysis bag against the 100-1000-fold of the original volume at a temperature of 4 °C. Alternatively, the protein solution was buffered in new buffer with a HiPrep Desalting column (Amersham, Uppsala, Sweden).

5.5.6 Standard purification of His6-tagged proteins

Solutions

Buffer 1: 40 mM Sodium phosphate, pH 7,5
200 mM KCl
5 mM Imidazole

Buffer 2: *40 mM Sodium phosphate, pH 7,5*
200 mM KCl
300 mM Imidazole

Buffer 3: *40 mM HEPES, pH7.5, 20mM KCl,(1mM DTT)*

Buffer 4: *40 mM HEPES, pH7.5, 1M KCl,(1mM DTT)*

Buffer 5: *40 mM HEPES, pH 7.5, 150 mM KCl,(1mM DTT)*

Buffer 6: *40 mM HEPES, pH 7.5, 50mM KCl,(1mM DTT)*

Procedure

100 ml overnight culture was used to inoculate eight liters of LB media (four 2 l

flasks) and the respective antibiotic to maintain the expression plasmid. Generally, cultures were grown to an OD_{600} of 0.5-0.7 at 30 °C and induced with 1 mM IPTG. Subsequently, cells were grown over-night and harvested the next day. Cells were centrifuged at 6000 rpm at 8 °C for 10 min and resuspended in Buffer 1 containing a DNase I and Serva HP Protease Inhibitor Mix. Cell was lysed in a disruption system with a pressure of 1.8 kbar. The soluble fraction was isolated by centrifugation at 18.000 rpm and 8 °C for 45 min. The supernatant was loaded on a His-trap FF column (1.5 ml/min) which was pre-equilibrated using Buffer 1. 7 % Buffer 2 were applied to wash away the unspecific bindings. The protein was eluted by a step gradient to 100% buffer 2. The eluted protein was dialyzed against the binding buffer for the IEC (buffer 3). After overnight dialysis, the protein was load onto a Rescource Q or Rescource S column which was pre-equilibrated using Buffer 3. Protein was eluted in a linear salt gradient which consisted of a mixture of buffer 3 and 4. The desired protein was collected, concentrated and loaded onto a gel filtration column (Superdex 75 Prep Grade or Superdex200 Prep Grade depends on the size of protein) which was pre-equilibrated by buffer 5. The protein of interest was eluted, collected and dialyzed against buffer 6. The dialyzed protein was concentrated and frozen to aliquots in liquid nitrogen and stored at -80 °C.

5.6 Methods in protein analytics

5.6.1 Solutions in protein chemistry

Running buffer (10x)	Tris	0.25 M
	Glycin	2 M
	SDS	1% (w/v)
5x-Laemmli loading buffer	SDS	10% (w/v)
	Glycerin	50% (w/v)
	Tris	300 mM
	Bromphenol blue	0.05% (w/v)
	2-Mercaptoethnal	5% (v/v)
Transfer buffer	Glycine	36g
	Tris	7.6g
	Menthanol	500ml
	SDS	0.3% (w/v)
	H_2O	ad 2.5 l
PBS(-T)	NaCl	5.84 g
	Na_2HPO4	11.5 g
	NaH_2PO4	2.96 g
	H_2O	ad 1 l
	(Tween-20	1 ml)

5.6.2 SDS-polyacrylamide electrophoresis

Discontinuous SDS-Polyacrylamide gelelectrophoresis (SDS-PAGE) was carried out in a buffer system to analyze protein extracts and cell lysates. The separation occurs on vertical 7 x 9 x 0.075 cm SDS-PAGE gels in a SDS-PAGE electrophoresis chamber at a constant current of 30 mA per gel for 60 min. Before loading on the gel, 16 µl of the protein solution was mixed with 4 µl 5x Laemmli loading buffer and heated at 95 °C for 3 min. To estimate the molecular weight of the proteins, either LMW marker or HMW marker was loaded on the gel depending on the size of the target protein. In the case of a subsequent Western-Blot, a prestained marker was

used instead.

5.6.3 Coomassie staining of SDS gels

Gels were stained using a modified protocol first described by Fairbanks and others to visualize proteins after SDS-PAGE. SDS polyacrylamide gels were stained in Fairbanks Solution A and then destained in Fairbanks Solution D. By heating up the solutions the incubation times could be shortened considerably. Staining was performed for 5 min, destaining was carried out for 45 min. The detection limit of this method is approx. 50 ng of the respective protein.

Fairbanks solutions:

Solution A	25% (v/v) Isopropanol, 10% (v/v) technical grade acetic acid, 0.05% Coomassie Blue R
Solution D	10% technical grade acetic acid

5.6.4 Pull downs from yeast extracts

Purified His_6-tagged Sti1 or Cpr6 was incubated with 10 µl Ni-Sepharose High Performance beads (GE Healthcare, Munich, Germany) in reaction tubes at room temperature for 30 min. Beads were spun down in a table top centrifuge at 1000 g for 30 seconds and the supernatant was discarded. The pellet was washed twice with binding buffer containing 40 mM HEPES, 50 mM KCl, 5 mM $MgCl_2$, pH7.5 (standard buffer) and then incubated with 500 µl precleared lysates of a STI1 or CPR6 deletion strain (STI1::kanMX and CPR6::kanMX, accession numbers Y01803 and Y04165 respectively, from the Euroscarf collection (293)), respectively at room temperature for 60 min. Beads again were spun down in a centrifuge at 1000 g for 30 seconds and the unbound lysate was discarded. Subsequently, the bound complexes were washed twice with standard buffer, twice with washing buffer containing 40 mM NaH_2PO_4, 150 mM NaCl and 50 mM imidazole and once with washing buffer containing 0.1% Zwittergent 3-14 (Calbiochem, La Jolla, USA). The bound complexes were eluted with 100 µl elution buffer containing 40 mM NaH_2PO_4, 500 mM NaCl and 300 mM imidazole. The eluted protein was separated by SDS-

PAGE and then transferred to a PVDF membrane for immunodetection. Detection was achieved with polyclonal antibodies directed against Sti1, Cpr6, Ssa1/Hsp70, Sba1, Aha1 and Hsp90 and a secondary α-rabbit-POD antibody (GE Healthcare, Munich, Germany). For quantification, purified proteins in different concentrations were used as standards. Bands were scanned and quantification of the bands was performed with Image J. Protein amounts were divided by their molecular weights in order to obtain relative stoichiometries.

5.6.5 Immunoblotting (Western Blot)

Proteins that were separated on a gel by SDS-PAGE were electrophoretically transferred on a PVDF or nitrocellulose membrane in a Semi-Dry blotting apparatus (Biometra, Göttingen, Germany). First, the SDS-PAGE gel, six Whatman 3MM filter papers and a methanol activated PVDF or nitrocellulose membrane were incubated in transfer buffer for five minutes. Second, a stack was formed with three Whatman 3MM filter papers at the bottom, the PVDF membrane with the SDS-PAGE gel above in the middle and three Whatman 3MM filter papers on the top. This stack was then placed in the Semi-Dry blotting apparatus and the transfer was started with a current of 72 mA per SDS-PAGE gel (1.5 mA/cm^2) for one hour. After transfer, the PVDF membrane was incubated in Roti-Block solution for 30 min to block unspecific binding sites. Nitrocellulose membranes were incubated in PBS-T containing 5% milk powder for 1 hour, respectively. The membrane was then incubated in a solution containing the primary antibody diluted in PBS-T/1% milk powder for 60 min. The dilution was dependent on the primary antibody and was individually different (mainly 1:4000). After three washing steps with PBS-T for 10 minutes, the membrane was incubated with secondary antibody for 45 minutes. The secondary antibody was either an anti-rabbit or anti-goat peroxidase-conjugated IgG and was diluted 1:5000 in PBS-T/1% milk powder. After three washing steps with PBS-T for 10 minutes, the antibody-enzyme conjugate was detected with an ECL detection kit (Amersham, Uppsala, Sweden). The detection method is based on chemoluminescence. In the presence of H_2O_2, peroxidase catalyzes the oxidation of cyclic diacylhydrazineluminol which is accompanied by light emission. To start the

reaction, a mixture of 975 µl of Reaction Buffer 1 (ECL1) and 25 µl of Reaction Substrate (ECL2) was added to the PVDF/nitrocellulose membrane. The membrane was placed between two plastic foils and light emission was detected on an X-Omat X-ray film (Kodak, Rochester, USA) by incubation up to 10 minutes.

5.6.6 Isothermal titration calorimetry (ITC)

Isothermal titration calorimetry (ITC) is a thermodynamic technique that directly measure the heat absorbed or released during a bimolecular interactions. The binding constants, reaction stoichiometry, enthalpy and entropy can be obtained from the ITC measurement. In the experiment, aliquots of a high concentration titrant are injected in the cell containing protein solution. Upon each titration the amount of heat absorbed or released in measured.

In this thesis, ITC experiments were used to determine the stoichiometry of the interaction between Hsp90 and AIP/Xap2 or Hop using a MicroCal VP-ITC (GE Healthcare, Munich, Germany) instrument operated at 25 °C. Buffer conditions were 40 mM HEPES/KOH pH 7.5, 50 mM KCl. Protein concentrations were 20 µM Hsp90 in the reaction chamber and 200 µM AIP/Xap2 or Hop in the injection syringe. A total of 36 injections of 8 µl were made. The intervals between the injections were six minutes. Data analysis was performed by following the manufacturer's manual, using the models for one binding site and for stepwise binding of two identical ligands in a cooperative system.

5.6.7 Protein labeling

Proteins were labeled at cysteine residues using Alexa Fluor 488 maleimide (Invitrogen, Carlsbad, USA). This dye reacts with thiol-groups to give tioether-coupled products. Disulfide bonds were reduced by supplementing the protein solution with a 10 fold excess of DTT. Before the labeling reaction was started, the protein was dialyzed against the labeling buffer (40 mM Hepes, pH 7.5, 50 mM KCl) in order to remove excess DTT. In general, a threefold molar excess of Alexa Fluor 488 was solved in 20 µl dimethyl sulfoxide (DMSO) and added drop wise to 500 µl protein solution. The reaction was allowed to proceed for 2 hours at room temperature or overnight at 4 °C protected from light. The reaction was quenched by

addition of 10 mM DTT and the protein was separated from free label by size-exclusion chromatography on a Superdex 75HR column (GE Healthcare, Ffreiburg, Germany) in a buffer containing 40 mM Hepes, pH 7.5, 50 mM KCl, 1 mM DTT. In this work, AIP/Xap2 was covalently lysine-coupled to the fluorescent dye Fluorescein (Invitrogen, La Jolla, USA), by incubating with the five times molar excess of the dye under the conditions recommended by the manufacturer. The coupling reaction of Xap2 was quenched by the addition of 1 M Tris, pH 8.5 and the protein was separated as described above. The concentration of the labeled protein and the degree of labeling was determined by the following equation:

$$\text{c(Protein)} = \frac{A_{280} - (A_{494} \times \textit{Correction Factor})}{\varepsilon_{protein}} \times \text{dilution factor}$$

$$\text{Moles dye per mole protein} = \frac{A_{494}}{\varepsilon_{fluor} \times \text{ protein concentration}} \times \text{ dilution factor}$$

5.6.8 Analytical ultracentrifugation

Analytical ultracentrifugation (aUC) is widely used to determine the exact molecular mass of a protein under native conditions (294). In this work aUC was used for the analysis of the oligomerization states as well as protein-protein interactions.

To analyze protein-protein interactions, aUC with a fluorescence detection device (E_m~520nm) was used (295,296). In the aUC experiments, the protein with lower molecular mass was labeled at cysteine residues or lysine residues with the Alexa Fluor 488 (Invitrogen, Carlsbad, USA) or Fluorescein (Invitrogen, La Jolla, USA) as described before. The labeled protein was subjected to aUC in a Beckman XL-A analytical ultracentrifuge equipped with an AVIV-FIS fluorescence detection system (AVIV Biomedical, Lakewood, USA). Sedimentation experiments were performed in standard 2-sector centerpieces in a Ti_{50} 8-hole rotor at 42,000 r.p.m. Scans at an excitation wavelength of 488 nm were recorded in 90 s intervals. The program SEDVIEW was used for the initial evaluation of the sedimentation run. Ultracentrifugation experiments were analyzed by converting sedimentation raw data

into dc/dt profiles to compare the S-values. The dc/dt analysis was performed by subtracting scans from each other and converting them into dc/dt profiles according to the method described by Stafford (297).

5.7 Spectroscopy

For all spectroscopic analyzes recorded spectra were corrected for the respective buffer spectra as reference. The reference buffer was either the dialysis buffer or the gel filtration buffer at the last purification step.

5.7.1 UV absorption spectroscopy

Proteins and peptides contain several function groups which absorb light. The peptide bond absorbs light in the far UV range (180 nm-230 nm) through its carbonyl group. The aromatic amino acids such as tyrosine and tryptophan also absorb light in the region between 240nm to 300nm. Besides, the disulfide bridges show an absorbance band near 260nm. The following table summarizes important determinants of protein absorption, their molar extinction coefficients and their wavelengths of maximum absorption in water.

Amino acid	**λ_{max} (nm)**	**ε_{max} (M^{-1} cm^{-1})**
Tryptophan	280	5600
Tyrosine	274	1400
Phenylalanine	257	200
Disulfide bridge	250	300
Peptide bond	190	~7000

UV spectroscopy was used in this work to determine the protein concentration of protein solutions. The protein concentration can be easily calculated if the molar extinction coefficient of the protein is known and the absorption of the protein solution at 280 nm is measured. The Lambert-Beer law gives the following relationship:

$$c = \frac{A}{\varepsilon_{280nm} \times d}$$

In the equation A is the absorbance at 280 nm, ε_{280} nm is the molecular extinction coefficient, d is the thickness of the cuvette and c is the concentration in mol/l. The extinction coefficient for a certain protein can be calculated on the basis of its amino acid composition. Program ProtParam provided by http://www.expasy.org was used to calculate the extinction coefficient of purified proteins (298-300).

5.7.2 Fluorescence spectroscopy

Fluorescence is the emission of light by a substance that has absorbed light or other electromagnetic radiation of a different wavelength. The occurrence of fluorescence is a three stage process including excitation, a short excited-state life time and fluorescence emission. In proteins, there are three amino acids with intrinsic florescence properties, tryptophan, tyrosine and phenylalanine. Tryptophan fluorescence is widely used in the study of protein folding. In the native folded state, it is generally located in the core of the protein, whereas in the partially folded or unfolded stated, it become exposed to the solvent and changes the fluorescence properties.

FRET is the non-recitative transfer of energy from an excited fluorophore (donor) to another fluorophore (acceptor) without emission of a photon when the two molecules are in very close proximity (1-10 nm). The efficiency of FRET is dependent on the inverse sixth power of the distance between the donor and acceptor fluorophore. The dependence on the distance renders FRET measurement a useful tool to study the protein -protein interactions. In this study, yeast Hsp90 was coupled with the acceptor dye ATTO550 (ATTO-TEC, Siegen, Germany) at an engineered cysteine residue in the middle domain (Cys385) or N-terminal domain (Cys61) as described earlier. Sti1 or other co-chaperone was labeled with the donor dye AlexaFluor488 on cysteine residues. Addition of ATTO550-Hsp90 (*Hsp90) to a solution of AlexaFluor488-Sti1 (*Sti1 or other co-chaperone) resulted in a marked increase in the acceptor fluorescence and a decrease in the donor fluorescence, implying that efficient FRET-transfer occurred between *Sti1 (or *other co-chaperone) and *Hsp90. Emission spectra from 510 nm to 650 nm were recorded using a Fluoromax 3

spectrometer (HORIBA Jobin Yvon, Munich, Germany) at 25 °C. Binding kinetics was monitored at the same temperature.

5.7.3 Circular dichroism (CD) spectroscopy

Circular dichroism is observed when optically active matter absorbs left and right hand circular polarized light with different intensity. It is measured with a CD spectropolarimeter, which is commonly used to assess the structural features of asymmetric molecular. The optical activity of protein is the result of asymmetric carbon atoms and/or aromatic amino acids. The complementary structural information can be obtained from several different spectral regions, such as the secondary structure composition and tertiary structure fingerprint. The absorption around 240nm and below is mainly due to the peptide bond. The different secondary structure elements in the proteins give rise to different characteristic spectra in the far-UV (summarized below).

Secondary structure	**Far UV CD**
α-helix	Negative band at about 222nm and a negative and positive couple at about 208nm and 190nm
β-sheet	Negative band at about 215nm and a positive band around 198nm
Random coil	Negative band at about 195nm and positive band at around 212nm

The spectra in the region 260nm to 320 nm arise from the aromatic amino acids. Trpytophan, Tyrsine and Phenylalanine show different characteristic wavelength profiles (summarized below). The information gained from this region indicates the tertiary environment around the aromatic residues.

Amino acid	**λ_{max} (nm)**	**$\varepsilon_{max}(M^{-1}cm^{-1})$**
Tryptophan	280	5700
Tyrosine	274	1400
Phenylalanine	257	200
Disulfide bond	250	300

All spectra were buffer corrected and normalized to the mean residual weight ellipticity Θ_{MRW} according to the following equation:

$$\Theta_{MRW} = \frac{\Theta \times 100}{d \times c \times N_{aa}}$$

with Θ as the obtained ellipticity (mdeg), d cell length (cm), c concentration (mM) and N_{aa} number of amino acids.

The measurement parameters used in this work are summarized below:

Parameter	**Far UV**
Wavelength (nm)	260-195
Speed (nm/min)	20
Response time (s)	4
Band width (nm)	1
Accumulation	8
Temperature	20
Cuvette thickness	0.1cm
Protein concentration	0.1 mg/ml

For determination of thermal stability, 0.1 mg/ml protein samples were heated with 20°C/h from 20°C to 80°C in a 1 mm Quartz cuvette and changes in CD signal at a certain wavelength was observed. The midpoint of the equation was determined by a Boltzmann fit.

5.7.4 Surface Plasmon Resonance spectroscopy

Surface plasmon resonance (SPR) spectroscopy is a powerful tool to determine the bimolecular interactions. SPR is based on the attenuation of reflected light when the incoming light is reflected on the interface of about 50nm thick metal layer through a prism, at a certain angle of incidence in total internal reflection. It is very sensitive to the change of the reflective index of the media. On the metal layer side, the irradiated light is totally reflected and generates the weak energy wave called evanescent wave, and the interaction between the materials induced on the sensor-chip surface differ the dielectric constant and influence the surface plasmon. Thus, the change of resonance can be used to measure the interactions between different molecules. The signal measured in resonance units (RU) is directly correlated to the amount of protein bound. Typically 1000 RU equals to 1 ng of protein per mm^2.

SPR experiments were performed with a Biacore X Instrument (Uppsala, Sweden). A CM5 chip was coupled with yeast Hsp90 or other proteins in a buffer containing 20 mM KH_2PO_4, pH4.5 using the amine coupling reagents EDC/NHS, yielding 1500 resonance units (RU) of immobilized protein. Measurements were performed at 25 °C in standard buffer at a flow rate of 20 µl/min. 65 µl injections of different protein concentrations were performed. Plateau values during binding reactions were determined and plotted against the concentration of injected protein. The corresponding curves were analyzed as suggested by the manufacturer using the Origin software (OriginLab Corporation, Northampton, USA).

5.8 Activity assay for proteins in vitro

5.8.1 ATPase assay with an ATP-regenerating system

The Hsp90 ATPase activity was characterized using an assay that is coupled to NADH consumption. The formed ADP is rapidly converted to ATP in the presence of phosphoenolpyruvate, pyruvate kinase, NADH and lactate dehydrogenase. Absorption at 340 nm is used to follow the conversion of NADH to NAD^+. In general, the following premix was prepared for the reaction:

Assay buffer (40 mM Hepes, 20 - 150 mM KCl, depending on the protein; $MgCl_2$)	*8500 µl*
100 mM phosphoenolpyruvate	*240 µl*
50 mM NADH	*35 µl*
Pyruvate kinase suspension (Roche Diagnostics)	*12 µl*
Lactate dehydrogenase suspension (Roche Diagnostics)	*44 µl*

100 µl of this premix were used for each 150 µl assay. The remaining volume was used for addition of the ATPase, ATP, co-chaperones or HKM buffer. The assays were conducted in a Cary 50 Bio UV/VIS spectrometer at 37 °C. Data were recorded with an average time of 1 sec. After a stable baseline was observed, the reaction was started by adding indicated amounts of ATP and measurements were performed for 20-30 min. The hydrolysis rates were calculated using the differential molar extinction coefficient of NADH and NAD^+ of 6200 $cm^{-1}M^{-1}$ at 340 nm.

$$v_{spez} = \frac{m}{d \times \left(-6200 \frac{1}{cm \times M} \right) \times c_{ATPase}}$$

m is the slope of the resulting lines, d is the thickness of the cuvette in cm and c_{ATPase} is the concentration of the respective ATPase in µM.

KM values for ATP were obtained by fitting the resulting plot with the ichaelis-Menten Equation:

$$v_{spez} = k_{cat} \times \frac{c}{c + K_M}$$

In the experiments, the concentration of Hsp90 was 4 µM. Assays were measured at 30 ºC (114). The Hsp90-specific ATPase activity was inhibited by adding 50 µM of the inhibitor radicicol (Sigma, St. Louis, USA) and subtraction of the remaining activity as background. The assays were evaluated using the Origin software (OriginLab Corporation, Northampton, USA).

5.8.2 Aggregation assay with citrate synthase

Citric acid synthase (CS) has a molecular mass of 49 kDa and forms homodimeres. Unfolding takes place at temperatures above 43°C leading to a loss of activity and later on to the aggregation of CS and thus it is usually used as a model substrate to understand the mechanism of protein aggregation and examine the chaperone activity (235). For the aggregation assay, 0.5 µM CS (monomer) was thermally denatured by incubation at 43 °C in 40 mM Hepes (pH 7.5) for 45 minutes. Aggregation of non-native CS was measured by monitoring the increase of turbidity at 360 nm in a UV-VIS spectrophotometer equipped with a temperature control unit using micro-cuvettes (120 µl) with a path length of 1 cm.

5.8.3 Activity assay with citrate synthase

Citrate synthase catalyzes the reaction between acetyl coenzyme A (acetyl CoA) and oxaloacetic acid (OAA) to form citric acid. The hydrolysis of the thioester of acetyl CoA results in the formation of CoA with athiol group (CoA-SH). The thiol reacts with the DTNB in the reaction mixture to form 5-thio-2-nitrobenzoic acid (TNB). This yellow product (TNB) is observed spectrophotometrically by measuring absorbance at 412 nm.

This assay was used to analyze the impact of AIPL1 or AIP on the thermal-induced unfolding behavior. 150 nM CS was mixed with AIPL1, AIP or their variants. Reactions mixtures were incubated at 25 °C in the cuvettes.

50 mM TE-buffer pH 8,0	*0.93 ml*
10 mM DTNB (in TE-buffer pH 8,0)	*0.01 ml*
10 mM Oxalacetat (in 50 mM Tris/Base)	*0.01 ml*
5 mM Acetyl-CoA (in TE-buffer pH 8,0)	*0.03 ml*

Aliquots from the CS mixture incubating at 43°C were mixed with the preincubated reaction mixture to assay the activity. The activity without incubation at 43°C was set to 100% as native protein. The specific activity of CS can be calculated using the extinction coefficient of the reacted DTNB of 13,600$M^{-1}cm^{-1}$.

6 Abbreviations

APS	Ammoniumpersulfate
ATPase	ATP-Hydrolase
AUC	Analytical ultracentrifugation
Bip	Heavy Chain Binding Protein
BSA	Bovin serum albumin
CD	Circular dichroism
Da	Dalton
DNA	Deoxyribonucleic acid
ε	Molar extinction coefficient
E.coli	*Escherichia coli*
EDC	1-Ethyl-3-(dimethylaminopropyl)-cardodiimid-HCl
EDTA	Ethylenediamine-tetraecetic acid
FPLC	Fast Protein Liquid Chromatography
FRET	
g	Gram
GdmHcl	Guanidinium hydrochloride
h	hour
Hcl	hydrochloric acid
HEPES	4-(2-hydroxyethyl)-1-piperazineethanesulfonic acid
HPLC	High Performance Liquid Chromatography
HR	High Resolution
Hsp	Heat Shock Proteins
ITC	Isothermal Titration Calorimetry
KDa	Kilodalton
λ	Wavelength
l	Liter
min	Minutes
ml	Milliliter

mM	Millimolar
µM	Micromolar
MW	Molekular Mass
NHS	N-hydroxy-succimid
nm	Nanometer
nM	Nanomolar
OD	Optical density
PAGE	Polyacrylamide gel electrophoresis
PEP	Phosphoenole pyruvate
PDI	Protein disulfide isomerase
pH	Potential of Hydrogen
PI	Isoelectric point
PPIase	Peptidyl-Prolyl-Isomerase
RNA	Ribonucleic acid
RNAase	Ribonuclease
RT	Room temperature
s	Second
S.cerevisiae	*Saccharomyces cerevisiae*
SDS	Sodium dodecyl sulfate
SPR	Surface Plasmon Resonance
TEMED	N, N, N', N'-Tetramethylethylendiamine
Tris/Hcl	Trihydroxymethylaminomethan Hydrochloride
rpm	Rounds per minute
UV	Ultraviolet
V	Volt
v/v	Volume per volume
w/v	Weight per volume

7 References

1. Dill, K. A., and Chan, H. S. (1997) *Nat Struct Biol* 4, 10-19
2. Fink, A. L. (2005) *Curr Opin Struct Biol* 15, 35-41
3. Dill, K. A., Bromberg, S., Yue, K., Fiebig, K. M., Yee, D. P., Thomas, P. D., and Chan, H. S. (1995) *Protein Sci* 4, 561-602
4. Anfinsen, C. B. (1973) *Science* 181, 223-230
5. Seckler, R., and Jaenicke, R. (1992) *FASEB J* 6, 2545-2552
6. Levinthal, C. (1968) *J Chim Phys* 65, 44-45
7. Ohgushi, M., and Wada, A. (1983) *FEBS Lett* 164, 21-24
8. Creighton, T. E. (1997) *Trends Biochem Sci* 22, 6-10
9. Brockwell, D. J., Smith, D. A., and Radford, S. E. (2000) *Curr Opin Struct Biol* 10, 16-25
10. Bieri, O., Wildegger, G., Bachmann, A., Wagner, C., and Kiefhaber, T. (1999) *Biochemistry* 38, 12460-12470
11. Tezcan, F. A., Findley, W. M., Crane, B. R., Ross, S. A., Lyubovitsky, J. G., Gray, H. B., and Winkler, J. R. (2002) *Proc Natl Acad Sci U S A* 99, 8626-8630
12. Wolynes, P., Luthey-Schulten, Z., and Onuchic, J. (1996) *Chem Biol* 3, 425-432
13. Veitshans, T., Klimov, D., and Thirumalai, D. (1997) *Folding & design* 2, 1-22
14. Gruebele, M. (2002) *Curr Opin Struct Biol* 12, 161-168
15. Clark, P. L. (2004) *Trends Biochem Sci* 29, 527-534
16. Lorimer, G. H. (1996) *FASEB J* 10, 5-9
17. Braakman, I., Hoover-Litty, H., Wagner, K. R., and Helenius, A. (1991) *J Cell Biol* 114, 401-411
18. Ellis, R. J. (2001) *Trends Biochem Sci* 26, 597-604
19. van den Berg, B., Ellis, R. J., and Dobson, C. M. (1999) *EMBO J* 18, 6927-6933
20. Soto, C. (2003) *Nature reviews. Neuroscience* 4, 49-60
21. Winklhofer, K. F., Tatzelt, J., and Haass, C. (2008) *EMBO J* 27, 336-349
22. Dobson, C. M. (2003) *Nature* 426, 884-890
23. Gothel, S. F., and Marahiel, M. A. (1999) *Cell Mol Life Sci* 55, 423-436
24. Wilkinson, B., and Gilbert, H. F. (2004) *Biochim Biophys Acta* 1699, 35-44
25. Hartl, F. U. (1996) *Nature* 381, 571-579
26. Goldberger, R. F., Epstein, C. J., and Anfinsen, C. B. (1963) *J Biol Chem* 238, 628-635
27. Bulleid, N. J., and Freedman, R. B. (1988) *Nature* 335, 649-651
28. Fischer, G., Bang, H., and Mech, C. (1984) *Biomed Biochim Acta* 43, 1101-1111
29. Munro, S., and Pelham, H. R. (1987) *Cell* 48, 899-907
30. Freedman, R. B., Brockway, B. E., and Lambert, N. (1984) *Biochem Soc Trans* 12, 929-932
31. Li, S. J., Hong, X. G., Shi, Y. Y., Li, H., and Wang, C. C. (2006) *J Biol Chem* 281, 6581-6588
32. Tian, G., Xiang, S., Noiva, R., Lennarz, W. J., and Schindelin, H. (2006) *Cell* 124, 61-73
33. Fischer, G., and Schmid, F. X. (1990) *Biochemistry* 29, 2205-2212
34. Lu, K. P., Finn, G., Lee, T. H., and Nicholson, L. K. (2007) *Nat Chem Biol* 3, 619-629
35. Takahashi, N., Hayano, T., and Suzuki, M. (1989) *Nature* 337, 473-475
36. Fischer, G., Wittmann-Liebold, B., Lang, K., Kiefhaber, T., and Schmid, F. X. (1989) *Nature* 337, 476-478
37. Harding, M. W., Galat, A., Uehling, D. E., and Schreiber, S. L. (1989) *Nature* 341, 758-760
38. Siekierka, J. J., Hung, S. H., Poe, M., Lin, C. S., and Sigal, N. H. (1989) *Nature* 341, 755-757
39. Laskey, R. A., Honda, B. M., Mills, A. D., and Finch, J. T. (1978) *Nature* 275, 416-420
40. Ellis, R. J. (1993) *Philos Trans R Soc Lond B Biol Sci* 339, 257-261

41. Hartl, F. U., and Hayer-Hartl, M. (2002) *Science* 295, 1852-1858
42. Gething, M. J., and Sambrook, J. (1992) *Nature* 355, 33-45
43. Ruddock, L. W., and Klappa, P. (1999) *Curr Biol* 9, R400-402
44. Ellis, J. (1987) *Nature* 328, 378-379
45. Freskgard, P. O., Bergenhem, N., Jonsson, B. H., Svensson, M., and Carlsson, U. (1992) *Science* 258, 466-468
46. Wang, C. C., and Tsou, C. L. (1993) *FASEB J* 7, 1515-1517
47. Richter, K., Haslbeck, M., and Buchner, J. (2010) *Mol Cell* 40, 253-266
48. Hemmingsen, S. M., Woolford, C., van der Vies, S. M., Tilly, K., Dennis, D. T., Georgopoulos, C. P., Hendrix, R. W., and Ellis, R. J. (1988) *Nature* 333, 330-334
49. Valpuesta, J. M., and Carrascosa, J. L. (2001) *J Struct Biol* 135, 83
50. Bertsch, U., Soll, J., Seetharam, R., and Viitanen, P. V. (1992) *Proc Natl Acad Sci U S A* 89, 8696-8700
51. Fayet, O., Ziegelhoffer, T., and Georgopoulos, C. (1989) *J Bacteriol* 171, 1379-1385
52. Lubben, T. H., Gatenby, A. A., Donaldson, G. K., Lorimer, G. H., and Viitanen, P. V. (1990) *Proc Natl Acad Sci U S A* 87, 7683-7687
53. Horwich, A. L., and Saibil, H. R. (1998) *Nat Struct Biol* 5, 333-336
54. Frydman, J., Nimmesgern, E., Erdjument-Bromage, H., Wall, J. S., Tempst, P., and Hartl, F. U. (1992) *EMBO J* 11, 4767-4778
55. Fenton, W. A., and Horwich, A. L. (2003) *Q Rev Biophys* 36, 229-256
56. Sigler, P. B., Xu, Z., Rye, H. S., Burston, S. G., Fenton, W. A., and Horwich, A. L. (1998) *Annu Rev Biochem* 67, 581-608
57. Xu, Z., Horwich, A. L., and Sigler, P. B. (1997) *Nature* 388, 741-750
58. Hartl, F. U., and Hayer-Hartl, M. (2009) *Nat Struct Mol Biol* 16, 574-581
59. Glover, J. R., and Lindquist, S. (1998) *Cell* 94, 73-82
60. Goloubinoff, P., Mogk, A., Zvi, A. P., Tomoyasu, T., and Bukau, B. (1999) *Proc Natl Acad Sci U S A* 96, 13732-13737
61. Barends, T. R., Werbeck, N. D., and Reinstein, J. (2010) *Current opinion in structural biology* 20, 46-53
62. Burton, B. M., and Baker, T. A. (2005) *Protein science : a publication of the Protein Society* 14, 1945-1954
63. Martin, A., Baker, T. A., and Sauer, R. T. (2005) *Nature* 437, 1115-1120
64. Doyle, S. M., Shorter, J., Zolkiewski, M., Hoskins, J. R., Lindquist, S., and Wickner, S. (2007) *Nature structural & molecular biology* 14, 114-122
65. Weber-Ban, E. U., Reid, B. G., Miranker, A. D., and Horwich, A. L. (1999) *Nature* 401, 90-93
66. Mayer, M. P., and Bukau, B. (2005) *Cellular and molecular life sciences : CMLS* 62, 670-684
67. Werner-Washburne, M., and Craig, E. A. (1989) *Genome / National Research Council Canada = Genome / Conseil national de recherches Canada* 31, 684-689
68. Haas, I. G. (1994) *Experientia* 50, 1012-1020
69. Voisine, C., Craig, E. A., Zufall, N., von Ahsen, O., Pfanner, N., and Voos, W. (1999) *Cell* 97, 565-574
70. Marshall, J. S., DeRocher, A. E., Keegstra, K., and Vierling, E. (1990) *Proceedings of the National Academy of Sciences of the United States of America* 87, 374-378
71. Kampinga, H. H., and Craig, E. A. (2010) *Nature reviews. Molecular cell biology* 11, 579-592
72. Rudiger, S., Germeroth, L., Schneider-Mergener, J., and Bukau, B. (1997) *The EMBO journal* 16, 1501-1507
73. Schlecht, R., Erbse, A. H., Bukau, B., and Mayer, M. P. (2011) *Nat Struct Mol Biol* 18, 345-351

74. Marcinowski, M., Holler, M., Feige, M. J., Baerend, D., Lamb, D. C., and Buchner, J. (2011) *Nat Struct Mol Biol* 18, 150-158
75. Wandinger, S. K., Richter, K., and Buchner, J. (2008) *J Biol Chem* 283, 18473-18477
76. Smith, D. F., and Toft, D. O. (2008) *Molecular endocrinology* 22, 2229-2240
77. Haslbeck, M., Franzmann, T., Weinfurtner, D., and Buchner, J. (2005) *Nature structural & molecular biology* 12, 842-846
78. Liberek, K., Lewandowska, A., and Zietkiewicz, S. (2008) *The EMBO journal* 27, 328-335
79. Lee, G. J., and Vierling, E. (2000) *Plant Physiol* 122, 189-198
80. Ehrnsperger, M., Gaestel, M., and Buchner, J. (2000) *Methods Mol Biol* 99, 421-429
81. Haslbeck, M. (2002) *Cellular and molecular life sciences : CMLS* 59, 1649-1657
82. McHaourab, H. S., Godar, J. A., and Stewart, P. L. (2009) *Biochemistry* 48, 3828-3837
83. Jakob, U., and Buchner, J. (1994) *Trends Biochem Sci* 19, 205-211
84. Haley, D. A., Horwitz, J., and Stewart, P. L. (1998) *Journal of molecular biology* 277, 27-35
85. Franzmann, T. M., Menhorn, P., Walter, S., and Buchner, J. (2008) *Molecular cell* 29, 207-216
86. Haslbeck, M., Walke, S., Stromer, T., Ehrnsperger, M., White, H. E., Chen, S., Saibil, H. R., and Buchner, J. (1999) *The EMBO journal* 18, 6744-6751
87. van Montfort, R. L., Basha, E., Friedrich, K. L., Slingsby, C., and Vierling, E. (2001) *Nature structural biology* 8, 1025-1030
88. Stromer, T., Fischer, E., Richter, K., Haslbeck, M., and Buchner, J. (2004) *The Journal of biological chemistry* 279, 11222-11228
89. Studer, S., Obrist, M., Lentze, N., and Narberhaus, F. (2002) *European journal of biochemistry / FEBS* 269, 3578-3586
90. Fu, X., Zhang, H., Zhang, X., Cao, Y., Jiao, W., Liu, C., Song, Y., Abulimiti, A., and Chang, Z. (2005) *The Journal of biological chemistry* 280, 6337-6348
91. Borkovich, K. A., Farrelly, F. W., Finkelstein, D. B., Taulien, J., and Lindquist, S. (1989) *Mol Cell Biol* 9, 3919-3930
92. Young, J. C., Moarefi, I., and Hartl, F. U. (2001) *J Cell Biol* 154, 267-273
93. Welch, W. J., and Feramisco, J. R. (1982) *J Biol Chem* 257, 14949-14959
94. Csermely, P., Schnaider, T., Soti, C., Prohaszka, Z., and Nardai, G. (1998) *Pharmacol Ther* 79, 129-168
95. Langer, T., Rosmus, S., and Fasold, H. (2003) *Cell Biol Int* 27, 47-52
96. Felts, S. J., Owen, B. A., Nguyen, P., Trepel, J., Donner, D. B., and Toft, D. O. (2000) *J Biol Chem* 275, 3305-3312
97. Mazzarella, R. A., and Green, M. (1987) *J Biol Chem* 262, 8875-8883
98. Sorger, P. K., and Pelham, H. R. (1987) *J Mol Biol* 194, 341-344
99. Buchner, J. (2010) *Mol Microbiol* 76, 540-544
100. Shiau, A. K., Harris, S. F., Southworth, D. R., and Agard, D. A. (2006) *Cell* 127, 329-340
101. Bardwell, J. C., and Craig, E. A. (1987) *Proc Natl Acad Sci U S A* 84, 5177-5181
102. Ali, M. M., Roe, S. M., Vaughan, C. K., Meyer, P., Panaretou, B., Piper, P. W., Prodromou, C., and Pearl, L. H. (2006) *Nature* 440, 1013-1017
103. Dutta, R., and Inouye, M. (2000) *Trends Biochem Sci* 25, 24-28
104. Hadden, M. K., Lubbers, D. J., and Blagg, B. S. (2006) *Curr Top Med Chem* 6, 1173-1182
105. Prodromou, C., Panaretou, B., Chohan, S., Siligardi, G., O'Brien, R., Ladbury, J. E., Roe, S. M., Piper, P. W., and Pearl, L. H. (2000) *EMBO J* 19, 4383-4392
106. Meyer, P., Prodromou, C., Liao, C., Hu, B., Mark Roe, S., Vaughan, C. K., Vlasic, I., Panaretou, B., Piper, P. W., and Pearl, L. H. (2004) *EMBO J* 23, 511-519

107. Retzlaff, M., Hagn, F., Mitschke, L., Hessling, M., Gugel, F., Kessler, H., Richter, K., and Buchner, J. (2010) *Mol Cell* 37, 344-354
108. Fontana, J., Fulton, D., Chen, Y., Fairchild, T. A., McCabe, T. J., Fujita, N., Tsuruo, T., and Sessa, W. C. (2002) *Circ Res* 90, 866-873
109. Scheufler, C., Brinker, A., Bourenkov, G., Pegoraro, S., Moroder, L., Bartunik, H., Hartl, F. U., and Moarefi, I. (2000) *Cell* 101, 199-210
110. Chen, S., Sullivan, W. P., Toft, D. O., and Smith, D. F. (1998) *Cell Stress Chaperones* 3, 118-129
111. Prodromou, C., Siligardi, G., O'Brien, R., Woolfson, D. N., Regan, L., Panaretou, B., Ladbury, J. E., Piper, P. W., and Pearl, L. H. (1999) *EMBO J* 18, 754-762
112. Obermann, W. M., Sondermann, H., Russo, A. A., Pavletich, N. P., and Hartl, F. U. (1998) *J Cell Biol* 143, 901-910
113. Panaretou, B., Prodromou, C., Roe, S. M., O'Brien, R., Ladbury, J. E., Piper, P. W., and Pearl, L. H. (1998) *EMBO J* 17, 4829-4836
114. Richter, K., Muschler, P., Hainzl, O., and Buchner, J. (2001) *J Biol Chem* 276, 33689-33696
115. Richter, K., Soroka, J., Skalniak, L., Leskovar, A., Hessling, M., Reinstein, J., and Buchner, J. (2008) *J Biol Chem* 283, 17757-17765
116. Graf, C., Stankiewicz, M., Kramer, G., and Mayer, M. P. (2009) *EMBO J* 28, 602-613
117. Hessling, M., Richter, K., and Buchner, J. (2009) *Nat Struct Mol Biol* 16, 287-293
118. Mickler, M., Hessling, M., Ratzke, C., Buchner, J., and Hugel, T. (2009) *Nat Struct Mol Biol* 16, 281-286
119. Street, T. O., Lavery, L. A., and Agard, D. A. (2011) *Mol Cell* 42, 96-105
120. McLaughlin, S. H., Smith, H. W., and Jackson, S. E. (2002) *J Mol Biol* 315, 787-798
121. Panaretou, B., Siligardi, G., Meyer, P., Maloney, A., Sullivan, J. K., Singh, S., Millson, S. H., Clarke, P. A., Naaby-Hansen, S., Stein, R., Cramer, R., Mollapour, M., Workman, P., Piper, P. W., Pearl, L. H., and Prodromou, C. (2002) *Mol Cell* 10, 1307-1318
122. Mayr, C., Richter, K., Lilie, H., and Buchner, J. (2000) *J Biol Chem* 275, 34140-34146
123. Pirkl, F., and Buchner, J. (2001) *J Mol Biol* 308, 795-806
124. Tai, P. K., Chang, H., Albers, M. W., Schreiber, S. L., Toft, D. O., and Faber, L. E. (1993) *Biochemistry* 32, 8842-8847
125. Johnson, J. L., and Toft, D. O. (1994) *J Biol Chem* 269, 24989-24993
126. Cox, M. B., Riggs, D. L., Hessling, M., Schumacher, F., Buchner, J., and Smith, D. F. (2007) *Mol Endocrinol* 21, 2956-2967
127. Riggs, D. L., Roberts, P. J., Chirillo, S. C., Cheung-Flynn, J., Prapapanich, V., Ratajczak, T., Gaber, R., Picard, D., and Smith, D. F. (2003) *EMBO J* 22, 1158-1167
128. Johnson, B. D., Schumacher, R. J., Ross, E. D., and Toft, D. O. (1998) *J Biol Chem* 273, 3679-3686
129. Richter, K., Muschler, P., Hainzl, O., Reinstein, J., and Buchner, J. (2003) *J Biol Chem* 278, 10328-10333
130. Chen, S., and Smith, D. F. (1998) *J Biol Chem* 273, 35194-35200
131. Brinker, A., Scheufler, C., Von Der Mulbe, F., Fleckenstein, B., Herrmann, C., Jung, G., Moarefi, I., and Hartl, F. U. (2002) *J Biol Chem* 277, 19265-19275
132. Hu, L. M., Bodwell, J., Hu, J. M., Orti, E., and Munck, A. (1994) *J Biol Chem* 269, 6571-6577
133. Kosano, H., Stensgard, B., Charlesworth, M. C., McMahon, N., and Toft, D. (1998) *J Biol Chem* 273, 32973-32979
134. Gangaraju, V. K., Yin, H., Weiner, M. M., Wang, J., Huang, X. A., and Lin, H. (2011) *Nat Genet* 43, 153-158

135. Marozkina, N. V., Yemen, S., Borowitz, M., Liu, L., Plapp, M., Sun, F., Islam, R., Erdmann-Gilmore, P., Townsend, R. R., Lichti, C. F., Mantri, S., Clapp, P. W., Randell, S. H., Gaston, B., and Zaman, K. (2010) *Proc Natl Acad Sci U S A* 107, 11393-11398
136. Chadli, A., Bouhouche, I., Sullivan, W., Stensgard, B., McMahon, N., Catelli, M. G., and Toft, D. O. (2000) *Proc Natl Acad Sci U S A* 97, 12524-12529
137. Grenert, J. P., Johnson, B. D., and Toft, D. O. (1999) *J Biol Chem* 274, 17525-17533
138. Weikl, T., Abelmann, K., and Buchner, J. (1999) *J Mol Biol* 293, 685-691
139. Weaver, A. J., Sullivan, W. P., Felts, S. J., Owen, B. A., and Toft, D. O. (2000) *J Biol Chem* 275, 23045-23052
140. Johnson, J. L., Beito, T. G., Krco, C. J., and Toft, D. O. (1994) *Mol Cell Biol* 14, 1956-1963
141. Johnson, J. L., and Toft, D. O. (1995) *Mol Endocrinol* 9, 670-678
142. McLaughlin, S. H., Sobott, F., Yao, Z. P., Zhang, W., Nielsen, P. R., Grossmann, J. G., Laue, E. D., Robinson, C. V., and Jackson, S. E. (2006) *J Mol Biol* 356, 746-758
143. Richter, K., Walter, S., and Buchner, J. (2004) *J Mol Biol* 342, 1403-1413
144. Grad, I., McKee, T. A., Ludwig, S. M., Hoyle, G. W., Ruiz, P., Wurst, W., Floss, T., Miller, C. A., 3rd, and Picard, D. (2006) *Mol Cell Biol* 26, 8976-8983
145. Echtenkamp, F. J., Zelin, E., Oxelmark, E., Woo, J. I., Andrews, B. J., Garabedian, M., and Freeman, B. C. (2011) *Mol Cell* 43, 229-241
146. Gaiser, A. M., Kretzschmar, A., and Richter, K. (2010) *J Biol Chem* 285, 40921-40932
147. Siligardi, G., Panaretou, B., Meyer, P., Singh, S., Woolfson, D. N., Piper, P. W., Pearl, L. H., and Prodromou, C. (2002) *J Biol Chem* 277, 20151-20159
148. Ferguson, J., Ho, J. Y., Peterson, T. A., and Reed, S. I. (1986) *Nucleic Acids Res* 14, 6681-6697
149. Reed, S. I. (1980) *Genetics* 95, 561-577
150. Dey, B., Lightbody, J. J., and Boschelli, F. (1996) *Mol Biol Cell* 7, 1405-1417
151. Brugge, J. S. (1986) *Curr Top Microbiol Immunol* 123, 1-22
152. MacLean, M., and Picard, D. (2003) *Cell Stress Chaperones* 8, 114-119
153. Roe, S. M., Ali, M. M., Meyer, P., Vaughan, C. K., Panaretou, B., Piper, P. W., Prodromou, C., and Pearl, L. H. (2004) *Cell* 116, 87-98
154. Vaughan, C. K., Gohlke, U., Sobott, F., Good, V. M., Ali, M. M., Prodromou, C., Robinson, C. V., Saibil, H. R., and Pearl, L. H. (2006) *Mol Cell* 23, 697-707
155. Lotz, G. P., Lin, H., Harst, A., and Obermann, W. M. (2003) *J Biol Chem* 278, 17228-17235
156. Koulov, A. V., Lapointe, P., Lu, B., Razvi, A., Coppinger, J., Dong, M. Q., Matteson, J., Laister, R., Arrowsmith, C., Yates, J. R., 3rd, and Balch, W. E. (2010) *Mol Biol Cell* 21, 871-884
157. Mayer, M. P., Nikolay, R., and Bukau, B. (2002) *Mol Cell* 10, 1255-1256
158. Wang, X., Venable, J., LaPointe, P., Hutt, D. M., Koulov, A. V., Coppinger, J., Gurkan, C., Kellner, W., Matteson, J., Plutner, H., Riordan, J. R., Kelly, J. W., Yates, J. R., 3rd, and Balch, W. E. (2006) *Cell* 127, 803-815
159. Peattie, D. A., Harding, M. W., Fleming, M. A., DeCenzo, M. T., Lippke, J. A., Livingston, D. J., and Benasutti, M. (1992) *Proc Natl Acad Sci U S A* 89, 10974-10978
160. Smith, D. F. (1993) *Mol Endocrinol* 7, 1418-1429
161. Ratajczak, T., Ward, B. K., Cluning, C., and Allan, R. K. (2009) *Int J Biochem Cell Biol* 41, 1652-1655
162. Duina, A. A., Chang, H. C., Marsh, J. A., Lindquist, S., and Gaber, R. F. (1996) *Science* 274, 1713-1715
163. Fanghanel, J., and Fischer, G. (2004) *Front Biosci* 9, 3453-3478
164. Bose, S., Weikl, T., Bugl, H., and Buchner, J. (1996) *Science* 274, 1715-1717
165. Freeman, B. C., Toft, D. O., and Morimoto, R. I. (1996) *Science* 274, 1718-1720

166. Ward, B. K., Mark, P. J., Ingram, D. M., Minchin, R. F., and Ratajczak, T. (1999) *Breast Cancer Res Treat* 58, 267-280
167. Sumanasekera, W. K., Tien, E. S., Davis, J. W., 2nd, Turpey, R., Perdew, G. H., and Vanden Heuvel, J. P. (2003) *Biochemistry* 42, 10726-10735
168. Meyer, B. K., and Perdew, G. H. (1999) *Biochemistry* 38, 8907-8917
169. Meyer, B. K., Petrulis, J. R., and Perdew, G. H. (2000) *Cell Stress Chaperones* 5, 243-254
170. Kazlauskas, A., Sundstrom, S., Poellinger, L., and Pongratz, I. (2001) *Mol Cell Biol* 21, 2594-2607
171. Fukunaga, B. N., Probst, M. R., Reisz-Porszasz, S., and Hankinson, O. (1995) *J Biol Chem* 270, 29270-29278
172. Edlich, F., Erdmann, F., Jarczowski, F., Moutty, M. C., Weiwad, M., and Fischer, G. (2007) *J Biol Chem* 282, 15341-15348
173. Okamoto, T., Nishimura, Y., Ichimura, T., Suzuki, K., Miyamura, T., Suzuki, T., Moriishi, K., and Matsuura, Y. (2006) *EMBO J* 25, 5015-5025
174. Kang, H., Sayner, S. L., Gross, K. L., Russell, L. C., and Chinkers, M. (2001) *Biochemistry* 40, 10485-10490
175. Wandinger, S. K., Suhre, M. H., Wegele, H., and Buchner, J. (2006) *EMBO J* 25, 367-376
176. Vaughan, C. K., Mollapour, M., Smith, J. R., Truman, A., Hu, B., Good, V. M., Panaretou, B., Neckers, L., Clarke, P. A., Workman, P., Piper, P. W., Prodromou, C., and Pearl, L. H. (2008) *Mol Cell* 31, 886-895
177. Austin, M. J., Muskett, P., Kahn, K., Feys, B. J., Jones, J. D., and Parker, J. E. (2002) *Science* 295, 2077-2080
178. Catlett, M. G., and Kaplan, K. B. (2006) *J Biol Chem* 281, 33739-33748
179. Lee, Y. T., Jacob, J., Michowski, W., Nowotny, M., Kuznicki, J., and Chazin, W. J. (2004) *J Biol Chem* 279, 16511-16517
180. Kadota, Y., Amigues, B., Ducassou, L., Madaoui, H., Ochsenbein, F., Guerois, R., and Shirasu, K. (2008) *EMBO Rep* 9, 1209-1215
181. Takahashi, A., Casais, C., Ichimura, K., and Shirasu, K. (2003) *Proc Natl Acad Sci U S A* 100, 11777-11782
182. Zhang, M., Kadota, Y., Prodromou, C., Shirasu, K., and Pearl, L. H. (2010) *Mol Cell* 39, 269-281
183. Zhao, R., Kakihara, Y., Gribun, A., Huen, J., Yang, G., Khanna, M., Costanzo, M., Brost, R. L., Boone, C., Hughes, T. R., Yip, C. M., and Houry, W. A. (2008) *J Cell Biol* 180, 563-578
184. Eckert, K., Saliou, J. M., Monlezun, L., Vigouroux, A., Atmane, N., Caillat, C., Quevillon-Cheruel, S., Madiona, K., Nicaise, M., Lazereg, S., Van Dorsselaer, A., Sanglier-Cianferani, S., Meyer, P., and Morera, S. (2010) *J Biol Chem* 285, 31304-31312
185. Young, J. C., Hoogenraad, N. J., and Hartl, F. U. (2003) *Cell* 112, 41-50
186. Qbadou, S., Becker, T., Mirus, O., Tews, I., Soll, J., and Schleiff, E. (2006) *EMBO J* 25, 1836-1847
187. Yang, Y., Yan, X., Cai, Y., Lu, Y., Si, J., and Zhou, T. (2010) *Proc Natl Acad Sci U S A* 107, 3499-3504
188. Crevel, G., Bennett, D., and Cotterill, S. (2008) *PLoS One* 3, e0001737
189. Ballinger, C. A., Connell, P., Wu, Y., Hu, Z., Thompson, L. J., Yin, L. Y., and Patterson, C. (1999) *Mol Cell Biol* 19, 4535-4545
190. Connell, P., Ballinger, C. A., Jiang, J., Wu, Y., Thompson, L. J., Hohfeld, J., and Patterson, C. (2001) *Nat Cell Biol* 3, 93-96
191. Riggs, D. L., Cox, M. B., Tardif, H. L., Hessling, M., Buchner, J., and Smith, D. F. (2007) *Mol Cell Biol* 27, 8658-8669

192. Smith, D. F., Sullivan, W. P., Marion, T. N., Zaitsu, K., Madden, B., McCormick, D. J., and Toft, D. O. (1993) *Mol Cell Biol* 13, 869-876
193. Pratt, W. B., and Toft, D. O. (1997) *Endocr Rev* 18, 306-360
194. Smith, D. F., Stensgard, B. A., Welch, W. J., and Toft, D. O. (1992) *J Biol Chem* 267, 1350-1356
195. Forafonov, F., Toogun, O. A., Grad, I., Suslova, E., Freeman, B. C., and Picard, D. (2008) *Mol Cell Biol* 28, 3446-3456
196. Freeman, B. C., Felts, S. J., Toft, D. O., and Yamamoto, K. R. (2000) *Genes Dev* 14, 422-434
197. Scroggins, B. T., and Neckers, L. (2007) *Expert Opinion on Drug Discovery* 2
198. Shao, J., Hartson, S. D., and Matts, R. L. (2002) *Biochemistry* 41, 6770-6779
199. Mollapour, M., Tsutsumi, S., Donnelly, A. C., Beebe, K., Tokita, M. J., Lee, M. J., Lee, S., Morra, G., Bourboulia, D., Scroggins, B. T., Colombo, G., Blagg, B. S., Panaretou, B., Stetler-Stevenson, W. G., Trepel, J. B., Piper, P. W., Prodromou, C., Pearl, L. H., and Neckers, L. (2010) *Mol Cell* 37, 333-343
200. Miyata, Y. (2009) *Cell Mol Life Sci* 66, 1840-1849
201. Duval, M., Le, B. F., Huot, J., and Gratton, J. P. (2007) *Mol Biol Cell* 18, 4659-4668
202. Lei, H., Venkatakrishnan, A., Yu, S., and Kazlauskas, A. (2007) *J Biol Chem* 282, 9364-9371
203. Aoyagi, S., and Archer, T. K. (2005) *Trends Cell Biol* 15, 565-567
204. Yang, Y., Rao, R., Shen, J., Tang, Y., Fiskus, W., Nechtman, J., Atadja, P., and Bhalla, K. (2008) *Cancer Res* 68, 4833-4842
205. Kekatpure, V. D., Dannenberg, A. J., and Subbaramaiah, K. (2009) *J Biol Chem* 284, 7436-7445
206. Kovacs, J. J., Murphy, P. J., Gaillard, S., Zhao, X., Wu, J. T., Nicchitta, C. V., Yoshida, M., Toft, D. O., Pratt, W. B., and Yao, T. P. (2005) *Mol Cell* 18, 601-607
207. Scroggins, B. T., Robzyk, K., Wang, D., Marcu, M. G., Tsutsumi, S., Beebe, K., Cotter, R. J., Felts, S., Toft, D., Karnitz, L., Rosen, N., and Neckers, L. (2007) *Mol Cell* 25, 151-159
208. Scroggins, B. T., and Neckers, L. (2009) *EMBO Rep* 10, 1093-1094
209. Hess, D. T., Matsumoto, A., Kim, S. O., Marshall, H. E., and Stamler, J. S. (2005) *Nat Rev Mol Cell Biol* 6, 150-166
210. Martinez-Ruiz, A., Villanueva, L., Gonzalez de Orduna, C., Lopez-Ferrer, D., Higueras, M. A., Tarin, C., Rodriguez-Crespo, I., Vazquez, J., and Lamas, S. (2005) *Proc Natl Acad Sci U S A* 102, 8525-8530
211. Retzlaff, M., Stahl, M., Eberl, H. C., Lagleder, S., Beck, J., Kessler, H., and Buchner, J. (2009) *EMBO Rep* 10, 1147-1153
212. Ziemiecki, A., Catelli, M. G., Joab, I., and Moncharmont, B. (1986) *Biochem Biophys Res Commun* 138, 1298-1307
213. Momose, F., Naito, T., Yano, K., Sugimoto, S., Morikawa, Y., and Nagata, K. (2002) *J Biol Chem* 277, 45306-45314
214. Mayor, A., Martinon, F., De Smedt, T., Petrilli, V., and Tschopp, J. (2007) *Nat Immunol* 8, 497-503
215. Pratt, W. B., Morishima, Y., Peng, H. M., and Osawa, Y. (2010) *Exp Biol Med (Maywood)* 235, 278-289
216. Picard, D., Khursheed, B., Garabedian, M. J., Fortin, M. G., Lindquist, S., and Yamamoto, K. R. (1990) *Nature* 348, 166-168
217. Whittier, J. E., Xiong, Y., Rechsteiner, M. C., and Squier, T. C. (2004) *J Biol Chem* 279, 46135-46142
218. Zou, J., Guo, Y., Guettouche, T., Smith, D. F., and Voellmy, R. (1998) *Cell* 94, 471-480

219. Guo, Y., Guettouche, T., Fenna, M., Boellmann, F., Pratt, W. B., Toft, D. O., Smith, D. F., and Voellmy, R. (2001) *J Biol Chem* 276, 45791-45799
220. Nadeau, K., Das, A., and Walsh, C. T. (1993) *J Biol Chem* 268, 1479-1487
221. Hubert, D. A., He, Y., McNulty, B. C., Tornero, P., and Dangl, J. L. (2009) *Proc Natl Acad Sci U S A* 106, 9556-9563
222. Liu, Y., Burch-Smith, T., Schiff, M., Feng, S., and Dinesh-Kumar, S. P. (2004) *J Biol Chem* 279, 2101-2108
223. DeZwaan, D. C., Toogun, O. A., Echtenkamp, F. J., and Freeman, B. C. (2009) *Nat Struct Mol Biol* 16, 711-716
224. Boulon, S., Pradet-Balade, B., Verheggen, C., Molle, D., Boireau, S., Georgieva, M., Azzag, K., Robert, M. C., Ahmad, Y., Neel, H., Lamond, A. I., and Bertrand, E. (2010) *Mol Cell* 39, 912-924
225. Geller, R., Vignuzzi, M., Andino, R., and Frydman, J. (2007) *Genes Dev* 21, 195-205
226. Shim, H. Y., Quan, X., Yi, Y. S., and Jung, G. (2011) *Virology* 410, 161-169
227. Taguwa, S., Kambara, H., Omori, H., Tani, H., Abe, T., Mori, Y., Suzuki, T., Yoshimori, T., Moriishi, K., and Matsuura, Y. (2009) *J Virol* 83, 10427-10436
228. Dmochewitz, L., Lillich, M., Kaiser, E., Jennings, L. D., Lang, A. E., Buchner, J., Fischer, G., Aktories, K., Collier, R. J., and Barth, H. (2011) *Cell Microbiol* 13, 359-373
229. Haug, G., Leemhuis, J., Tiemann, D., Meyer, D. K., Aktories, K., and Barth, H. (2003) *J Biol Chem* 278, 32266-32274
230. Li, R., Soosairajah, J., Harari, D., Citri, A., Price, J., Ng, H. L., Morton, C. J., Parker, M. W., Yarden, Y., and Bernard, O. (2006) *FASEB J* 20, 1218-1220
231. Citri, A., Harari, D., Shohat, G., Ramakrishnan, P., Gan, J., Lavi, S., Eisenstein, M., Kimchi, A., Wallach, D., Pietrokovski, S., and Yarden, Y. (2006) *J Biol Chem* 281, 14361-14369
232. Gould, C. M., Kannan, N., Taylor, S. S., and Newton, A. C. (2009) *J Biol Chem* 284, 4921-4935
233. Terasawa, K., Yoshimatsu, K., Iemura, S., Natsume, T., Tanaka, K., and Minami, Y. (2006) *Mol Cell Biol* 26, 3378-3389
234. Falsone, S. F., Leptihn, S., Osterauer, A., Haslbeck, M., and Buchner, J. (2004) *J Mol Biol* 344, 281-291
235. Jakob, U., Lilie, H., Meyer, I., and Buchner, J. (1995) *J Biol Chem* 270, 7288-7294
236. Muller, P., Ceskova, P., and Vojtesek, B. (2005) *J Biol Chem* 280, 6682-6691
237. Walerych, D., Kudla, G., Gutkowska, M., Wawrzynow, B., Muller, L., King, F. W., Helwak, A., Boros, J., Zylicz, A., and Zylicz, M. (2004) *J Biol Chem* 279, 48836-48845
238. Walerych, D., Gutkowska, M., Klejman, M. P., Wawrzynow, B., Tracz, Z., Wiech, M., Zylicz, M., and Zylicz, A. (2010) *J Biol Chem* 285, 32020-32028
239. Rudiger, S., Freund, S. M., Veprintsev, D. B., and Fersht, A. R. (2002) *Proc Natl Acad Sci U S A* 99, 11085-11090
240. Park, S. J., Borin, B. N., Martinez-Yamout, M. A., and Dyson, H. J. (2011) *Nat Struct Mol Biol* 18, 537-541
241. Hagn, F., Lagleder, S., Retzlaff, M., Rohrberg, J., Demmer, O., Richter, K., Buchner, J., and Kessler, H. (2011) *Nat Struct Mol Biol*
242. Goasduff, T., and Cederbaum, A. I. (2000) *Arch Biochem Biophys* 379, 321-330
243. Fuller, W., and Cuthbert, A. W. (2000) *J Biol Chem* 275, 37462-37468
244. Gusarova, V., Caplan, A. J., Brodsky, J. L., and Fisher, E. A. (2001) *J Biol Chem* 276, 24891-24900
245. Meacham, G. C., Patterson, C., Zhang, W., Younger, J. M., and Cyr, D. M. (2001) *Nat Cell Biol* 3, 100-105

246. Sanchez, E. R., Toft, D. O., Schlesinger, M. J., and Pratt, W. B. (1985) *J Biol Chem* 260, 12398-12401
247. Fan, M., Park, A., and Nephew, K. P. (2005) *Mol Endocrinol* 19, 2901-2914
248. Xu, W., Marcu, M., Yuan, X., Mimnaugh, E., Patterson, C., and Neckers, L. (2002) *Proc Natl Acad Sci U S A* 99, 12847-12852
249. Nillegoda, N. B., Theodoraki, M. A., Mandal, A. K., Mayo, K. J., Ren, H. Y., Sultana, R., Wu, K., Johnson, J., Cyr, D. M., and Caplan, A. J. (2010) *Mol Biol Cell* 21, 2102-2116
250. Ehrlich, E. S., Wang, T., Luo, K., Xiao, Z., Niewiadomska, A. M., Martinez, T., Xu, W., Neckers, L., and Yu, X. F. (2009) *Proc Natl Acad Sci U S A* 106, 20330-20335
251. Nanbu, K., Konishi, I., Mandai, M., Kuroda, H., Hamid, A. A., Komatsu, T., and Mori, T. (1998) *Cancer Detect Prev* 22, 549-555
252. Liu, X. L., Xiao, B., Yu, Z. C., Guo, J. C., Zhao, Q. C., Xu, L., Shi, Y. Q., and Fan, D. M. (1999) *World J Gastroenterol* 5, 199-208
253. Neckers, L., Mimnaugh, E., and Schulte, T. W. (1999) *Drug Resist Updat* 2, 165-172
254. Yano, M., Naito, Z., Yokoyama, M., Shiraki, Y., Ishiwata, T., Inokuchi, M., and Asano, G. (1999) *Cancer Lett* 137, 45-51
255. Whitesell, L., Mimnaugh, E. G., De Costa, B., Myers, C. E., and Neckers, L. M. (1994) *Proc Natl Acad Sci U S A* 91, 8324-8328
256. Stebbins, C. E., Russo, A. A., Schneider, C., Rosen, N., Hartl, F. U., and Pavletich, N. P. (1997) *Cell* 89, 239-250
257. Scheibel, T., and Buchner, J. (1998) *Biochem Pharmacol* 56, 675-682
258. Schulte, T. W., and Neckers, L. M. (1998) *Cancer Chemother Pharmacol* 42, 273-279
259. Niikura, Y., Ohta, S., Vandenbeldt, K. J., Abdulle, R., McEwen, B. F., and Kitagawa, K. (2006) *Oncogene* 25, 4133-4146
260. Schulte, T. W., Akinaga, S., Soga, S., Sullivan, W., Stensgard, B., Toft, D., and Neckers, L. M. (1998) *Cell Stress Chaperones* 3, 100-108
261. Sharma, S. V., Agatsuma, T., and Nakano, H. (1998) *Oncogene* 16, 2639-2645
262. Clevenger, R. C., and Blagg, B. S. (2004) *Org Lett* 6, 4459-4462
263. Marcu, M. G., Schulte, T. W., and Neckers, L. (2000) *J Natl Cancer Inst* 92, 242-248
264. Soti, C., Racz, A., and Csermely, P. (2002) *J Biol Chem* 277, 7066-7075
265. Sgobba, M., Forestiero, R., Degliesposti, G., and Rastelli, G. (2010) *J Chem Inf Model* 50, 1522-1528
266. Kim, Y. S., Alarcon, S. V., Lee, S., Lee, M. J., Giaccone, G., Neckers, L., and Trepel, J. B. (2009) *Curr Top Med Chem* 9, 1479-1492
267. Flom, G., Behal, R. H., Rosen, L., Cole, D. G., and Johnson, J. L. (2007) *Biochem J* 404, 159-167
268. Ghaemmaghami, S., Huh, W. K., Bower, K., Howson, R. W., Belle, A., Dephoure, N., O'Shea, E. K., and Weissman, J. S. (2003) *Nature* 425, 737-741
269. Johnson, J. L., Halas, A., and Flom, G. (2007) *Mol Cell Biol* 27, 768-776
270. Yi, F., Doudevski, I., and Regan, L. (2010) *Protein Sci* 19, 19-25
271. Sinars, C. R., Cheung-Flynn, J., Rimerman, R. A., Scammell, J. G., Smith, D. F., and Clardy, J. (2003) *Proc Natl Acad Sci U S A* 100, 868-873
272. Sullivan, W. P., Owen, B. A., and Toft, D. O. (2002) *J Biol Chem* 277, 45942-45948
273. Chang, H. C., Nathan, D. F., and Lindquist, S. (1997) *Mol Cell Biol* 17, 318-325
274. Owens-Grillo, J. K., Czar, M. J., Hutchison, K. A., Hoffmann, K., Perdew, G. H., and Pratt, W. B. (1996) *J Biol Chem* 271, 13468-13475
275. Eisen, M. B., Spellman, P. T., Brown, P. O., and Botstein, D. (1998) *Proc Natl Acad Sci U S A* 95, 14863-14868

276. Gasch, A. P., Spellman, P. T., Kao, C. M., Carmel-Harel, O., Eisen, M. B., Storz, G., Botstein, D., and Brown, P. O. (2000) *Mol Biol Cell* 11, 4241-4257
277. Harst, A., Lin, H., and Obermann, W. M. (2005) *Biochem J* 387, 789-796
278. Johnson, J., Corbisier, R., Stensgard, B., and Toft, D. (1996) *J Steroid Biochem Mol Biol* 56, 31-37
279. van der Spuy, J. (2006) *Exp Eye Res* 83, 1307-1308
280. Weleber, R. G., Francis, P. J., and Trzupek, K. M. (1993) Leber Congenital Amaurosis. in *GeneReviews* (Pagon, R. A., Bird, T. D., Dolan, C. R., and Stephens, K. eds.), Seattle (WA). pp
281. Sohocki, M. M., Sullivan, L. S., Tirpak, D. L., and Daiger, S. P. (2001) *Mamm Genome* 12, 566-568
282. Zoldak, G., Aumuller, T., Lucke, C., Hritz, J., Oostenbrink, C., Fischer, G., and Schmid, F. X. (2009) *Biochemistry* 48, 10423-10436
283. Hidalgo-de-Quintana, J., Evans, R. J., Cheetham, M. E., and van der Spuy, J. (2008) *Invest Ophthalmol Vis Sci* 49, 2878-2887
284. Ozfirat, Z., and Korbonits, M. (2010) *Mol Cell Endocrinol* 326, 71-79
285. Cazabat, L., Bouligand, J., and Chanson, P. (2011) *The New England journal of medicine* 364, 1973-1974; author reply 1974-1975
286. Lin, B. C., Sullivan, R., Lee, Y., Moran, S., Glover, E., and Bradfield, C. A. (2007) *J Biol Chem* 282, 35924-35932
287. Kuzhandaivelu, N., Cong, Y. S., Inouye, C., Yang, W. M., and Seto, E. (1996) *Nucleic Acids Res* 24, 4741-4750
288. Akey, D. T., Zhu, X., Dyer, M., Li, A., Sorensen, A., Fukada-Kamitani, T., Daiger, S. P., Craft, C., Kamitani, T., and Sohocki, M. M. (2003) *Adv Exp Med Biol* 533, 287-295
289. Kirschman, L. T., Kolandaivelu, S., Frederick, J. M., Dang, L., Goldberg, A. F., Baehr, W., and Ramamurthy, V. (2010) *Hum Mol Genet* 19, 1076-1087
290. van der Spuy, J., Chapple, J. P., Clark, B. J., Luthert, P. J., Sethi, C. S., and Cheetham, M. E. (2002) *Hum Mol Genet* 11, 823-831
291. Ruaro, E. M., Collavin, L., Del Sal, G., Haffner, R., Oren, M., Levine, A. J., and Schneider, C. (1997) *Proc Natl Acad Sci U S A* 94, 4675-4680
292. Ball, L. J., Kuhne, R., Schneider-Mergener, J., and Oschkinat, H. (2005) *Angew Chem Int Ed Engl* 44, 2852-2869
293. Winzeler, E. A., Shoemaker, D. D., Astromoff, A., Liang, H., Anderson, K., Andre, B., Bangham, R., Benito, R., Boeke, J. D., Bussey, H., Chu, A. M., Connelly, C., Davis, K., Dietrich, F., Dow, S. W., El Bakkoury, M., Foury, F., Friend, S. H., Gentalen, E., Giaever, G., Hegemann, J. H., Jones, T., Laub, M., Liao, H., Liebundguth, N., Lockhart, D. J., Lucau-Danila, A., Lussier, M., M'Rabet, N., Menard, P., Mittmann, M., Pai, C., Rebischung, C., Revuelta, J. L., Riles, L., Roberts, C. J., Ross-MacDonald, P., Scherens, B., Snyder, M., Sookhai-Mahadeo, S., Storms, R. K., Veronneau, S., Voet, M., Volckaert, G., Ward, T. R., Wysocki, R., Yen, G. S., Yu, K., Zimmermann, K., Philippsen, P., Johnston, M., and Davis, R. W. (1999) *Science* 285, 901-906
294. Laue, T. M., and Stafford, W. F., 3rd. (1999) *Annual review of biophysics and biomolecular structure* 28, 75-100
295. Kroe, R. R., and Laue, T. M. (2009) *Anal Biochem* 390, 1-13
296. MacGregor, I. K., Anderson, A. L., and Laue, T. M. (2004) *Biophys Chem* 108, 165-185
297. Stafford, W. F., 3rd. (1992) *Anal Biochem* 203, 295-301
298. Edelhoch, H. (1967) *Biochemistry* 6, 1948-1954
299. Gill, S. C., and von Hippel, P. H. (1989) *Anal Biochem* 182, 319-326

300. Pace, C. N., Vajdos, F., Fee, L., Grimsley, G., and Gray, T. (1995) *Protein Sci* 4, 2411-2423

8 Declarations

I, Jing Li, hereby declare that this thesis was prepared independently using only the references and resources stated here. This work has not been presented to any examination board yet. Parts of this work have been published in scientific journals.

9 Publications

J. Li, K. Richter and J. Buchner, Mixed Hsp90-cochaperone complexes are important for the progression of the reaction cycle, *Nat Struct Mol Biol*, 18 (2011) 61-66.

J. Li*, J. Soroka* and J. Buchner, The Hsp90 chaperone machinery: conformational dynamics and regulation by co-chaperones, *Biochim.Biophys.Acta* (2011), doi:10.1016/j.bbamcr.2011.09.003 (*both author contributed equally)

10 Acknowledgements

First and foremost I would like to thank my supervisor, Prof. Johannes Buchner for the unique opportunity to work on my Ph.D. thesis in his group, and for the continuous support in my Ph.D. study and research. His patience, understanding, encouraging and wide knowledge guided me all the time.

I sincerely thank Dr. Klaus Richter for his detailed and constructive advice and for his important support throughout my Ph.D. study.

I wish to express my thanks to the rest member of my thesis advisory committee, Prof. Peter Becker and Prof. Jürgen Soll for their encouragement and insightful discussion.

I warmly thank Dr. Hans Jörg Schäffer, Maxi Reif and Dr. Ingrid Wolf from the IMPRS coordination office for continuous support, for organizing the great scientific and soft-skill workshops, for supporting the methods training and conference. I am happy and proud to be a member of this graduate school.

As well I would like to thank all the members of the Buchner group for their kind help and stimulating discussions.

I owe my loving thanks to my wife, Yikai Chen. Her love and support makes my stay in Munich extremely pleasant and valuable.

Last but importantly, I wish to thank my parents for bringing me into this world, for their understanding and encouragement, for their continuous support throughout my undergraduate and postgraduate years of study.